FIRE ANT SELF-ASSEMBLAGES

A Dissertation
Presented to
The Academic Faculty

by

Nathan J Mlot

In Partial Fulfillment
of the Requirements for the Degree
Doctor of Philosophy in the
School of Mechanical Engineering

Georgia Institute of Technology
December 2013

FIRE ANT SELF-ASSEMBLAGES

Approved by:

Dr. David Hu, Advisor
School of Mechanical Engineering
Georgia Institute of Technology

Dr. Craig Tovey, Co-Advisor
School of Industrial Systems Engineering
Georgia Institute of Technology

Dr. Michael Leamy
School of Mechanical Engineering
Georgia Institute of Technology

Dr. Alexander Alexeev
School of Mechanical Engineering
Georgia Institute of Technology

Dr. Michael Goodisman
School of Biology
Georgia Institute of Technology

Date Approved: August 9, 2013

DEDICATION

I dedicate my adventures in fire ant studies to my wife and to my advisor Dr Hu.

Thanks to my wonderful wife who put up with all my long days and nights working in the lab. We were married during the thick of my qualifying exam studies. Through it all she was never short of encouraging and loving.

Before arriving at Georgia Tech to begin graduate school in Mechanical Engineering, never would I have imagined studying such a unique and "out there" topic as fire ant self-assemblages. I am thankful for my advisor and his unique approach and outlook on life that has made such a project possible. His was the first and only office I walked into when looking for a research advisor, but since then he has become so much more: a friend and mentor. His influence will have a lasting impact on my life perspective.

TABLE OF CONTENTS

LIST OF TABLES

LIST OF FIGURES

SUMMARY

Fire ants link their legs and jaws together to form functional structures called self-assemblages. Examples include floating rafts, towers, bridges, and bivouacs. We investigate these self-assemblages of fire ants. Our studies are motivated in part by the vision of providing guidance for programmable robot swarms. The goal for such systems is to develop a simple programmable element from which complex patterns or behaviors emerge on the collective level. Intelligence is decentralized, as is the case with social insects such as fire ants.

In this combined experimental and theoretical study, we investigate the construction of two fire ant self-assemblages that are critical to the colony's survival: the raft and the tower. Using time-lapse photography, we record the construction processes of rafts and towers in the laboratory. We identify and characterize individual ant behaviors that we consistently observe during assembly, and incorporate these behaviors into mathematical models of the assembly process. Our models accurately predict both the assemblages' shapes and growth patterns, thus providing evidence that we have identified and analyzed the key mechanisms for these fire ant self-assemblages.

We also develop novel techniques using scanning electron microscopy and micro-computed tomography scans to visualize and quantify the internal structure and packing properties of live linked fire ants. We compare our findings to packings of dead ants and similarly shaped granular material packings to understand how active arranging affects ant spacing and orientation. We find that ants use their legs to increase neighbor spacing and hence reduce their packing density by one-third compared to packings of dead ants. Also, we find that live ants do not align themselves in parallel with nearest neighbors as much as dead ants passively do.

Our main contribution is the development of parsimonious mathematical models of how the behaviors of individuals result in the collective construction of fire ant assemblages. The

models posit only simple observed behaviors based on local information, yet their mathematical analysis yields accurate predictions of assemblage shapes and construction rates for a wide range of ant colony sizes.

ACKNOWLEDGEMENTS

I acknowledge the following for their contributions:

- David Hu for advising the project, for his endless creativity, and for the adventures in fire ant research.
- National Science Foundation for funding portions of the research through a grant (IOS-0920402).
- Craig Tovey for development of the rafting and tower models and for his enthusiasm, inspiration, guidance, and direction involving the rafting and tower experiments and modeling.
- Michael Goodisman for his help in the early stages of the research by providing direction for ant procurement, care, and all things biology.
- Paul Foster for development of the Matlab code to analyze the CT scan data and for contributing his genius.
- Dan Goldman and Darya Monaenkova for their contributions with tower x-rays
- Sho Shinotsuka for carrying out preliminary tower experiments.
- Tim Nowack for his many beautiful and creative ant photographs.
- Nick Gravish for his selfless insight and direction.
- Victor Breedveld for his early contributions to the rheology research.
- Michael Gerov for being a model research assistant and friend at the same time.
- John Hyatt and his advisor Alberto Fernandez for their extensive use of their rheometer, training on the equipment, and their insight into the world of rheology.

- The following undergraduates for their hard work and contributions: Sulisay Phonekeo for his ingenuity on constructing ant bridges, Zhongyang Liu for his hard work on ant rheology, Adrian Martinez for experimenting with fire ant tunnels, Solomon Equbai for counting ants, and Yun Lee for painting ants.

- The following high-school students for their hard work and contributions: Raghuveer Gummadi, Kaitlyn Murdock, and Madeline O'Connell.

- My wife for her patience and love during my many long nights in the lab and office.

CHAPTER I

INTRODUCTION

"Go to the ant, you sluggard; consider its ways and be wise! It has no commander, no overseer or ruler, yet it stores its provisions in summer and gathers its food at harvest."
-The Holy Bible (NIV), Proverbs 6:6-8

1.1 Motivation

Swarm behavior is a general term used to describe cooperative aggregate behavior exhibited by many animal groups such as the coordinated schooling of fish, the harmonized flocking of birds, or the efficient foraging of ant colonies. Swarm behavior, also referred to as collective behavior, is characterized by many agents in a system cooperating to achieve a common goal but without following commands from a leader or a global plan. The term 'swarm intelligence' refers to the phenomenon of relatively incapable individuals interacting with one another based on simple local rules to govern their actions, resulting in the emergence of an ability to accomplish tasks and goals far beyond the abilities and intelligence of an individual. As an illustration, the movements of a single bird within a flock are not orchestrated by a "leader bird." Rather, a bird's position is dictated by its attempt to stay close to its neighbors while avoiding collisions [5].

Recently mathematicians and system engineers have begun modeling swarms with the hopes of understanding the individual's role in the emergence of group function. Ultimately, a driving force behind the modeling is development of functional swarm robots that operate on the same swarm intelligence principles dictating natural swarm behavior. Benefits of swarm robots include relatively simple programming and lower costs per agent. The robots should be designed to be interchangeable, autonomous, and versatile. Such robots could benefit many fields such as flexible manufacturing systems, spacecraft, inspection/maintenance, defense, construction, agriculture, and medicine work [5].

Our research attempts to bridge the gap between biologists and roboticists by providing empirical results based on the motion of individual ants within a swarm. We use fire ants as our model species since they are readily available in the southeast USA and are known for their ability to link and build floating rafts, using only their bodies, as a means to survive floods. They also naturally form towers, ladders, and other functional aggregates both in nature and in the lab. We conduct experiments to better understand and characterize the individual's role in providing function to the swarm. We also develop models to predict the growth of both ant rafts and towers. These speed and shape predications are validations of

our model assumptions, providing an explanation for individual ant behavior that leads to the aggregate behavior. Swarm roboticists could use such data as inspiration for defining engagement rules between robots in a swarm. Aspects such as ability to self-heal, interchangeability, water-repellancy, and individual agent versatility are attractive qualities of fire ants to roboticists attempting to emulate swarm behavior.

Many researchers today are looking into ways in which robotic swarms can learn from the actions of natural ones [6]. Implementations of swarm intelligence logic such as discrete optimization, task optimization, and collective decision making, are all inspired by mechanisms employed by social insects such as fire ants [7]. To many, our future lies in the development of "smart" robots that touch all aspects of our lives, from household robots that communicate with appliances, to autonomous security bots which patrol a given area, to post-natural-disaster search and rescue bots [6].

Our research also has inherent value in its interdisciplinary contributions to the field of biological organisms and systems engineering. Since the research we are performing is interdisciplinary, we are creating a link between two fields that in the past rarely overlapped. But a growing trend among scientists today is interdisciplinary modeling projects [8] that focus on bridging the gap between these research fields. According to E.O. Wilson, the integration of disciplinary knowledge is the most promising path to scientific advancement, intellectual adventure, and human awareness. Also, mathematical modeling of biological systems has seen a recent rise in interest from applied mathematicians, physicists, and engineers. Such studies can provide much insight and understanding of very complex systems.

We have also contributed to the field of behavioral biology by using engineering principles and techniques to uncover previously unknown fire ant behaviors in constructing self-assemblages. We have probed and fine-tuned the experimental conditions to initiate fire ant self-assemblage construction in a lab. These methods are useful for biologists wishing to replicate our experiments so they can study ant behaviors. For example: in our studies, we attempted to remove queens, males, and broods from the construction process whereas a biologist may want to leave these colony elements in to better understand colony function in a biological context. Our methods are easily repeatable, controlled, and easily analyzable.

We have used many mechanical engineering tools to study ant assemblages. Some of these tools include particle tracking software, image manipulation software, CAD software to visualize assemblage formation, advanced MATLAB scripts to visualize and quantify internal assemblage structure, x-ray image capture to visualize ant movement within a live assemblage, and CT scanning and SEM to visualize structure and connections. In addition to the data processing software used we designed and built many complex experimental setups to collect data. This often involved using image capture equipment including HD cameras, high-speed cameras, macro and telescoping lenses, a CT scanner, SEM, and fine

depth composition microscopy. As we are also interested in the aesthetics of our images in addition to the quality of our data, we often went the extra step to ensure the images we captured would be visually appealing. This often involved inventive camera angles, backgrounds, lighting setups, mastery of our image capture equipment controls, and lots of patience. We also used engineering and mathematical principles and methods to develop simulations and models and to analyze our experimental findings.

1.2 Preview

Fire ant self-assemblages are functional structures fire ants form by linking together using legs and jaws. **Fig.1** shows an assortment of fire ant assemblages. Chapter 2 introduces the relevant literature on insect assemblages. We review recent and significant experiments and models involving insect self-assemblages. We also highlight researcher's attempts to formally define ambiguous terms in the field of collective behavior. We follow this with a summary of robotic applications, a review of granular media studies relative to active matter, and highlights of the few studies on insect water-repellency. In Chapter 3, we present experimental methods for constructing a fire ant raft. We use experimentally gathered trajectory statistics to formulate a predictive model of raft construction growth rate for rafts of any size. In Chapter 4, we present the first time images of insect self-assemblage internal structure and provide insight into the physical implications of the assemblage packing properties. In Chapter 5, we present experimental methods for constructing a fire ant tower and justify the tower shape with a model of constant strength. In addition we present a model to explain tower construction dynamics. In Chapter 6, we discuss our contributions to the relatively new field of active matter rheology by probing ant assemblage bulk properties in a rheometer. In Chapter 7, we present areas where future work is needed and include interesting phenomena we observed that should be further explored. In Chapter 8, we summarize the main findings of the research. Appendices that follow include publications and conference talks (Appendix A), and supplementary information for detailed calculations and procedures. References cited in the document are provided at the end.

Figure 1: An array of fire-ant self assemblages

The variables used in each chapter are compiled and listed here for reference.

Table 1: Variables used in the raft chapter

Raft Variables	
γ	Planar ant packing (ants/cm^2)
δ	Distance between ant centers-0f-mass (cm)
v, u	Ant speed on raft (cm/s)
F	Maximum ant tensile force (dyne)
σ_f	Tensile yield stress (dyne/cm^2)
θ_e	Ant body-water contact angle (°)
ρ	Material density of linked ants (g/cc)
m	Ant mass (g)
V	Volume occupied by linked ants (cc)
Φ	Area fraction of the ant-water contact
N	Number of ants in a raft
σ	Surface tension of ants (dynes/cm)
L_a	Capillary length for ants (cm)
r	Raft radius at time t (cm)
t	Time elapsed during raft growth (sec)
α	Expected distance ant travels on a raft
h	Raft thickness at equilibrium (ant layers)
t_∞	Time for an ant raft to reach equilibrium (sec)
n_∞	Number of ants in raft's bottom layer at t_∞
p	Probability an ant will "bounce" of raft edge
n	Number of ants in raft's bottom layer at t
n_0	Number of ants in raft's bottom layer at t=0
s	Walking distance on raft between turns (cm)
D	Diffusion coefficient for ants (cm^2/s)
e	Eccentricity of ant raft shape

Table 2: Variables used in the structure chapter

Structure Variables	
α	Aspect ratio
Φ	Packing fraction
c	Contact number
N	Number of samples
n	Ants in a sample
NND	Nearest neighbor distance (mm)
V	Volume of ant (mm^3)
V_{total}	Volume of containing ants in a sample (mm^3)
l	Staple barb length
w	Staple spine length
c_{in}	Incoming ant connections
c_{out}	Outgoing ant connections
c_{total}	Total ant connections
r	Sphere radius
$\mathbf{P}$	Unit vector pointing along ant principle axis
Ψ	Relative orientation correlation
θ	Angle between neighboring ant principle axes (°)

Table 3: Variables used in the tower chapter

Tower Variables	
t	Time elapsed during tower construction (sec)
h	Tower height at time t (mm)
w	Tower width at height h and time t (mm)
N	Total tower layers
n	The n^{th} tower layer
X_n	Number of ants in layer n
α	Ant strength in a tower (ant weights)
N_h	Total human layers in a tower
n_h	The n^{th} human layer in a tower
α_h	Human strength in a tower (human weights)
ρ	Density of mobile ants on the tower surface (cm^2)
v	Ant speed on tower surface (cm/sec)
p	Probability of sticking to rod vs bouncing
d	Distance traveled before changing direction
χ	Density of ants in the tower ($ants/cm^3$)
ψ	Thickness of ant layer (cm)
s	Downward speed of ant waterfall (cm/min)
g	Growth rate of the tower height (cm/sec)
T	Time waterfall starts after construction begins (sec)
D	Rod diameter (cm)
R	Number of available spaces for ants around the rod

Table 4: Variables used in the rheology chapter

Rheology Variables	
η	Viscosity (Pa-s)
$\dot{\gamma}$	Shear rate (s^{-1})
γ	Shear strain
m	Consistency index
n	Power law exponent
λ	Characteristic time of the fluid (sec)
t_{flow}	Characteristic time of the flow (sec)
τ	Shear stress
τ_y	Yield stress
ω	Frequency (rad/s)
T	Torque (mNm)
G'	Storage modulus (Pa)
G''	Loss modulus (Pa)

CHAPTER II

BACKGROUND

2.1 Insect self-assemblages

Very few intensive studies exist that attempt to quantify or even characterize self-assemblages formed by insect societies using their own bodies as building blocks. This is because insect self-assemblages can often times be elusive [9], difficult to reproduce in a lab setting, or pose a danger to the experimenter. Despite these difficulties, they are a striking example of self-organization and provide a model opportunity for study of a decentralized system of individuals acting cohesively as a unit.

A review by Carl Anderson *et al* in 2002 provides an exhaustive compilation of all known self-assemblage structures formed collectively by social insect societies. It categorizes assemblage according to function and complexity and provides a detailed description for each type of assemblage [10]. Some assemblage are difficult to categorize as the function is not clear to researchers. A sampling of the structures includes bridges, bivouacs, curtains, droplets, ladders, ovens, rafts, and pulling chains. The functions of these adaptive configurations include colony defense, thermoregulation, and temporary shelter.

While insect societies function both as a unit on the colony level and at the individual level, Anderson *et al* remark in another study that between these levels lie numerous "intermediate-level parts" that function as adaptive units, but don't require participation from the entire colony. In fact these parts usually act as a tool for accomplishing a higher colony function [11]. Insect self-assemblages are intermediate-level parts.

The earliest review of animal aggregations dates to the 1920s when Allee discussed the significance of animal and insect groupings [12]. He breaks insects into two groups: those in constant contact and those in which physical contact is not normal. He also notes though that these two groups are not mutually exclusive, and some species may transition between groups. This is the case for fire ants, the subject of our studies, since they can transition from foraging or exploring individually while still in the company of colony members, to being directly connected to neighbors as one static link in a bridge across flooded terrain.

Another more recent study by Halley *et al* reviews many publications on self-assembly and attempts to harmonize them by discussing consistent concepts [13]. Halley *et al* create a distinction between self-organization and self-assembly based on thermodynamics. The term "self-assemblage" is limited to those spontaneous processes that tend towards equilibrium. A requirement that demands some components remain unchanged throughout the self-assembly process. While Halley *et al* state that the term "self-assembly" is overused today,

Anderson and other experts agree that the process of fire ants constructing bivouacs or rafts is indeed a self-assembling process.

While formal definitions are important for continuing in the field, the quest for understanding how and why insects form self-assemblages continues [14–16]. Today more researchers studying insect swarms are developing models and simulations based on experimental observations to better understand the driving mechanisms behind self-assembly [17–23]. Such models can also be used to predict insect behavior outside of a laboratory context. Modeling self-assemblages can provide insight into the forces distributed between members and the role of an individual in carrying out the group functions.

While modeling insect behavior in general is non uncommon, the modeling specifically of self-assemblage formation, equilibrium states, and deconstruction is rare in the literature. The earliest such study was in 1997 by Bonabeau *et al*, and discusses a phenomenon of the Argentine ant *Linepithema humile* that is only known to occur under particular experimental conditions. Bonabeau *et al* observe that a continuous flow of ants on a bent rod forms into droplets and falls off the end of the rod much like water droplets from a leaky faucet. In fact, the authors found that the similarities are not just superficial, but that the competing cohesive and gravity forces play a similar role in determining system dynamics.

Several years later, the authors followed up their study, this time led by Theraulaz, with a discrete probabilistic model based on experiments of Argentine ant droplet formation. By recording time intervals between droplets, Theraulaz *et al* find that a rapid succession of two droplets is likely followed by a longer time interval because the ant supply at the end of the rod is temporarily depleted. The nonlinear dynamics of droplet formation makes sense when considering that colony bridge and chain formation are highly nonlinear events that emerge under changing colony and environmental situations.

Another notable study was performed by Lioni *et al* to model the chain formation of African Weaver ant *Oecophylla longinoda* used to bridge gaps and improve colony traveling efficiency [16]. The model describes the evolution of the number of individuals in the chain during the development and breakup phases of the chain. The study showed that probability of an ant joining or leaving a chain is highly dependent on the number of ants present in the chain, and depends little on visual stimulus. Lioni's model provides an accurate predictor of chain formation and breakup dynamics in the ant species. Three years later, Lioni *et al* published modeling results that show chain building logic need not involve complex cognition such as direct comparison between attachment sites in the chain [18]. A key finding of this study is that when two chains to bridge a gap are formed simultaneously, one of these chains will usually breakup, leaving the other intact. The ants are able to accomplish this without any direct visual or tactile communication between chain sites.

Azzag and Lebbah drew inspiration from the self-assembly behavior found in ants, to develop a model for data clustering. In their model, ants are added to a structure from

a single point and progressively build that structure by first linking to the point and then recursively to the newly connected ants [19]. Lastly, Zirbes *et al* provide the first evidence of self-assemblages in earthworms. They examine the mechanisms governing earthworm behavior in joining or leaving self-assemblages, finding that size of the cluster is a key factor determining structure stability.

Ant self-assemblages have inspired swarm roboticists for many years, but these systems are extremely complex, and are not easy to analyze. Drawing useful algorithms can be challenging, but understanding only a small aspect or specific instance of self-assembling can reap large rewards. Our research on fire ants self-assemblages follows naturally in the path of the published studies on insect assemblages. By experimentally observing the formation of self-assemblages such as the raft or tower, we use the behaviors of the individual that we believe lead to the overall function of the greater structure to develop a mathematical model. A model that matches the experimental observations verifies that we discovered the key mechanisms that lead to self-assembling.

2.2 Collective behavior, swarm intelligence, and self-organization

Many papers written recently aim define collective behavior, swarm intelligence, and self-organization in the animal world [5–7, 24–28]. How do these three fields relate and how much overlap exists among them? Beginning with collective behavior, it can simply be described as the spontaneous emergence of structure from the unorchestrated interaction of many individuals. Examples that occur naturally include the synchronized schooling of hundreds of herring, the massive swarms of dancing starlings, or the intricate system of underground tunnels built to house ant colonies.

How is it that such low level intelligence creatures are able to accomplish tasks which are far beyond the intelligence level of any individual without any global coordination? In order to answer this question and hopefully use that answer to further science and engineering, scientists attempt to define and describe a set of rules called behavioral algorithms. These algorithms serve as the basis for math models that can explain and predict behavior of these self-organized systems. It is the hope of a few researchers that a single model will be developed to universally describe the collective behavior of biological systems [28].

Despite scientists' attempts at creating a universal swarm model, no such all-encompassing set of behavioral rules has been found [28]. Sumpter proposes instead a method which studies systems on a case-by-case basis, and for each particular system, defines the rules according to which the individuals interact with each other and their environment [28]. However, there are some principles which seem to apply to nearly every case of collective behavior: positive and negative feedback, redundancy, synchronization, and response thresholds are a few [28].

Swarm intelligence is an area of study closely related to collective behavior. Swarm intelligence refers particularly to the emergent collective intelligence of groups of simple autonomous agents. The agents use simple local rules to govern their actions, and because of the compounded interactions of the group, an objective is achieved [5, 29–31]. Swarm intelligence as a scientific discipline was born from observations of the impressive abilities of social insects to solve challenging problems. Some important fields that have developed from swarm intelligence are swarm optimization and distributed control in robotics [7].

Self-organization, a field which is almost indistinguishable from collective behavior, has roots in physics and chemistry which date at least back to the 1940s [24]. It refers to the system-level patterns that spontaneously arise solely from interactions among subunits of the system. Group-level behavior is not encoded into each individual, and emergence of complex patterns implies non-additive, nonlinear interactions involved implicating the role of positive feedback [26, 32]. In the case of social insects, complex colony level features arise without individual complexity [24]. Defining the properties and basic ingredients of self-organization has helped us to describe and better understand many group behaviors of social insects. Ants in particular display a wide range of group behaviors including foraging, nest building, and piling of dead ants [24].

Animal aggregations have been studied for over half a century, but little is known about how these aggregations are formed or sustained. Flocks of birds, schools of fish, stampeding herds, milling crowds, and swarming insects have raised intriguing questions about the collective behavior of animals [28] [33]. One such question is how can the behavior of individuals, without a central method of communication, prompt the emergence of organized patterns and structures? [7]

A paper by Goldstone *et al* provides a look at collective behavior and where the surrounding research stands today from swarms of bees to non-communicated decisions in sports teams [27]. Goldstone *et al* attribute the recent rise in collective behavior interest to technology advances, and raises some very intriguing questions about collective behavior: "Does group behavior always reduce to individual behavior, is group cognition possible, and what is the value of formal modeling for understanding group behavior?" Such questions put advancement in the field in perspective, showing that the major themes surrounding collective behavior remain a mystery. Despite this, we should still explore the field trying to decipher one small section of the code at a time.

For example, we examine literature on general swarming aggregations and present trends in swarm participant spacing normalized by body length as seen in **Fig.2**. Swarming animal aggregations occur across all animal scales. Except in the case of flocking birds, swarming requires the participants to be around 1 body length or closer. For smaller creatures such as insects, swarming is based on tactile cues. For larger creatures such as birds and fish, visual cues become increasingly more important as body contact can prove disastrous during

high velocity swarming. This is especially true for birds as their swarming includes rapid and spontaneous direction changes: a property that likely can be attributed to the higher neighbor distance required during swarming.

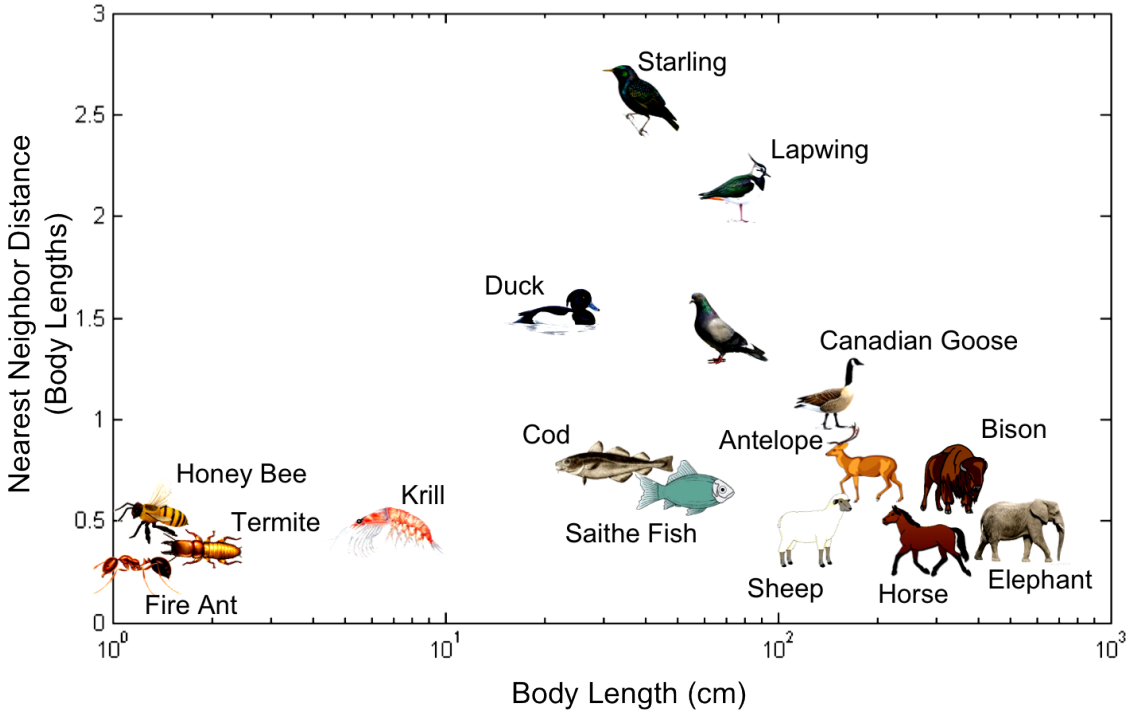

Figure 2: Swarming animal aggregations occur across all animal scales. Except in the case of flocking birds, swarming requires the participants to be around 1 body length or closer. For smaller creatures, swarming is based on tactile cues. For larger creatures, visual cues becomes increasingly more important as body contact can prove disastrous during high velocity swarming.

2.3 Application to robotics

The direct and obvious application of self-organization and swarm intelligence studies is in the field of swarm robotics development [29, 34–42]. Often, the goal of swarm robotics is the design and fabrication of interlocking and interchangeable modular robots that are operating on the same principles that govern insect swarms [43]. Robot swarms provide the possibility of enhanced task performance, high reliability, low unit complexity, and decreased cost over traditional robotic systems. Swarm robots have applications in many fields, including flexible manufacturing systems, search and rescue, demolition, construction, defense, inspection/maintenance, sorting, agriculture, and medicine work [5].

Imagine a group of robots that can travel as individuals into tight spaces, and later link together forming a larger versatile robot that can accomplish difficult or dangerous tasks in hard to reach spaces. Each unit is dispensable and interchangeable. The collective robot is

self-healing, adaptable, and greater than the sum of the individual parts. This is not only one vision for swarm robots, but also an accurate description of natural self-assembling ant structures. It makes sense then that we should look to these naturally forming systems of little programmed robots for our inspiration in developing synthetic swarm robots.

The Symbrion program [44], a project funded by the European Union to develop shape-changing, self-organizing mini robots that work together as a team, is an example of a research project inspired by the natural behaviors that ants and other social insects display. The robots are interchangeable, removing concerns such as task allocation and distinct programming. Another example of ant inspired robot design is the ant-like robot algorithms developed by Deneubourg et al. inspired by how ants sort their brood [45].

With several papers and a dissertation on the topic, Grob is a leader in self-assembling, biologically-inspired robot development. He reviews the leading systems, providing a taxonomy of the systems, discussing their design and function [46]. Grob shows that self-assembly offers adaptive value to robotic groups in task performance.

2.4 Active matter and cohesive granular media

Studies of fire ants aggregations have implications and applications in the closely related fields of granular physics and active matter. Active matter consists of particles that convert energy into movement [47, 48]. This is not the case for most of the materials traditionally considered by continuum mechanics such as non-living materials like air and water or living materials like tree trunks with a movement time-scale much longer than that of daily applied forces [47]. Consideration of active material is important for many living systems and their constituent molecular motors, as well as synthetic analogues in which energy is added to the system, such as vibrated copper wire segments [47].

The majority of active particle work has been on those in a fluid. Active particles such as the bacteria *Chlamydomonas* or *Bacillus subtilis* can generate turbulence and can change the viscosity of the medium [47]. Such motile bacteria can be classified into pushers and pullers. Ants have been observed to push and pull, as well as reverse their direction for short spurts. They can also drag their nest mates around when necessary. The ants have numerous mechanisms such as adhesive pads and claws to prevent slipping, even when walking on challenging porous surfaces such as other ants [49]. Because of their small size and great strength, locomotion against gravity impedes ants minimally. Their intrinsic metabolic power exceeds the rate of working to climb vertical surfaces [50]. As a result, an ant expends the same energy to walk horizontally as on walls. This ability suggests that models of ant swarming need not consider the inclinations of the environment traversed. Research has shown however that ants can recognize inclination.

Fire ants also do not seem capable of sensing over even short distances, as suggested by their bumper car behavior of frequent bumping into each other and consequently stopping.

Such phenomena would be disastrous for birds and fish given their high velocities. Ants instead run into each other and then use tactile information from antennuating each other and reading pheromone trails [51].

Most granular media cannot resist tensile forces, and as a result most granular materials when assembled can only form a conical pile with a constant angle of repose [52]. Cohesion and thus the ability to resist tensile stress is a necessary property for building a wider array of 3D structures. Recently, there have been several studies on cohesive granular media that can be used as construction materials [53]. The most familiar is wet granular materials such as wet sand: the capillary forces between sand grains is sufficient for structures such as sand castles to be built [54].

Within the study of granular media, there have been few studies of non-convex particles, which are defined as containing sets of points where one can draw line segments, between the two points, that will reach outside the set [55]. Many shapes in nature are non-convex, including the shapes of ants. These shapes permit entanglement, the penetration of objects within the cavities of other particles. Entangled granular media such as staples use a combination of friction and the elasticity of the staple to cohere together.

Ants are a special class of active cohesive granular materials in that they can control their cohesion. Ants possess tarsal claws and adhesive pads that they can intentionally open or close, permitting the creation or removal of junctures. They also possess muscles that can provide tensile or contractile forces in an analogous way to actin networks with a cell.

2.5 Water repellency of insects

The underwater breathing mechanism of aquatic insects has been formally studied since the late 1800s. The work of early contributors such as Ege and Brocher revealed that many insects can survive underwater through trapping a layer of air in the numerous tiny hairs covering the insect's body [56]. These hairs render the insect's bodies water repellent by creating a barrier between the water's surface and the insect's body even when the insect is fully submerged. This trapped air layer is termed the "plastron" and serves as a breathing mechanism as well as facilitates resurfacing of submerged insects [57].

The wettability of rough porous surfaces was examined by Cassie and Baxter in 1944 when they discovered that water-repellency could be improved through surface roughening [58]. Previously, Wenzel had postulated that a water drop on a rough surface would fill in the air voids [59]. Cassie's findings showed instead that when roughened, hydrophobic surfaces tended to create pockets of air underneath a water droplet so that the drop rests on islands of solid in a sea of air [60]. Cassie found that the apparent contact angle of a water drop could be increased by decreasing the ratio of solid actually contacting the water to the perceived water droplet contact area. The hairy foot of an insect is analogous to the kinds of rough porous surfaces studied by Cassie and Baxter.

The locomotion of water walking creatures such as the water strider has been investigated by researchers [60–63]. For all such creatures, tiny leg hairs abutting the water's surface provide support for resting on the water's surface and for driving against it during locomotion. Fire ants also possess similar hairs on their legs and on a majority of their body (**Fig.3**b,c). Their hairs are angled at approximately 30° which is consistent with findings on water strider legs [60].

Few studies exist on the water-repellency of lone insects, and even fewer on the water-repellent self-assemblages formed by swarms. One study was found which focused on the mechanisms used by swarms of honey bees to form a water repellent curtain of bees over the swarm cluster when rained upon [15]. The study focused mostly on the behaviors of bee swarms during curtain formations. Their studies showed that during rainstorms, bees orient themselves similar to a phalanx formation so that water rolls off the bees' wings.

CHAPTER III

THE ANT RAFT

3.1 What is an ant raft?

Insect societies are remarkable natural examples of collective behavior that includes such activities as nest construction, complex foraging strategies, and collective decision making [10]. Our research focuses on one of the most understudied, but at the same time, one of the most visually striking examples of collective behavior –the functional structures that insects are able to build by linking their bodies together, termed "self-assemblages" [10]. Their bodies make up the building block for such structures, and the flexibility of their attachment mechanisms ensures that no two structures are built in the exact same way. We focus our studies on fire ants because they are both readily available and readily form these structures in a laboratory under certain conditions.

One of the most notable structures formed by fire ants is the floating raft. While fire ants are not the only species observed to form rafts [10], again they are very easy to collect here in the south and therefore are the species for experimentation despite their powerful bite and subsequent poisonous sting.

The raft serves a two-fold purpose for the fire ant colony. First and foremost, the raft is a mechanism for survival during flooding. Fire ants, part of the *Solenopsis* species, are native to the Pantanal flood plain of South America–an area that sees frequent flooding [3, 64]. Since ants are social creatures, they cannot survive without the colony; a single ant left alone will quickly die. Ants need the stochastic foraging and digging behavior of the many colony members to collect food and build nests. This makes the fire ants' ability to form cohesive rafts during flooding crucial for survival, since dispersal of the ants in random directions would leave them unlikely to gather again and reestablish themselves after the floodwaters have subsided. Also crucial for survival is the inclusion of the queen and brood (larvae) in the raft.

The second function of the raft is to allow the ants to spread to new areas. This is how the ants have been able to spread across the southeast of the United States [65]. If a colony formed two separate rafts during flooding, then the presence of a queen in each raft would allow the original colony to potentially split and form two separate colonies upon reestablishment on land [66]. This is made possible since some fire ant colonies are polygyne (having multiple queens) [67].

The raft is formed as rainwater starts to seep into the colony and flood the tunnels. The nest evacuation process is slow; it can take several hours for the ants to collect all the brood

and bring them to the surface. When the water rises above the level of the ground, the ants are already milling around in a massive pile on top of the location of their now flooded colony. They begin to float effortlessly and are at the mercy of the flowing water. They are now easy prey for an attacking creature and thus increase their defensiveness while rafting [64]. The ants are able to float for weeks at a time until stable ground is once more available [3].

A natural question to raise when observing the ant raft is how do the ants on the bottom breathe?' Contrary to previous research on the raft [12, 66, 68], we have found that fire ants in a raft do not cycle positions to breathe. Rather, the tight weave of the ant structure and their natural hydrophobicity allows linked ants to repel water extremely well and to keep water from seeping through the raft. Ants in the bottom layer of the raft, except in rare occasions, remain fixed in position contacting the water surface. The ants on the top are free to mill about on the surface of the raft. In one sense, as long as the water's surface is free of surfactants, all the ants remain dry, since they all rest atop the surface of the water, and even the ants who may break through the surface tension of the water retain a plastron layer around their bodies while submerged [57].

An ant raft is a model example of collective behavior among social insects. Thousands of individuals interact to form a functional structure without any individual knowledge of the final objective. Despite the impressive feat of intertwined ants forming floating aggregations, little detailed work has been carried out to characterize the ant raft, the ant behavior within the raft, and to quantify its measurable characteristics. We studied the ant raft in a lab, under controlled conditions. We designed experiments to determine measurable parameters describing both *1)* individual ant motion within the raft, which yields the overall resulting dynamics of construction rate, and *2)* equilibrium sizes. These experimentally gathered parameters are then used to develop a model for predicting the raft construction rates.

3.2 Introduction

A raft is defined as a flat vessel for flotation or transport on water. Usually, it is characterized by the lack of a hull and floats simply by the buoyancy of its materials rather than by watertight integrity. By Archimedes' Law, the buoyancy force of a raft is given by $(\rho - \rho_w)Vg$ where g is gravity, V is the displaced volume of the fluid and ρ and ρ_w are the densities of the raft materials and water, respectively. Using low-density materials is thus a necessity, as was known in 5,000 B.C. when the first rafts were built by humans using logs and twine [69]. In the natural world, aquatic plants raft by virtue of the air stored in underwater stolons. Animals generally cannot trap air pockets in this manner and so instead raft by stowing away upon mats of floating vegetation [70].

Individual ants may float if the water surface is free of surfactants. Although denser than water, they rely upon surface tension forces in the manner of water-walking insects

and certain biomimetic robots [61, 71, 72]. However, surface tension is generally too weak to support objects that have the density of water and a size much larger than the capillary length $l_c = \sqrt{\sigma_w/(\rho_w g)} \approx 2.3$ mm, where σ_w is the surface tension of water. Consequently, it is not immediately obvious how colonies of thousands of ants can float so easily.

3.3 Experimental methods for small rafts

3.3.1 General ant procurement and care

To study rafting behaviors fire ant colonies were collected in fields approximately 60 miles east of Atlanta city limits, near the city of Madison. Fire ant colonies were chosen primarily for largest average worker size as well as overall size of the colony. Colonies were dug up and placed into 5 gallon buckets with talcum powdered sides [73]. Attempts were made to dig as deeply as possible in the center of the nest so as to maximize the number of workers gathered in each shovel scoop as well as to increase the chances of collecting queen and brood.

Upon return to the lab, ants were extracted from the soil using established techniques [74, 75] of dripping water slowly into the buckets over an 8 hour period. The dripping rate must be slow because it takes significant time for the ants to gather themselves to the surface, and sudden inundation of the colony will trap the ants in the soil and kill them. When the water level rises above the soil, the floating colony of ants and brood were scooped from the water and placed into plastic tubs (18 qt Sterilite container) coated with talc. The tub contained covered petri dishes for colony housing, water, and a food source of both crickets and protein bars.

Single colonies that exceeded the size of the plastic tubs were split into several marked tubs. Ants were provided water 3 times a week and food twice a week. In between experiments, ants were allowed to return to the colony for at least 4 hours to return to typical behavior before ants were randomly chosen for subsequent experimenting.

3.3.2 Time-lapse video

Ants were scooped with spoons into 100-mL beakers rimmed with talc powder and weighed to count their numbers. Using the natural adhesion of the ants, a few swirls of the beaker was sufficient to roll the ants into balls (Figure 3c). Ant balls were placed on the water surface and held stationary by impalement upon a pair of wires of an inverted LED affixed to the aquarium bottom. Top and side views of the ant raft were filmed using a high-definition digital video camera (Sony HDR-HC9). Fluid-distortion of the side view of the raft was minimized by filming through a glass sheet coated with Fluoropel^{TM}. Films were digitized using Matlab to determine the area of the raft as as a function of time.

3.3.3 Cohesive force

We glued a live ant onto the bottom of a glass slide. Clinging to this ant was another ant, harnessed with an elastic band (length 5 cm, diameter 1mm). By pulling on the elastic slowly (for a duration of 3 sec), the maximum extension of the band was measured (5-7 mm) upon release of the ant's grip, where we accounted for the 1-mm extension of the ant's arms. The tensile force was estimated using the spring constant of the elastic (0.20 N/m).

3.3.4 Ant viscosity

To measure viscosity, we measured the settling speed $U \sim 10^{-2}$ cm/s of a sphere of radius $a = 4.8$ mm and density $\rho_s = 7.5$ g/cc in an ant raft of 8000 ants floating in a water-filled beaker of radius $3a$. Settling speed was estimated using the height of the raft and the duration elapsed before the sphere exited the raft. Stokes drag on this system indicates that the viscosity $\mu = \frac{2}{9}(\rho_s - \rho)ga^2/U$.

3.3.5 Ant separation distance

To measure the distance between ant centers of mass, rafts of ants were frozen in liquid nitrogen. Ants were removed manually until a single layer remained, whose number of ants was counted manually.

3.3.6 Raft edge bounce probability

We measured the bounce probability by tracking the motion of ants constructing their raft. Specifically, we observed a raft of 500 ants for 20 seconds, tracking 5 separate points on the raft's circumference. During this observation we could distinguish the motion of 9-16 ants at each point. In terms of X, the number of ants ricocheting and Y, the number adhering, the bounce-probability was found to be $p = X/(X + Y) = 0.64 \pm 0.04$ (N=5).

3.4 Results for small rafts

We conducted a series of laboratory experiments to determine how ants respond to floods, from which we observed ants constructing rafts when placed into water. Fire ants in a colony vary in size, with heights of 0.5 - 2.5 mm, lengths of 1 - 4.5 mm and masses of 0.5 - 5 mg [72]. Their average mass, 1.3 ± 0.8 mg (N=16), was used to estimate the number of ants in a raft. We characterized ant rafts by a planar ant packing of $\gamma = 34 \pm 2$ (N=4) ants per cm^2, found by counting ants in 4 rafts of fixed size. This packing corresponds to a distance between ant centers-of-mass of $\delta = 1/\sqrt{\gamma} = 0.17 \pm 0.02$ cm. The average ant speed

while walking on the raft is $u \approx 0.39 \pm 0.18$ cm/s (N=8), measured by observing ants atop the raft.

3.4.1 Cohesive strength

We froze ant rafts in liquid nitrogen to visualize how ants are linked together within the raft. We found that ants grip each other by using either mandibles or tarsal claws (**Fig.3**b-c). We observed that frozen ant rafts are brittle, disintegrating upon handling, and so infer that the strength of ant gripping depends on the squeezing force applied by the ant's grip. By harnessing two live ants with an elastic band, we found that the maximum tensile force between them is $F = 620 \pm 100$ dynes (N=11), or more than 400 times body weight. This force is significantly weaker than other mechanisms of ant-attachment to complex surfaces. One example is the velcro-like attachment (5700 times body weight) between ant claws and the fuzzy loops on certain plant leaves [76]. Conversely, the gripping force is twice as strong as the ant adhesion to smooth surfaces such as glass (370± 90 dynes, N=10) or plastic (1-150 times body weight) [77, 78]. On such surfaces, ants extrude fluid drops with their feet, adhering by using the associated capillary and viscous forces [72, 79, 80].

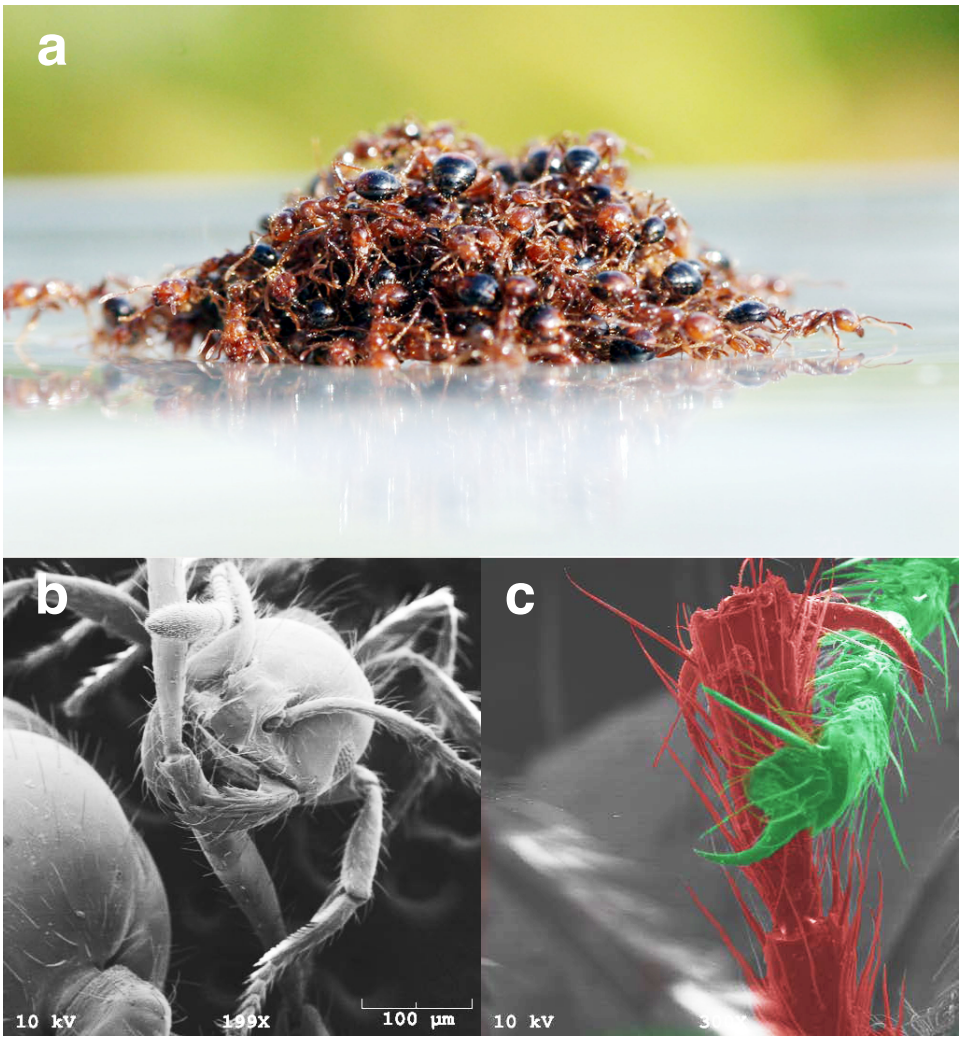

Figure 3: (a) A raft of 500 fire ants, composed of a partially wetted layer of ants on the bottom and dry ants on top. (b & c) Scanning electron micro- graphs of links between ants in the raft, consisting of mandibletarsus and tarsustarsus attachments. Note that the mandibular grip requires particular care to minimize pain to the recipient of the bite.

When many ants are placed in a beaker, they readily clump, forming a porous visco-elastic material. The material can be easily broken apart by hand, without injuring any of the ants. This is consistent with rough estimations of the material's low tensile strength, $\sigma_f \approx F/\delta^2 \approx 2 \times 10^4$ dynes/cm^2 = 2000 Pa, which is several orders of magnitude less than the strength (10^6 Pa) of connective stolons of floating plants [81]. However, the strength is sufficient to hold an ant raft together on the water surface. We note that the cohesion of the ants is highly dependent on the water surface being clean. Traces of surfactant cause ants to release their grip upon each other, causing the raft to fall apart. It is thus possible that ant-to-ant cohesion on the water surface may be aided by capillary forces, which have been shown to help other insects aggregate on the water surface [82].

3.4.2 Water-repellency and buoyancy

In order to prevent dehydration or bacterial growth, many natural surfaces are water-repellent. On plant leaves [83] and insect cuticle [60, 84], water drops bead up, demonstrating high contact angles θ_e with the solid. As shown in **Fig.4**a, an ant's cuticle is mildly hydrophobic, with a contact angle θ_e of $102 \pm 4^\circ$ (N=10), a value consistent with measurements on other terrestrial insects [60]. An advantage of having a hydrophobic cuticle is that it enables ants and semi-aquatic insects to trap a plastron layer of air around their bodies, without which they would sink. We verified the necessity of the plastron by measuring the volume-displacement of ant rafts. We find that clean water permits plastron retention while soapy water minimizes it. The average material density of ants was measured by $\rho = m/V$, where m is their mass and V the volume of water they displaced when submerged. We found that their average density without plastrons was $1.1\pm$ 0.3 g/cc (N = 3), which is greater than the density of water. Thus, ants in soapy water will struggle to swim and eventually sink. In clean water, however, ants are clearly able to trap plastrons, as shown by the bubbles attached to submerged ants (**Fig.4**d). These bubbles are enlarged in submerged ant rafts, as shown by the large air pockets in **Fig.4**e. These trapped air pockets decrease the ants' mean density by 75% to $\rho = 0.2 \pm 0.04$ g/cc (N=4). The presence of the plastron also explains why ants in rafts rarely drown: their plastron enables them to breathe even when they are at the bottom of the raft.

To understand why water does not penetrate a raft, we investigated its water-repellency. We deposited drops on ant rafts and observed that the contact angles of ant rafts were $133 \pm 12^\circ$ (N=6), which is 30% higher than that of individual ants (**Fig.4**b). This water-repellency is consistent with predictions using the Cassie-Baxter Law of wetting [60, 85, 86]. This law states that the contact angle θ^* of a textured solid is given by the relation $\cos(\theta^*) = \phi(\cos\theta_e + 1) - 1$, where ϕ is the area fraction of the ant-water contact. Using the ant area fraction, $\phi = (\rho/\rho_w)^{2/3} = 0.35$, yields that $\theta^* = 136^\circ$, which corresponds well with our observations. This enhanced water-repellency prevents the raft from sinking when submerged (**Fig.4**c) and aids in water-proofing during rainstorms. While natural water-repellency has been previously viewed as a static property of a surface [85], the ant raft represents the first example of a surface rendered water-repellent by cooperative behavior.

In response to mechanical perturbations or submergence (**Fig.4**d), the ants contract their muscles in unison, squeezing the raft into a tight mass. Consequently, the raft suffers a slight loss of buoyancy due to the increased raft density, $\rho_{max} = 0.27 \pm 0.01$ g/cm^3 (N=3). A benefit of this behavior is the decrease in ant separation distance, which rigidifies the raft. Moreover, the tighter weave increases the submergence depth at which fluid imbibition occurs [60]. A rough estimate of this depth, without taking into account the ant legs, yields $z \sim 2\sigma/(\delta\rho_w g) \sim 1$ cm; in our experiments we observed some air bubbles escaping at 3-10 cm, and others remaining trapped at depths over 20 cm.

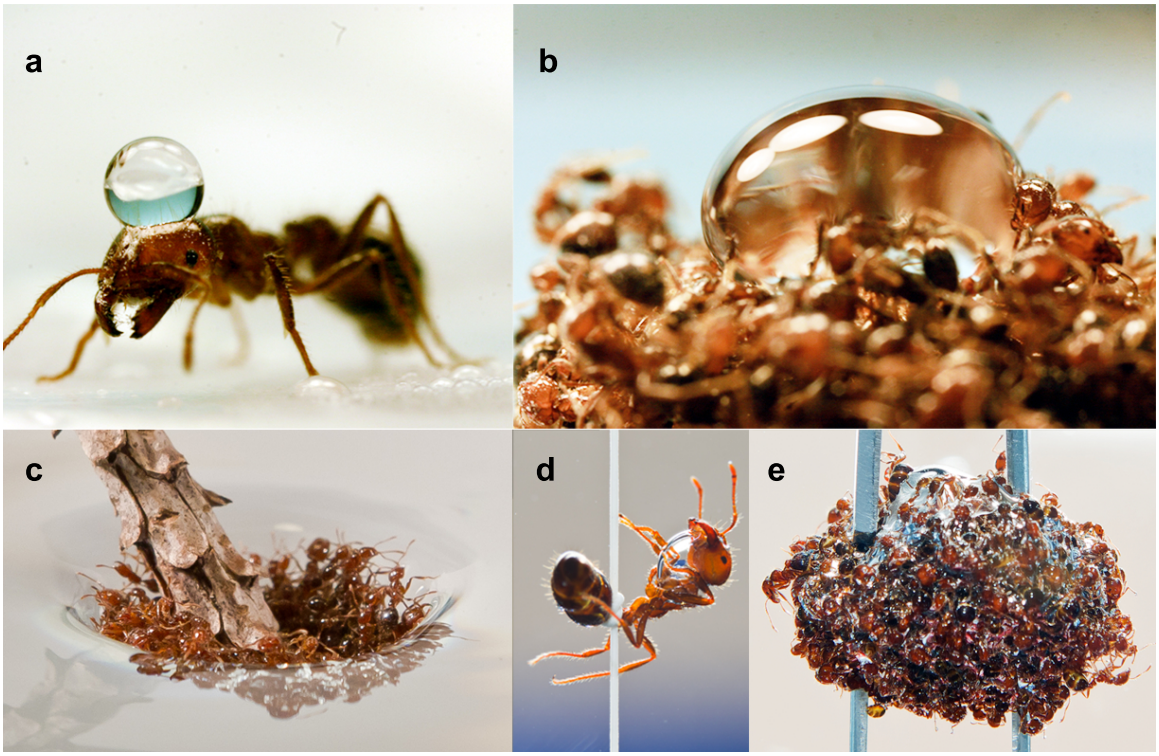

Figure 4: Water repellency of the ant rafts. (a) An individual ants exoskeleton is moderately hydrophobic, as shown by the contact angle of the water drop. (b) Enhanced water repellency of a raft of ants, as shown by the increased contact angle of the water drop. (c) Buoyancy and elasticity of the ant raft, as shown by attempted submersion by a twig. (d) The plastron air bubble of an ant in soap-free water. The bubble makes the ant buoyant, necessitating the use of a thread to hold it underwater. (e) An air pocket trapped in a submerged ant raft. The shimmery layer around the ants is the airwater interface.

3.4.3 Construction rate

We observed raft construction using spheres of ants, each containing $N = 1000 - 7000$ ants (**Fig.5**c). Not surprisingly, ant spheres that are placed on solid surfaces quickly disintegrate as the ants flee in all directions. However, when placed on the water surface, ant spheres redistribute and reconnect themselves into a raft, as shown in the video sequence in **Fig.5**a-b. The raft reaches a stable equilibrium within several minutes. At equilibrium, the rafts are pancake-shaped, whereby a dry portion of the colony stands atop a monolayer of ants. Visually, the spreading of the raft resembles that of a drop of fluid, so we first consider modeling ants as a continuum.

3.4.4 Ants as a fluid

Spreading drops have been studied in the context of water, blood, lava and shampoo [87–89]. By crudely estimating the continuum properties of ants, we may model the raft as a fluid composed of ant "molecules". Table 1 gives order-of magnitude estimates for the

density, viscosity, and surface tension of ants compared to water. The surface tension of ants, $\sigma = F/\delta$, was estimated using the characteristic ant force F and spacing δ. Ant viscosity was inferred from the very slow settling speed (10^{-2} cm/s) of a metal sphere in a beaker of ants (see Methods). Compared to water, ant rafts have 1/5 the density, but 10 times the surface tension and 10^6 times the viscosity. Their surface tension is 5 times higher than that of mercury (487 dynes/cm); and their viscosity is similar to that of high-viscosity silicone oil (10^6 cP). The capillary length for ants is $L_a = 3$ cm, which is 10 times larger than that for water. In our experiments, a sphere of $N = 3000$ ants (with a volume Ω of 15 cc), spreads from $R = 1.5$ cm to 3.6 cm in 150 seconds. Given that ants are significantly more viscous than water, the physical picture of an ant raft is that of a viscous lens (a large pancake-shaped drop) floating on an immiscible non-viscous liquid. The associated physics is well-understood, and closed-form solutions have been derived by previous investigators [85, 89] for the final drop radius R as a function of time. Drops smaller than L_a spread at time-scales of $t \sim (\pi/16)R^4/(\Omega\sigma/\mu)$; larger drops at time-scales of $t \sim (1/2)R^2\mu/(\tilde{\rho}g\Omega)$ where ρ, μ, σ are the density, viscosity and surface tension of ants given in Table 1, Ω is the droplet volume, $\tilde{\rho} = \rho(1 - \rho/\rho_w) = 0.25$ is the ant material density corrected for the Archimedes' pressure. Using these relations, we predict a spreading time of 10^3 seconds, which is nearly an order of magnitude greater than in our experiments.

In the lubrication limit of a spreading drop, flow is two-dimensional and radial: fluid particles tend to follow the ones in front of them. Such simple flows have arisen in previous studies of ants, for example in the raids of army ants, where they travel in straight lines, and in "circular ant mills", where ants travel in circles endlessly [51]. Do rafting ants travel in such simple patterns? Tracking the trajectories of ants on rafts of various sizes, we find that they move using a stereotyped sequence of behaviors, as shown in **Fig.5**d. This includes walking in straight lines, ricocheting off the edges of the raft, and walking again until finally adhering to an edge. The expected distance of travel α is on average over three times the radius of the raft. The discrepancy between α and unity indicates a potential problem in modeling ants as fluids. One view of a fluid is that of an ideal cooperative organism, in that all particles travel radially. In comparison, ant motion is not radial, but in fact randomly oriented.

Another potential problem in modeling ants as fluids is that such models suggest that ant rafts should spread according to simple power laws with respect to time. **Fig.5**e shows the time course of the number of ants on the raft bottom n, with colors denoting the raft size, $N = 1000$-7000 ants (N=21). The trends, plotted in log-log, are sigmoid rather than linear, indicating that a power-law fails to account for ant-raft spreading. One last difference in the two systems is that ants are a source of kinetic energy, in contrast to a drop of fluid, in which gravitational energy is dissipated by viscosity. Given these discrepancies, we turn to a discrete model of ants, modeled as self-propelled independent agents.

3.4.5 Straight-path model

An important input parameter into our model is the raft thickness at equilibrium. Clearly, the ant raft has some topology as shown in **Fig.5**b. We can estimate the spatially-averaged thickness using n_∞, the number of ants on the bottom of the raft at time t_∞: the thickness is then $h = N/n_\infty \approx 2.5\pm\ 0.4$ (N=30) layers of ants. Physically, h corresponds to 8 mm, a quantity that appears to be conserved for all rafts. **Fig.5**e (inset) shows that the n_∞, is approximately 40±10 % the total number of ants, N. Thus, ant rafts appear to exhibit some level of fairness, in that no more than half the colony is on the bottom of the raft. The selection of the raft thickness is beyond the scope of this study; presumably, it results from a competition between raft strength and the ants' aversion to be on the bottom of the raft.

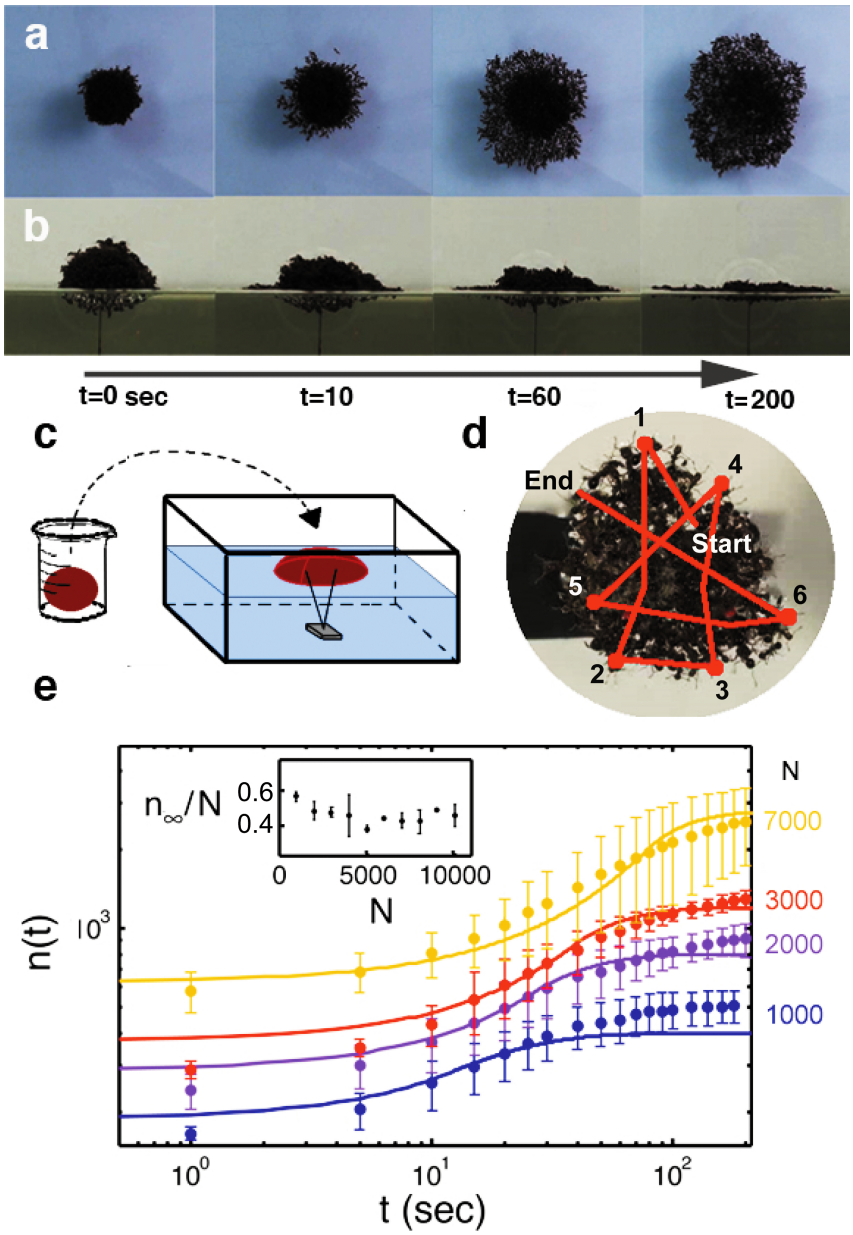

Figure 5: Dynamics of ant-raft construction. (a & b) Top and side views of growth of a 3,000-ant raft. (c) Schematic of experimental setup. Ants are rolled into balls in a beaker and then placed onto a pronged stabilizer in a partially filled aquarium. (d) The trajectory of a single ant on the raft, tracked over a duration of 40 s. (e) The relation between time t and the number of ants on the bottom of the raft $n(t)$. Data are shown for four raft sizes, characterized by the number of ants in the raft N. Solid lines are given by the predictions of our theoretical model. (Inset) The relation between the number of ants in the raft N and the proportion of ants on the bottom at equilibrium

In our model, we assume that only the top layer of ants can move and the remaining layers of ants are jammed. As previously discussed, ants walk in straight lines and either stick to an edge or bounce off. The probability p that an ant will bounce off the raft edge,

rather than sticking and adding to the edge, is $p = 0.64 \pm 0.04$ (N=5). As shown in Appendix B, the expected travel distance on a unit disk during this sequence of randomly-directed walks is $\alpha = \frac{8}{3\pi} + \frac{4}{\pi}(\frac{p}{1-p}) \approx 3.1$. In our model, we will thus distinguish two stages in the raft construction, short times for which $n(t) \leq N/(h+1)$, when a full top layer of ants may move; and long times, for which $n(t) > N/(h+1)$, when there is only a partial layer of $N - hn(t)$ ants that can move. Keeping track of these regimes is important because the number of ants on top strongly influences the deposition rate of ants at the edge.

If the ants have a uniform packing of γ (ants per square cm), the area of the raft can be written as a corresponding number of ants using $\pi r^2 = n(t)/\gamma$. The radius of the raft in cm is $r = \sqrt{n(t)/\gamma\pi}$. If there are $n(t)$ ants in the moving layer, on average $n(t)u/\alpha r$ ants attach to the boundary per second. Considering that the ants distribute themselves to form a new exterior boundary h ants thick, the rate of new ants on the bottom equals $\beta\sqrt{n(t)}$ numbers of ants per second, where $\beta = \frac{u\sqrt{\gamma\pi}}{\alpha h} \approx 0.52$ sec^{-1}. Conversely, if there are $N - hn(t)$ ants in the moving layer, then $\beta(N - hn(t))/\sqrt{n(t)}$ add to the bottom per second. Thus, the rate of change in the number of ants $n(t)$ on the bottom layer at time t, evolves according to

$$\frac{dn}{dt} = \begin{cases} \beta\sqrt{n(t)} & \text{if } n(t) < N/(h+1) \\ \beta(N - hn(t))/\sqrt{n(t)} & \text{if } n(t) \geq N/(h+1). \end{cases} \quad (1)$$

The initial values for the differential equation Eq. (1), $n_0 \approx 2.6N^{0.62}$ were estimated using the number of ants in the cross-section of a sphere of N ants. Integrating Eq. (1), we obtain the solution,

$$\begin{aligned} n(t) &= (\frac{1}{2}\beta t + \sqrt{n_0})^2 && \text{if } t \leq t^* \\ t - t^* &= -\frac{2}{\beta h}(\sqrt{n(t)} - \sqrt{n^*}) + \frac{2\sqrt{N}}{\beta h^{3/2}}\left(\tanh^{-1}\sqrt{\frac{hn(t)}{N}} - \tanh^{-1}\sqrt{\frac{hn^*}{N}}\right) && \text{if } t > t^* \quad (2) \end{aligned}$$

where the inflection point is given by $t^* = \frac{2}{\beta}\left(\sqrt{\frac{N}{h+1}} - \sqrt{n_0}\right)$ and $n^* = \frac{N}{h+1}$. The solution, shown by the solid lines in **Fig.5**e, exhibits close agreement to the expansion rates observed for ant rafts up to $N = 7000$ ants.

Modifications to this model are possible. For example, ants at the bottom will at times exchange positions with those on top. However these rates are slow, and during construction, such negative feedback is not required, as the rate of raft expansion is controlled by the number of ants remaining on top. We also implemented a brownian diffusion model [90] (see Appendix B), but found that it was unable to account for the high rate of growth of the raft.

3.4.6 Discussion on small rafts

Overlooking its diminutive size and its shortcomings in soapy solutions, the ant raft has attractive traits with respect to man-made flotation devices. It simultaneously provides cohesion, buoyancy and water-repellency to its passengers. It can be constructed quickly (in ~ 100 seconds) without any additional equipment. It can accommodate thousands to millions of passengers with zero casualties, but perhaps most strikingly, it is self-assembling.

Many of these benefits are due to the ant's small size. At the scale of millimeters, ants have great strength, high speed, and the ability to trap air pockets when submerged, which in turn makes their rafts water-repellent. These abilities will likely vanish at large sizes. Roboticists interested in building biomimetic ant rafts will need to design robots that can both reversibly attach to one another and traverse over one another. Moreover, they will need to understand which processes of the raft assembly process are coordinated (such as ant-to-ant gripping) as opposed to stochastic (ant trajectories).

In the ant raft, passengers are used interchangeably as flotation devices. This feature of the raft makes its construction reversible. We conducted experiments in which free ants were removed one-by-one from the top of the raft. This caused the raft to self-heal: ants on the bottom moved to the top to preserve the average thickness of the raft. We surmise that ants are able to sense how many of their colony members are walking on top of them. Similar behavior was shown to be important in ant bridge construction in which bridges made of ants were maintained as long as ants were crossing atop of them [10].

Self-assembly and self-healing are hallmarks of living organisms [91, 92]. The ant raft demonstrates both these abilities, providing another example that an ant colony behaves like a super-organism [51]. In addition, we observed that large numbers of organisms can behave similarly to a fluid. This viewpoint has been used to model the flow in human crowds [93]. We found that understanding ant rafts also requires an additional consideration, namely that they are water-repellent en masse. Future studies of swarms of other insects may find that they too exhibit an aversion or repellency to water or rain that affects their cooperative behaviors.

3.5 Introduction to large ant rafts

Previously we had made observations of ants moving only on small ant rafts, composed of $N = 3000$ ants. We observed that ants would morph their raft into a pancake shape of 2-3 ant layers in thickness, as shown in **Fig.6**. We predicted the spreading rate of this pancake by tracking ant walking patterns to formulate a differential equation in terms of the number of ants n on the bottom layer of the raft. The current study represents two improvements to this model based on the following two motivations:

One motivation for the current study is the absence of analysis or explanation of the overall shape of the raft which had been circular in our previous experiments. In fact our previously published analysis implicitly assumed circularity but gave no explanation to how it arises. A second motivation is our observation that our model was a better fit for small rafts of 1,000-6,000 ants than for large rafts greater than 8,000 ants. Fire ant rafts found in nature often comprise entire colonies of ants, and thus can span tens of centimeters and carry tens of thousands of ants, as shown in **Fig.7**a. In order to build a model that can better account for the largest of rafts, we have re-investigated the growth of ant rafts, focusing on those of large size.

In this study on large ant rafts, we report the results of a model specifically for large ant rafts. We begin by providing details of our experimental methods. Next we present our new experimental results for the trajectories of ants atop large rafts and discuss the resulting implications to our model. We also include a justification for the circular shape of the ant raft. We continue with a presentation of our mathematical modification to our model from 2011 and compare its predicted results to those of our previous model. Lastly we discuss the implications of our work, and suggest directions for future research.

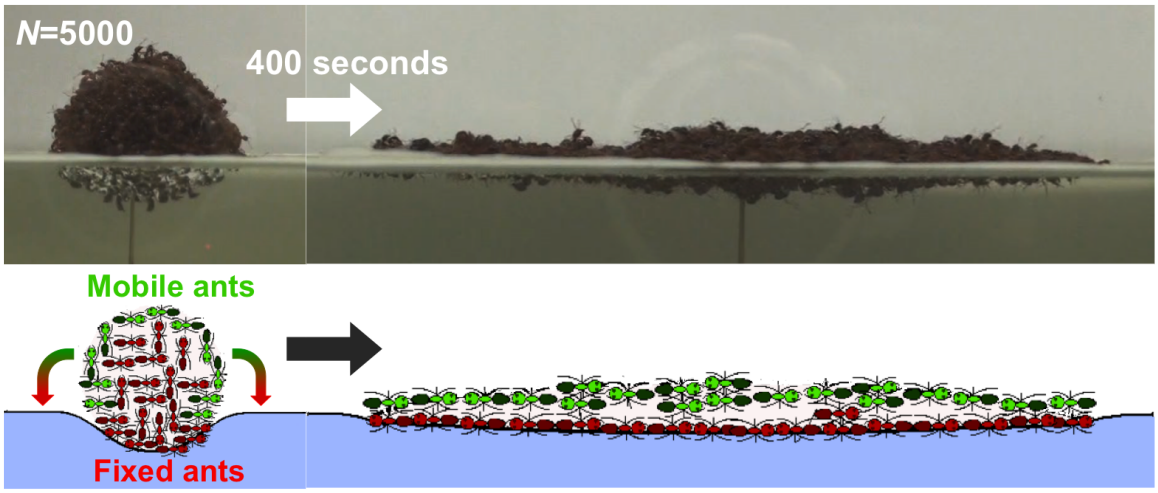

Figure 6: A sphere of ants will spread out to a pancake in a matter of minutes. Mobile ants on the top layer walk towards the edge and become part of the fixed bottom layers. This leaves a new mobile layer of ants that follow the same pattern. This behavior continues until the raft reaches an equilibrium thickness of 2.5 ants.

3.6 Experimental methods for large rafts

3.6.1 Filming of large ant rafts

Using high-definition video cameras, we film the construction of ant rafts floating on the water surface. We parameterize the raft size by the number of ants in the raft N, and perform experiments on rafts of N =6000, 10000, 15000 and 22500, measured by weighing the rafts. Ants are initially collected from bins and placed into a beaker, taking care to avoid collection of queens and males. The beaker is then swirled so that ants clump together forming a cohesive spherical aggregation. To ensure a spherical aggregation, beaker size is chosen such that when the ants are formed into a ball and centered in the beaker, there is at least a 1-cm and no more than a 2-cm gap between the ball edge and beaker wall. Using tweezers, ant balls are placed on the surface of clean, room-temperature water, and centered upon a partially submerged pin to prevent drifting. Resulting ant motion is recorded from above until equilibrium is reached. Four trials for each raft size N are performed and filmed. The average top-view projected-area change of the ant raft in number of ants is digitized using image processing for each N.

By tracking individual ants as we played videos frame-by-frame, we determined values for several parameters in the model. These parameters include the average walking speed v, the probability p of joining the bottom layer during the growth phase, the walking distance s between turns, and ant planar density γ in ants per centimeter squared.

3.7 Results for large rafts

3.7.1 Step size measurement

Fig.7b shows the canonical trajectory of a single ant in a small raft as found previously. As shown, the ant tends to move in straight-line paths separated by ricocheting paths off the raft edge. An important aspect of this motion is that the ants do not change direction until they reach the raft edge. Next, we made observations of single ants atop styrofoam discs of the same size as the rafts, approximately 4 cm. We chose the styrofoam due to the problem of visually resolving a small ant on a large raft of live ants. We found no qualitative differences between motion on the two surfaces. This similarity is consistent with observations by Fourcassié, who finds there is no significant difference in trajectory characteristics between solitary ants and groups of ants, although there are velocity differences [94].

Conducting experiments on a larger styrofoam disc ($r > 4$ cm), we found that the ant trajectories vary from those on small disks. Previously, we found that ants did not make changes in direction until they reached the disk edge. On this larger disk, we observed a different behavior: ants walked in straight line segments of length s, interspersed by turns in a random direction, as shown in **Fig.7**c. In our modeling section we refer to this distance s as the step size. Using a sample size of $m = 14$ random turns by one ant, we found s to be 4 ± 1.5 cm.

Although the ants make more turns on larger rafts, we note that their walking speed remained the same as on small rafts. Average walking speeds along the straight line-paths were $v \approx 0.39$ cm/s. The speeds on large rafts matched our previously measured speeds on small rafts, as well as measurements of ant speed made by Gordon [95].

Unraveling the intricacies of the bulk motion of the ants boils down to accurately describing the motion of a single ant. Based on our observations of individual ants, we hypothesize the following algorithms for individual behaviors:

1. An ant only moves if there are no ants on top of it.

2. When an ant moves, it travels straight in a random direction (uniformly distributed over 360 degrees) for a distance s, changes direction randomly, and repeats this pattern until it reaches an edge.

3. Upon reaching an edge, an ant gets stuck with probability $\rho \approx 0.3$, and with complementary probability $1 - \rho$ "bounces" off the edge, and begins traveling straight in a random direction away from the edge (uniformly distributed over 180 degrees), continuing with behavior *2*.

Experimentally, we found the raft reaches equilibrium when $N/n_\infty = 2.5 = h$, where h is measured in ant heights. If the raft gets thinner than $hn(t)$, then there are insufficient ants on top of the raft to keep the ones at the edge pinned by walking on top of them.

Ants follow the algorithms above until they are pinned at the edge of the raft by other ants. Note that the modification from the previous algorithm is the inclusion of a step size s.

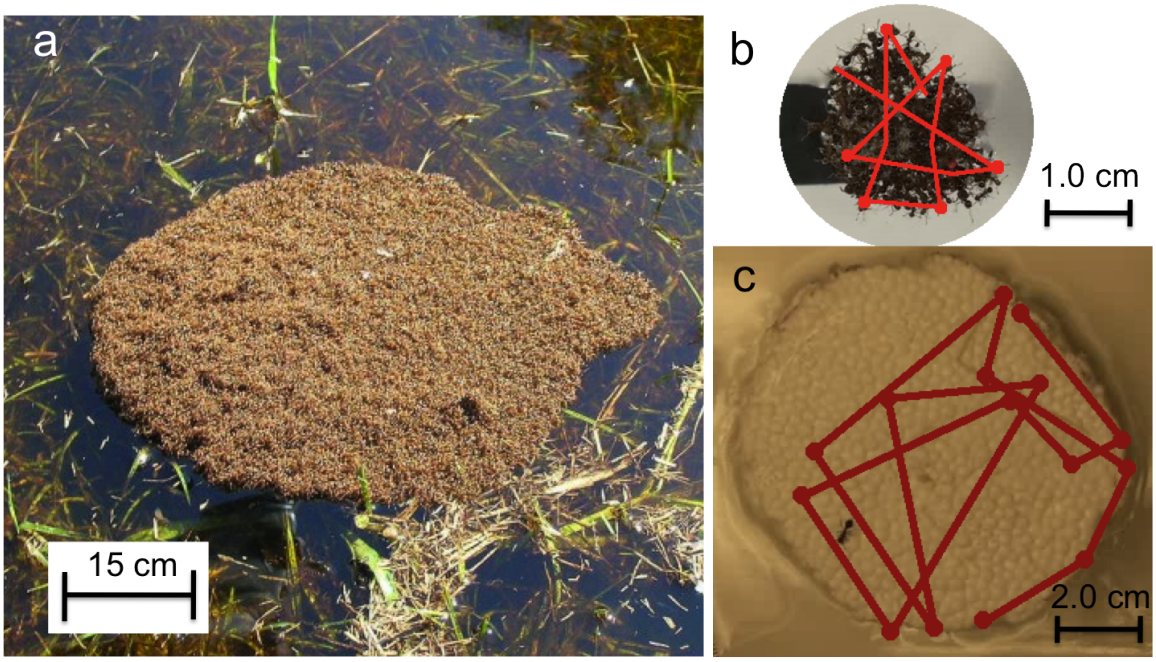

Figure 7: Ant rafts (a & b) and a styrofoam raft (c) for measuring ant trajectories. In (b & c), the lines show sample ant trajectories interrupted by the dots indicating turns made by the ant.

3.7.2 Diffusive model

For the purpose of modeling, we idealize the single ant's behavior as choosing a new random direction after traveling a step size s. This behavior is consistent with our previous observations: if the radius r of the raft is less than s, then one would simply observe ants traveling in a straight line until reaching an edge, as was the case of our previous observations. At the other extreme, when r is very large compared to s, this behavior ought to, in the limit, approach Brownian motion.

We had observed previously how clumps of ants behave as a viscoelastic solid as the raft flows from an initially spherical shape to form a pancake. We see that their diffusive motion is also consist with this view of ants as a fluid. Using the measured step size s and walking speed v, we can roughly estimate a diffusion coefficient D for ants, given by vs, to be 1.6 cm^2/s. For some comparison, D is largest in gases (10^3 cm^2/s), intermediate (0.01 cm^2/s) in liquids and smallest in solids (10^{-7} cm^2/s). This hierarchy is due to the kinetic energy of the respective phases and their inter-atomic spacing. Larger values of D means the molecules spread out at higher rates. Our diffusion coefficient for rafting ants falls in between those of gases and liquids.

In Brownian motion, the expected time to reach the boundary of a disc of radius r from the center is proportional to r^2 [90]. The *effective velocity* u of an ant is therefore proportional to $\frac{r}{r^2} = \frac{1}{r}$. The effective velocity also ought to be proportional to v, by scaling reasoning. Moreover, the effective velocity ought to be proportional to the step size s, again by scaling reasoning. This is because if one took k steps of size s, then irrespective of the direction in which each step is taken, one would end up exactly s times as far away as if one had taken the same k steps of size 1. Hence the effective velocity of an ant, when r is large, should be $\frac{vs}{r}$. Combining these two cases, we may write the ant's effective velocity u as a function of the raft size:

$$u(r) = \begin{cases} v & \text{if } r \leq s \\ \frac{vs}{r} & \text{if } r \geq s. \end{cases} \tag{3}$$

Note that the effective velocity $u(r)$ is a continuous function of r and is consistent with ant-trajectory observations in both **Fig.7**b-c.

We note the formula $\frac{vs}{r}$ for the ant's effective velocity is also at least fairly accurate for intermediate values of r. Approximate the circle as a square, and ant motion as random vertical and horizontal steps of length s. The expected number of horizontal steps to reach a boundary equals the expected number of steps a simple one-dimensional random walk takes to get $\frac{r}{s}$ steps to the left or right of its starting location, which is well known to equal $(\frac{r}{s})^2$ [96]. The total time for the horizontal motion to reach a boundary is therefore r^2/sv. Hence the effective speed is $\frac{r}{r^2/sv} = \frac{vs}{r}$. Vertical motion behaves identically. Neglecting constant factors, then, the effective speed is again $\frac{vs}{r}$, as found previously.

Using this effective speed given in Eq. (3), we re-formulate our previous model. Our modified differential equation to predict the rate of growth of the ant raft is defined in terms of four regimes as follows:

$$\frac{dn}{dt} = \begin{cases} \beta\sqrt{n(t)} & \text{if } r(t) \leq s \text{ and } n(t) \leq N/(h+1), \quad RegimeA \\ s\beta\sqrt{\gamma\pi} = \frac{sv\gamma\pi}{\alpha h} = 21.5 & \text{if } r(t) \geq s \text{ and } n(t) \leq N/(h+1), \quad RegimeB \\ s\beta\sqrt{\gamma\pi}(N/n(t) - h) & \text{if } r(t) \geq s \text{ and } n(t) \geq N/(h+1), \quad RegimeC \\ \beta(N - hn(t))/\sqrt{n(t)} & \text{if } r(t) \leq s \text{ and } n(t) \geq N/(h+1), \quad RegimeD, \end{cases} \tag{4}$$

where $n(t)$ is the number of ants on the bottom surface of the raft and t is in seconds. This model involves a number of parameters, measured from experiment, that are previously defined and are reiterated here. The initial condition for the equation can be found using N, the total number of ants forming the raft, which sets the number of ants on the bottom when the ant raft begins as a sphere. The local parameters include the following: h=2.5, the eventual thickness of raft in terms of number of ants; α= 3.1, the average number of circle radii traveled by a straight-line motion ant until sticking to circle boundary; $\gamma = 34$, the ant

density in an ant layer in ants per cm^2; $v = 0.39$, the speed of an ant's straight motion in cm/sec; and the fraction $\beta = \frac{v\sqrt{\gamma\pi}}{\alpha h} \approx 0.52$ sec^{-1}. We use the following expression converting raft radius to an equivalent number of ants on the bottom layer: $r(t) = \sqrt{n(t)/\gamma\pi}$, where the radius of the raft at time t is in cm. Finally, in Eq. (3) we use the parameter s=4 for the ant step size in cm. An ant's idealized motion is to change direction randomly every s centimeters unless a boundary is reached first.

3.7.3 Comparison to straight-path model

We use a first-order scheme to numerically integrate our governing equation for dn/dt given in Eq. (4), incorporating the effective velocity given in Eq. (3). In this section we report results of this new diffusive model to our previous straight-path model.

Previously, [17] we limited N to 10,000 ants. We now present new results for experiments with larger ant rafts of N=15,000 and 22,500. **Fig.8**a-d shows the time course of the number of ants n on the bottom of the raft for various sizes of raft as indicated. Experiments are denoted by the open symbols, and associated predictions from theory are given by the solid line (diffusive model) and dashed line (straight-path model). Both models are a good fit for short times ($t \leq 50$ seconds) when r is small, as expected. For instance, for the intermediate-sized raft of $N = 6{,}000$ ants in **Fig.8**a, the results for both models are nearly indistinguishable. This is because these rafts are small enough ($r \approx s$) that the diffusive behavior in Eq. (3) doesn't take effect until the raft is almost complete.

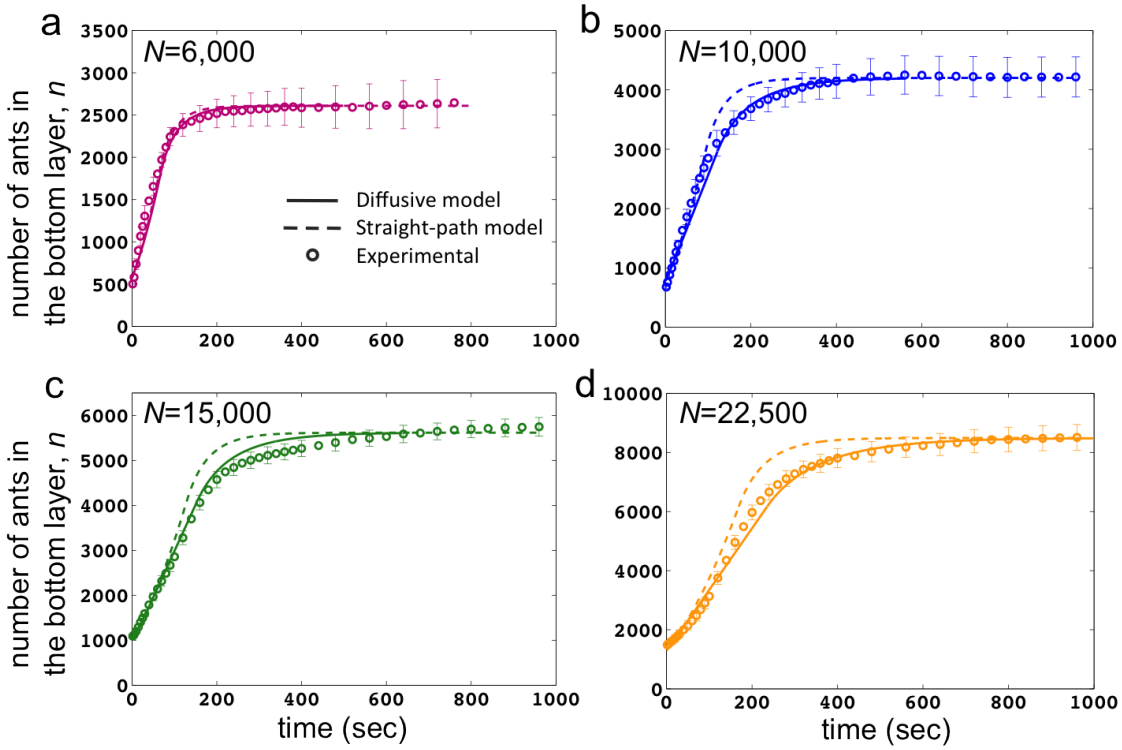

Figure 8: The growth of ant rafts N=6000, 10000, 15000, and 22500. The vertical axis is n, the number of ant on the bottom layer. The floating ant ball spreads out on the water's surface and reaches an equilibrium size. The plots compare experimental findings to both our previous straight-path only model and our new model that incorporates a Brownian element, accounting for the diffusive nature of ant motion. The diffusive element is triggered when the radius of the raft reaches a critical size. For large N, the diffusive model is clearly a better fit than the straight-path only model.

For larger N, the discrepancy between the models is more apparent, with the diffusive model providing a better fit for the experimental results (**Fig.8**a-d). The raft of size N = 22,500 ants (**Fig.8**d) is a good example of a clear deviation between the two models. While our previous model failed to accurately predict the growth rates for very large rafts, our new results show that the diffusive element of our new model accurately captures the dynamics of the larger raft. Specifically, the straight-path model over-predicts the construction rate in **Fig.8**d, as shown by the higher rate of growth between 100-250 seconds. In contrast, the diffusive model shows a raft growth rate that is slower and more consistent with the experiments. This difference occurs because the new model increases the time for the ants to reach the edge of the raft.

By using a range of values for the step size s in our diffusive model, we find that the raft growth rate is highly sensitive to step size. **Fig.9** shows the time course of the number of ants on the bottom of the raft for a series of values of s = 2, 4, and 10 cm. As s approaches the final raft radius (the solid purple line signifying s = 10), the diffusive model approaches

the straight-path model (the dashed black line). A large step size means that the ants do not change direction until reaching the raft's edge, thus exhibiting the same behavior as in our straight-path model. Also, as s approaches zero (solid orange line signifying $s = 2$), the ant behavior becomes purely diffusive and raft construction time approaches infinity. Cases $s = 2$ and $s = 10$ shown in **Fig.9** demonstrate the high sensitivity of the model to step size, highlighting the importance of measuring step size accurately. The s value of 4 cm found in our experiments (solid red line) yields diffusive model results that match closely to our experimental results (red circles).

We now comment on the significance of the four regimes given in Eq. (4). We use as an example the model predictions given by the red solid line in **Fig.9**, the diffusive model with $s = 4$. Here, *Regime A* is the same as the original model, but it only lasts while the raft radius $r(t)$ is less than the step size s, or $n(t)/\gamma\pi = n(t)/34\pi = n(t)$ cm^2 / 107 $\leq$ 16 cm^2, or $n(t) \leq 1,710$ ants. For very large rafts, $N >$ 35,000 ants, *Regime A* does not occur at all because the initial sphere of ants is so large that $r(t = 0) > s$. In **Fig.9**, *Regime A* occurs during time 0 to approximately 40 seconds. *Regime B* has linear growth of $n(t)$. This can be seen in **Fig.9** in the time interval approximately $[40, 105]$ seconds, where the experimental data fits this linear growth very well. During *Regime C*, $n(t)$ grows at a decreasing rate, approaching a growth rate of 0 as $n(t)$ approaches N/h. *Regime D* does not occur at all unless $N/(h + 1) \leq n(t) \leq s^2\gamma\pi = 1,710$ ants, which is impossible for $N > (h + 1)s^2\gamma\pi$ =3.5 (16cm^2)(34 ants/cm^2)π =6,000 ants. Since $n(t)$ never exceeds $N/h = N/2.5$ (i.e., $2.5n(t) \leq N$) and the new model doesn't kick in unless $n(t)$ >1,710 ants, the new model never takes effect unless $N > 2.5(1,710) \approx 4,300$ ants.

In summary, for $N \leq 4,300$ our new model behaves exactly like the straight-path model of our previous paper, transitioning directly from *Regime A* to *Regime D*, where the four regimes are listed in Eq. (4). For 35,000$\geq N \geq$ 6,000 our new model behaves like *Regime A*, as in the straight-path model, for a short time period, and then progresses to the linear growth of *Regime B*, ending with *Regime C*. For $N > 35,000$ our new model begins immediately with the linear growth of *Regime B*, ending with *Regime C*. For the narrow range 4,300$\leq N \leq$ 6,000 our new model progresses from *Regime A* to *Regime D* to *Regime C*.

In our derivation of the regimes of validity, we use an approximation that does not appear to affect the accuracy of our model substantially (as shown in **Fig.9**), but is worth noting here. Although *Regimes B* and *C* don't kick in until $r \geq s$, it is more complicated than a simple switch at $r = s$. Instead it is a gradual shift between regimes. The point at which $r = s$ is roughly in the middle of the shift. The beginning of the shift is at $2r = s$, which is the smallest diameter at which the ant might change direction, but occurs zero percent of the time. As r increases and approaches s the probability of random direction changes will increase. At $r = s$, a direction change occurs 2/3 of the time after bouncing off a boundary, but less than 1/2 and more than 1/3 of the time when starting at a random

point on the raft surface, yielding slightly more than a 1/2 probability that an ant will change direction. Therefore, $r \gg s$ marks the end of the shift, but even when $r \gg s$, there will still be a few short moves that hit a boundary before the travel distance reaches s.

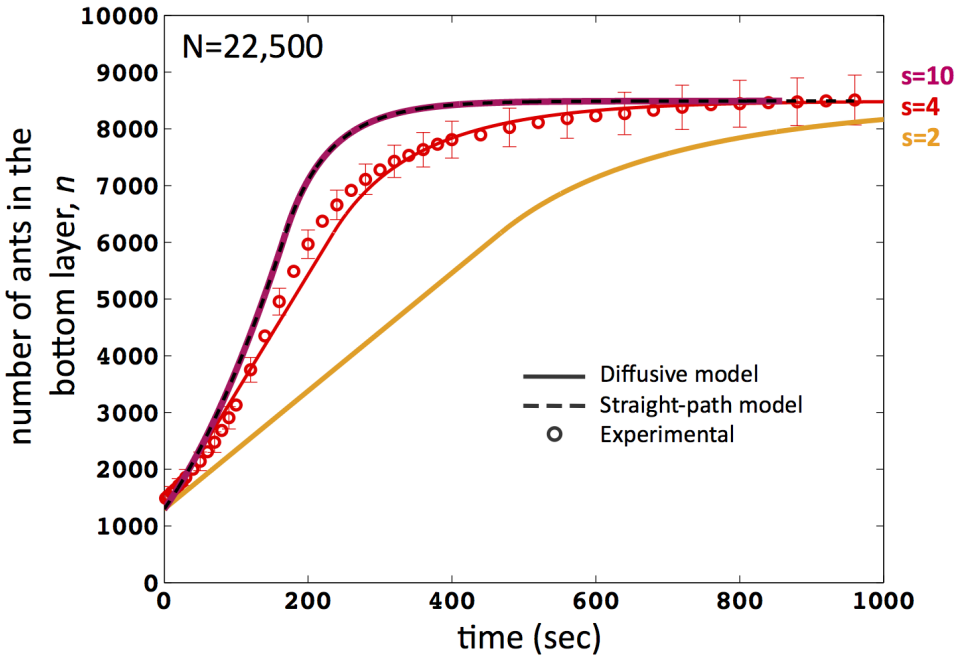

Figure 9: Time course for the number n of ants on the raft bottom for a raft $N = 10{,}000$ ants. Solid lines are the diffusive model for various values of ant step size s. The plot for $s = 10$ is consistent with the straight-path (dashed line) model since an ant won't change direction before reaching an edge. The value $s = 2$ shows longer construction times for the raft since the ants must make many direction changes before reaching an edge. The value $s = 4$, found experimentally, yields model results that are consistent with our experimental findings and are also clearly a better fit than the straight-path only model.

3.7.4 Raft circularity

It has been established [97] that when N random elements starting at the origin of a two-dimensional grid each in turn performs a simple random walk until reaching an unoccupied site, the set of occupied sites will form a disc whose circularity approaches perfection with probability 1 as N approaches ∞. The behavior of ants on large rafts can be idealized in this manner for analyzing the raft's shape. We expect that as the number of ants in the raft N increases, the equilibrium profile shape will become more circular. To measure the raft's deviation from circular, top view images of rafts (size $N = 5$, 10, 50, 100, 1000, 5000,

and 10000) at equilibrium (**Fig.10**a) are processed using Matlab to find an ellipse which best fits the raft profile. We define eccentricity of the ellipse as $e = 1 - \frac{min}{maj}$, where min and maj are the lengths of the minor and major axes of the ellipse respectively. An e value of 0 indicates a perfect circle where $min = maj$. The e values for the raft profiles are plotted against $\log N$ revealing a declining trend in e as expected (**Fig.10**c). These results show that the raft is indeed nearly circular and approaches that limit as N approaches infinity.

Asymptotic formulae for circularity are known, [97] but to compare actual ant raft shapes to the random walk growth model around an origin for moderate values of N, it is necessary to run our own simulation. A single 1x1 element rests at an origin (0,0). Each iteration, another element starts at the origin and follows a random walk of unit steps until it reaches an unoccupied site. For the first element added, this would be either (1,0), (0,1), (-1,0), or (0,-1). The second element to be added then starts at the origin and performs the random walk on this new two element shape. This continues until the number of elements reaches N. We ran this simulation 20 times each for $N = 10$, 50, 100, 1000, 5000, and 10000. Select images of the shapes formed are shown in **Fig.10**b. **Fig.10**c plots the average eccentricity value against $\log N$. Before plotting, values of N from 50 through 10,000 for the simulation were multiplied by 2.5 for comparison to our experimental findings. This was done because all elements in a simulation form a single layer, but real ants form a raft 2.5 layers thick. This means that a simulation of N elements corresponds to a raft of $2.5N$ real ants. The value $N = 10$ was not multiplied by 2.5 because a raft of only 10 ants forms a single layer.

The simulation follows the experimental data very closely. The closeness of this fit supports our hypothesis that the individual ant random movements cause the circular shape of the ant raft. If circularity were due to some other cause, it seems unlikely that the relationship between raft size and raft circularity would be the same.

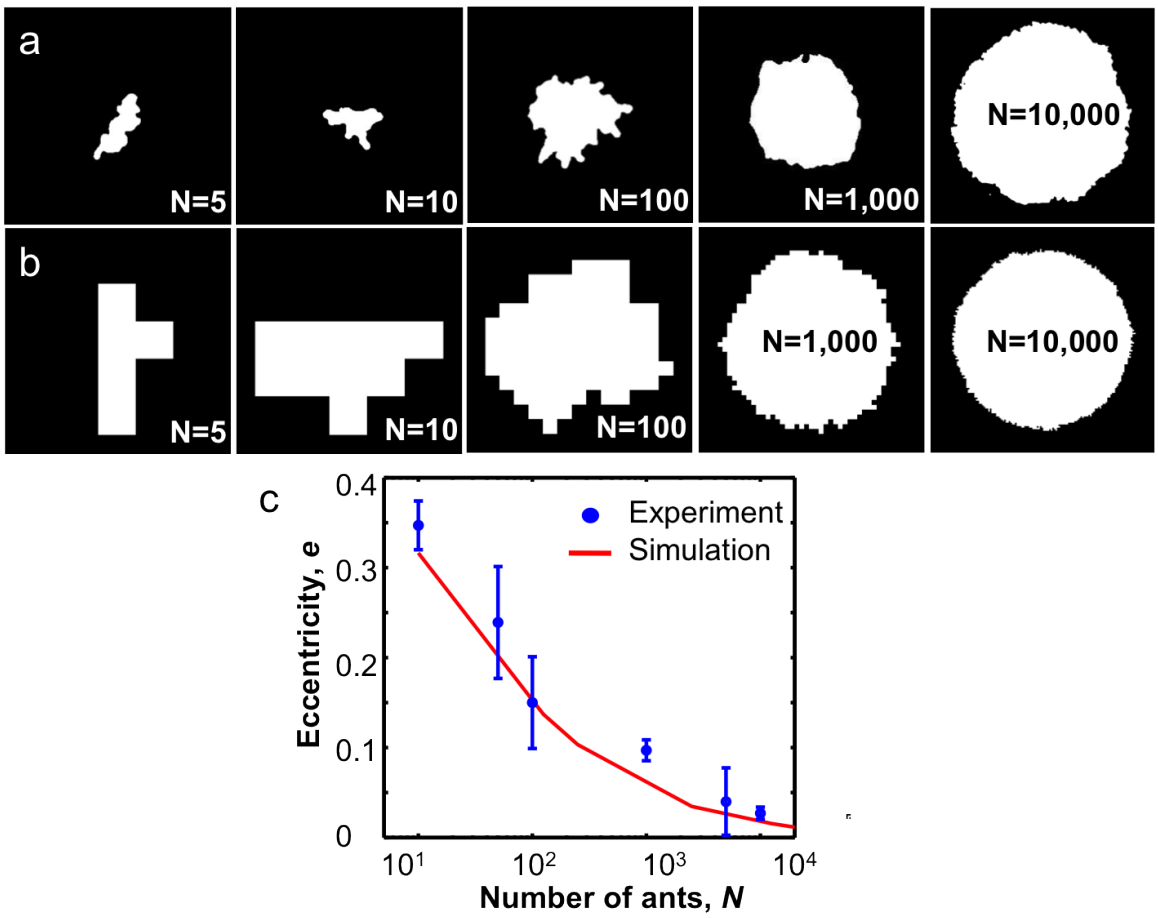

Figure 10: (a) Selection of raft profiles at equilibrium (b) Sample profiles from our simulation that randomly adds individuals to the edges. (c) Plot comparing the eccentricities for experimental rafts and average values of simulation data.

3.7.5 Discussion on large rafts

The two main contributions of this work are the following: *1)* We improve the accuracy of our previous model's assumptions of individual behavior, and thereby improve the accuracy of the model's predictions for larger rafts without sacrificing accuracy for smaller ones. We verify this through a comparison to new data gathered from observing large rafts, the results of which clearly show the new model's improvement. *2)* Through describing the behavior of an individual ant within the raft with a few simple rules, we show that ants can build circular rafts despite the inability of individuals to perceive the overall shape of the raft. Our numerical simulation of this phenomenon predicts a pattern of greater circularity as the raft size increases, a pattern that closely matches our experimental data.

Our earlier model of rafting fire ant motion [17] described their individual behavior as strictly straight-line motion combined with a bounce probability function to describe raft edge conditions. Our current model uses a Brownian element based on new observations

of the step size s of ants ants moving diffusively on large rafts. Using an s value from experiments yields relaxation times in the model which more accurately reflect those found in experiments. We have also presented the time-regimes of validity of our new model in Eq. (4), which are based on the initial size of the raft with respect to s. Our previous model also made an implicit assumption of raft circularity. Our new simulations based on a random walk from an origin provide an explanation for the circular raft shapes we observe. The close fit between the shape simulations and the actual raft shape supports the validity of our explanation.

Incorporating a Brownian element is more in line with previous work on animal behavior. In previous literature, diffusion models have shown broad applicability to modeling animal motions such as the swarming behavior of insects. Specifically Harkness developed a model that incorporates both straight-line and diffusive elements to describe the foraging behavior of ants. [22] Others such as Schweitzer and Theraulaz both suggest a diffusive mechanism behind the ant's walking patterns. [98, 99] Helland discusses the effectiveness of diffusion models for the dispersion of insect populations attracted towards a point. [23] Such diffusive behaviors are especially important when the number of agents, be they ants or robots, is very large, as in the case of ant rafts, which can exceed 100,000.

We have observed fire ants in a raft moving in random directions interspersed by a distance s. Rather than systematic searching, ants typically employ random search strategies. [100] This allows moving to be optimized so as to increase their chances of locating resources by increasing the chances of covering certain regions. The optimal solution often arises by merely carrying out a random-walk search strategy. [100] In the case of rafting, the step size may be a behavior originally adapted for moving on land.

The diffusive behavior observed sheds light on Detrain's claim that ants are not simply "behaving like molecules," but rather are acting upon the complex and changing parameters of their surroundings based on response thresholds. [101] Studies have shown that ants can collectively "make decisions," demonstrating capabilities far beyond simple molecules. [102, 103] Conversely, our research reveals that when ants form self-assemblages, such as the floating raft, they begin to exhibit behavior similar to the diffusive nature of some molecules. Moreover, a short set of behavior rules is sufficient to predict their group motion. These results suggest that in times of emergency, such as rapid raft construction, ants do in fact behave like molecules to some extent.

There are a number of other factors that likely could have an effect on rafting dynamics. Chemical signals have been shown to affect a colony's exploration of new space through recruitment. [95] The rate of antennal contact is a way for ants to measure raft-mate density. [104] The presence of queen and brood in a raft, such as occurs in nature, affects the worker distribution of ants within a raft. A heightened defensiveness while rafting will cause behavioral changes in the ants. [64]

The above factors, as well as the position of ambient lights, may affect raft equilibrium shape in natural settings. Also, a floating or partially submerged object such as grass or twigs (as in **Fig.7**a) appears to strongly affect the shape of the portion of the raft adjacent to the object. We also have observed the raft forming "appendages" that seem to be reaching out towards nearby land masses as an attempt to dock the raft.

The model we have presented omits these factors. In particular, it omits chemical signaling and antennal contact, which occur in both natural and laboratory settings. Yet, it provides an accurate representation of the growth rate and shape of large and small ant rafts in laboratory settings. This suggests that we have identified the critical elements of the individual ant behaviors that result in the observed raft formation.

CHAPTER IV

THE ANT ASSEMBLAGE STRUCTURE

4.1 Introduction

Ants and bees link their bodies together to build self-assemblages such as curtains, rafts, bridges and bivouacs [15, 32, 105]. Such assemblages perform functions similar to their counterparts in human architecture, but are built and maintained in a completely different manner. Self-assemblages can react to their environments, self-heal under environmental damage, and self-assemble using interchangeable parts without central control. Understanding how such structures are built may inspire similar feats with modular robotics and other synthetic materials [46].

The most significant barrier in characterizing self-assemblages is their opacity, which makes it impossible to measure the arrangement and connectivity of the network with the naked eye. Network properties such as connectivity have significant implications on the structure's strength, buoyancy, and rate of construction, which in turn directly affect the survivability of the colony. In this investigation, we employ micro-computed tomography (micro CT) and scanning electron microscopy (SEM) to elucidate the network structure of a fire ant self-assemblage.

In 2002, Anderson *et al* coined the term self-assemblage[32] for assemblies in which an individual is the building block for a variety of adaptable colony configurations. Such assemblages are often observed in a static state: individuals on the outside of the assemblages grip one another with legs or mandibles and remain in position until a specific task or goal is reached [11, 32, 106]. Colonies of fire ants can easily be observed building self-assemblages, such as a raft (**Fig.11**a), bivouac (**Fig.11**c), hanging column (**Fig.11**b), and an escape droplet and tower (**Fig.11**d, e). The dynamics of formation of the escape drop and the ant raft has been studied with great detail [17, 21, 107], and we now understand how the motion of ants within these structures leads to their distribution of sizes and shapes.

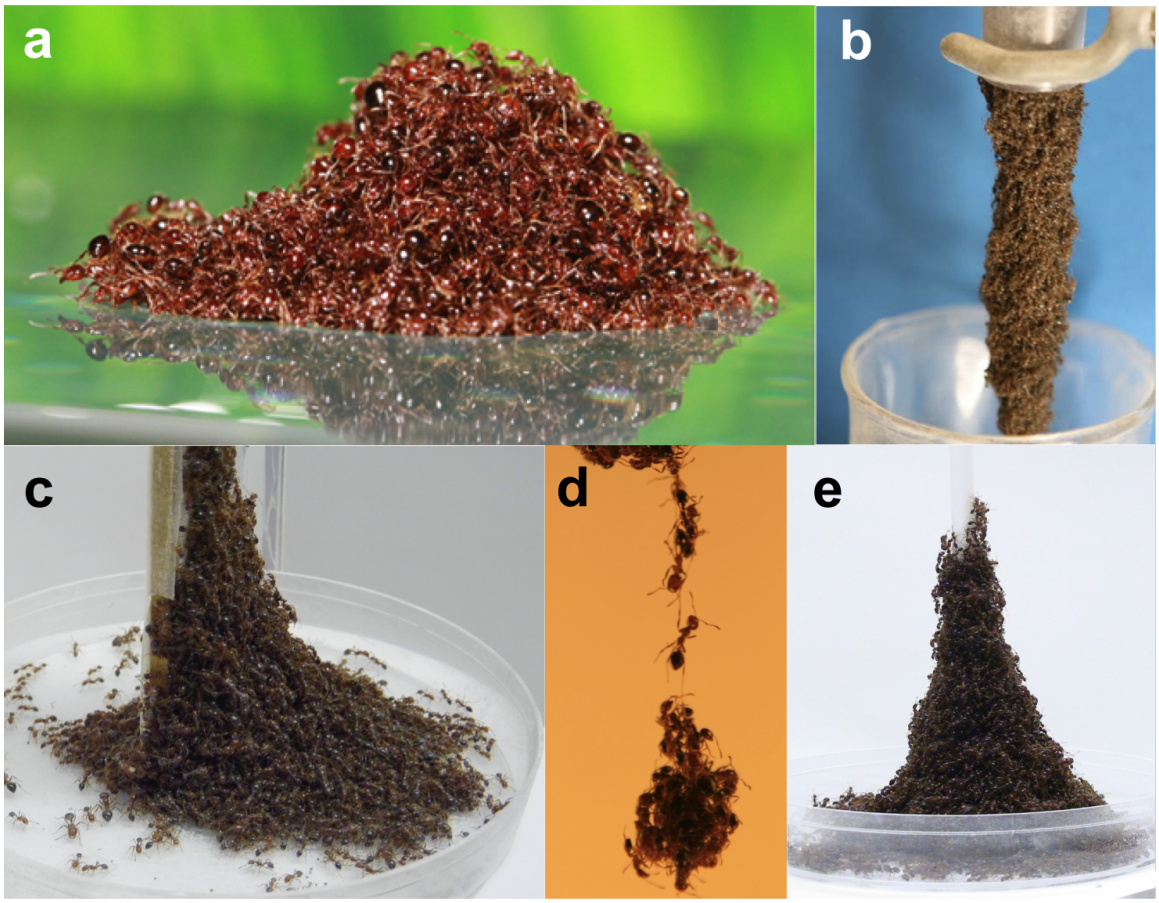

Figure 11: Ant self-assemblages: (a) raft, (b) hanging column, (c) bivouac, (d) escape droplet, and (e) escape tower.

The physical properties of ant assemblages has received very little attention. Indeed, in his review on self-assemblages, Anderson states "virtually nothing is known regarding the . . . *physical constraints* these structures are under; these are the most important avenues for future research" [32]. Mlot *et al* found that ant rafts have a variety of properties making them appropriate for seafaring [17]. They are hydrophobic, a property used to keep bottom of the raft dry when the raft floats. They are buoyant, by virtue of their density of one-fifth that of water, which elicits a sizable restoring force if the raft is submerged. Mlot *et al* also provided measurements of the strength and speed by which ant rafts are built. Ants can grip one another with a force of 400 times their own weight. Despite the great strength holding the raft together, rafts can be built rather quickly: thousands of ants are able to rearrange themselves from a ball of ants to a two-layer stable raft in only 200 seconds. In this study, we will provide micro-structural context for how these attractive properties are maintained, giving us a view of the ant assemblages across scale.

In studying the network structure of the ants, it is useful to view the aggregation as an active granular system. A theory of active granular system, one which particles can sense

their surroundings and adjust their bodies accordingly, currently does not exist. An active area of research is the study of inert granular particles, examples of which include sand, nuts, or medical pills. Such granular materials are the second-most manipulated material in industry, and have attracted attention because they can appear both as liquids and solids. This phase-change behavior is the focus of many experimental and computational studies to understand bulk properties [108]. We review here the studies most amenable to comparisons with ants.

In our study, we will compare the actively constructed aggregations of ants to several control groups of granular particles. The first group is an aggregation of dead ants, which shows how ants would pack if they were not actively seeking connections with their legs. The second group is an aggregation of cylinders of the same aspect ratio α as the ants, giving insight into how ants would pack if ants had no legs. This latter system also falls under the class of prolate granular particles, which has beens studied by several investigators. Franklin and Desmond showed that elongate particles, such as nails, cohere together into solids if their aspect ratio α is sufficiently high [109]. Blouwolff and Fraden measured the distribution of the contact number c for randomly packed cylinders [110]; in § 4.3.2, we compare these values to those exhibited by ants. Experimental limitations have motivated the use of simulations to predict critical packing parameters. Zhao et al simulated spherocylinder packings varying aspect ratio α and observed the effects on packing fraction ϕ and contact number c [111]. These studies, whose results are re-printed in § 4.3.1, will provide insight into how ants improve their packing properties using both behavior and their geometry.

This study also may shed light into the ability of biological systems to entangle. Entanglement is the ability of convex particles to interpenetrate one another and act cohesively. Gravish *et al* studied packings of staples, also known as geometrically entangled u-shaped particles [1]. They elicited a phase transition in a plug of entangled staples from solid to liquid to gas by vibrating the plug, finding that staple barb length is a key parameter for determining activation energy for such a transition. Similar to staple barbs, ant legs penetrate the spaces around neighboring ants to increase connectivity. Also, like staple barbs, ant legs can occlude neighboring ants from filling nearby space, having the effect of reducing packing fraction relative to staples without their barbs.

In this study, we identify the key principles ants use to maintain favorable packing properties. We begin in § 4.2 by presenting a new methodology for generating 3-D renderings of the self-assemblage and extracting quantitative data on the network of ants. Next in § 4.3 we discuss our findings on ant connectivity, packing fraction, spacing, and orientation within an assemblage. In § 4.4 we contextualize our results and discuss the implications of our findings, and summarize our work in § 4.5.

4.2 Methods

Here we present our methods for ant husbandry, sample preparation, and imaging using both scanning electron microscopy and computed tomography scanning.

Ant husbandry. Three ant colonies are procured from roadsides near Atlanta, Georgia during the summer of 2011. In selecting colonies, we aim for an average ant weight of 1.5 mg by looking at average ant size. Colonies are removed from the soil, placed into bins, and cared for according to our previous methods [17], and are fed crickets and water three times a week.

SEM imaging. A small group of about 15 live ants are confined to a petri dish. We swirl the dish to link the ants together into a cluster against the side of the dish. The cluster is then quickly flash frozen with liquid nitrogen before it can disassemble, then gold-sputtered using a Cressington Sputter Coater 108 and examined for intact connections using a Phenom G2 Pro Scanning Electron Microscope.

Freezing ants. We scan two types of ant samples, *live* and *dead*.

The schematic in **Fig.12** demonstrates our methods for preparing *live* ant samples. In such a sample, all leg connections result from ants reaching out and linking to one another. To prepare the *live* samples, we flash freeze a small self-assemblage using liquid nitrogen. This kills the insects instantly, but doesn't harm the network structure, preserving connections between ant legs and relative ant positions. The frozen sample is then lightly coated with cyanoacrylate vapor by boiling ethyl cyanoacrylate beneath the sample. This prevents motion in the sample due to thawing, which can produce noisy images during the hour-long scanning process.

A *dead* sample refers to a random arrangement of recently frozen individual ants. In dead samples, contacts result from dead ants laying next to one another. Ants are allowed to walk freely in a 13 cm x 13 cm container. The ants are flash frozen, and allowed to thaw completely for 20 minutes. Any incidentally connected ants are carefully separated, before all the ants are placed into a CT scanning tube. The tube is shaken, allowing ant bodies to settle randomly. Dead ant samples do not need to be coated with cyanoacrylate vapor because they are already thawed and will not more during scanning. We then scan and limit time between freezing and scanning to 3 hours to prevent desiccation and subsequent deforming of bodies.

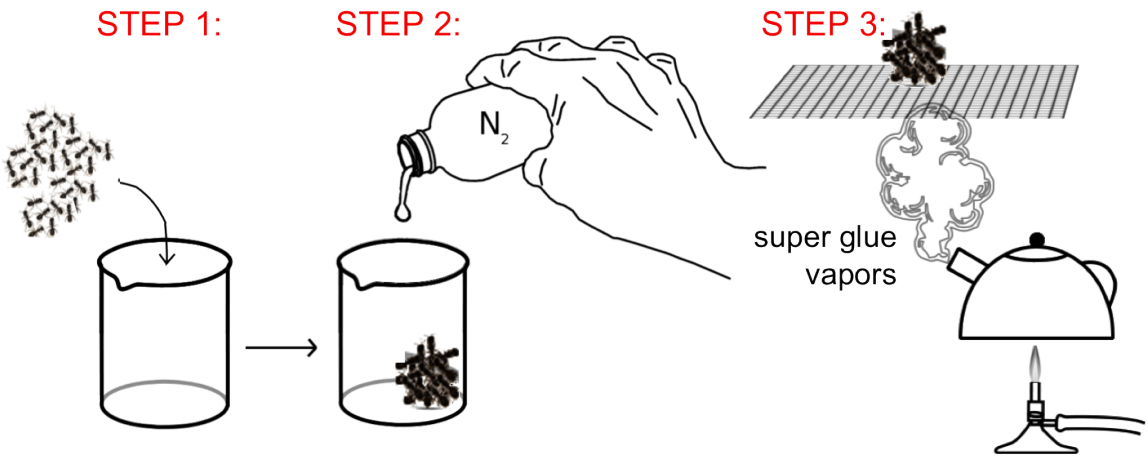

Figure 12: Method schematic to prepare ant samples for scanning. Step one: collect ants in a beaker and allow ants to group together. Step two: freeze ants with liquid nitrogen. Step three: preserve structure for scanning by coating with cyanoacrylate vapor.

CT scanning. Once the samples are prepared, both live and dead ants are scanned in the same fashion. Ant counts are made first by weighing; the counts are later verified using analysis of our CT-scans. A sample is placed in a 14-mm diameter tube and scanned using a Scanco μCT 50 CT-scan machine with 7 μm voxel size, 14 mm FOV, 2048 x 2048 pixel matrix, $E = 55$ kVp, and $I = 200\,\mu$A. Greyscale slice tomograms were converted to dicom format for further segmentation and image processing. Our CT-scans produce thousands of images each representing a thin horizontal slice 7 μm thick as shown in **Fig.13**a. These scans are digitally stacked to produce a 3-D rendering of the assemblage.

Image processing. For all data processing we use custom-written MATLAB algorithms designed to gather from the CT Scan files the number of connected neighbors, connections per ant, packing fraction, orientation, and neighbor spacing. These algorithms work by labeling ant bodies and appendages in the CT scan. Due to the noise in the data, we generally find that some mistakes remain after labeling, so the labels are hand reviewed and corrected before calculating statistics. More details on the algorithms used can be found in Appendix C.

4.3 Results

We begin by presenting CT-scan renderings and our characterization of the 3-D network structure. Particular attention is paid to the connections, spacing and relative orientation between neighbors. We follow by providing insight into the benefits of polymorphism in increasing network connectivity.

We employ methods of CT scanning to characterize the 3-D network across large numbers of ants. In this part of the study, we consider four live samples each containing 110

ants, for a total of n_{live}=440 ants We also consider 2 dead samples, each with 110 ants, for a total of n_{dead}=220 ants. **Fig.13**b is a representative rendering of 30 large ants illustrating the resolution obtainable through this method. In supplementary movie *antmoviesides.mov* we simultaneously pan through the CT scan cross-sections and the resulting 3-D rendering. A typical scan comprises over 100 ants, and over 600 legs which obscure viewing the image. To more easily visualize the ant bodies for image processing, we use MATLAB to digitally remove ant legs. **Fig.13**c shows a rendering of ants with legs removed, and color assignments to improve visualization of the arrangement and orientation of ants in an assemblage.

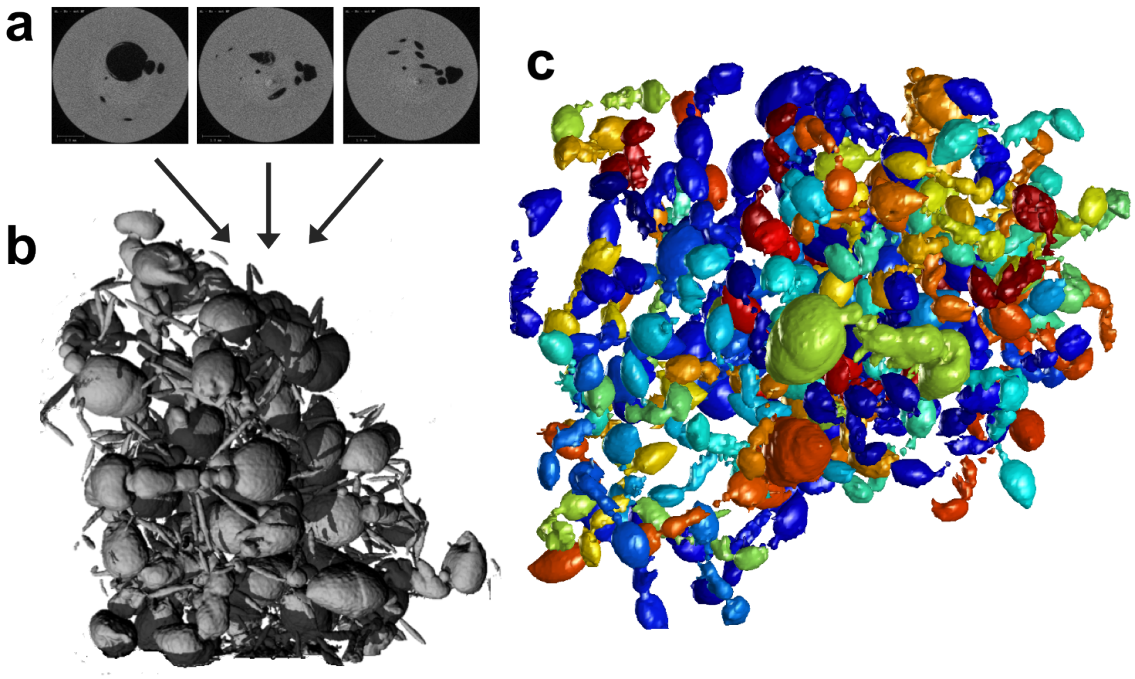

Figure 13: (a) Ant samples are scanned with a micro-computed tomography scanner producing thousands of 2-D image layers. (b) These layers are stacked digitally to create 3-D renderings of the connected ant network. For this particular image of an ant assemblage, we isolated 30 of the largest ants in a colony. (c) In another sample, ant legs are digitally removed to leave only ant bodies that are then colored to create an image that is easier to process visually.

4.3.1 Ants maintaing spacing using active pushing of their legs

The spacing between ants is an important characteristic that determines the weight of the assemblage, its porosity, buoyancy and water-repellency. The more lightweight a structure, the taller it can be built and the more easily it can be buoyed up to the water surface if submerged. We report nearest neighbor distance and packing fraction, two parameters that vary inversely with one another and give both local and bulk views of spacing between ants.

Consider an ant A_i within an assemblage, shown in **Fig.14**. Its neighbors consist of all ants who share a connection with A_i by a linkage. This linkage may be either a mandible, or an outgoing or incoming leg. We define nearest neighbor distance NND_1 as the distance between neighboring ant centroids. Live ants have a nearest neighbor distance $\mathrm{NND}_{1,\,avg} = 0.99 \pm 0.25$ mm, which is within 0.001mm of the corresponding value for dead ants. This is a surprising result as we would expect live ants to use their legs to increase distance between their neighbors. However, ant legs have a limited range of motion because of the joint angular range and their attachment at certain positions on the lateral side of the body. Consequently, they are unable to push away the nearest neighbor.

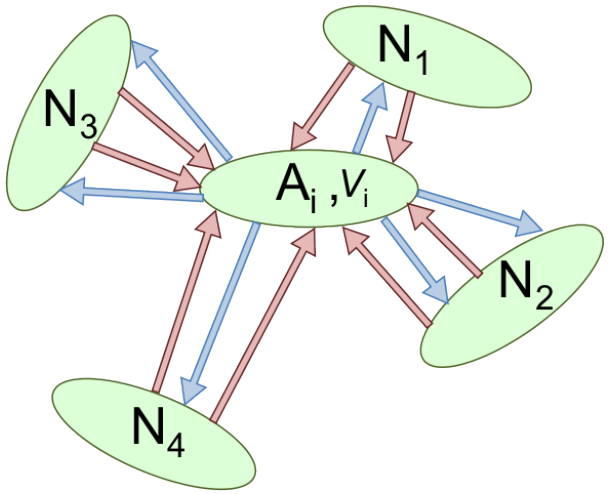

Figure 14: Schematic showing the connections of the ith ant A_i with volume V_i. Volume containing the ants is V_{total}. Each of the ant's 6 legs counts as outgoing connections, shown by the blue arrows. Incoming legs, shown by red arrows, originate from neighboring ants N_j and terminate on ant A_i. On average, each ant sees 8.3 incoming connections, for a total connectivity c_{total} of 14.3.

The active behavior of ants is however manifested in the second through fourth nearest neighbors distance (NND_2 - NND_4). The average of nearest neighbor NND_1 through NND_4 for live ants is 1.82 ± 0.31mm, which is 48% larger than for dead ants (1.23 ± 0.26 mm). Although dead ants possess legs, they are unable to use them to make connections with neighbors to keep them at bay, as is done by live ants.

To compare packing of ants to other granular materials, it is useful to discuss packing fraction rather than the equivalent nearest-neighbor distance. We define packing fraction for a sample of ants,

$$\phi = \frac{\sum_{i=1}^{n} V_i}{V_{\mathrm{total}}}\,, \tag{5}$$

where V_i is the volume of the i^{th} ant and the numerator is summed over all n ants in a sample (see **Fig.14**). V_{total} is the container volume, determined by using our software by

dilating the ant ball until 95% of the interior is filled according to the methods provided by Haralick [112].

Live ants, with packing fraction $\phi_{live} = 0.25 \pm 0.1$, are packed 34% less tightly as dead ants, with packing fraction $\phi_{dead} = 0.38 \pm 0.02$, as shown in **Fig.15**. We conclude ants are actively using their legs to increase spacing between one another. We verify this claim by conducting a t-test with resulting p-value ≤ 0.0001.

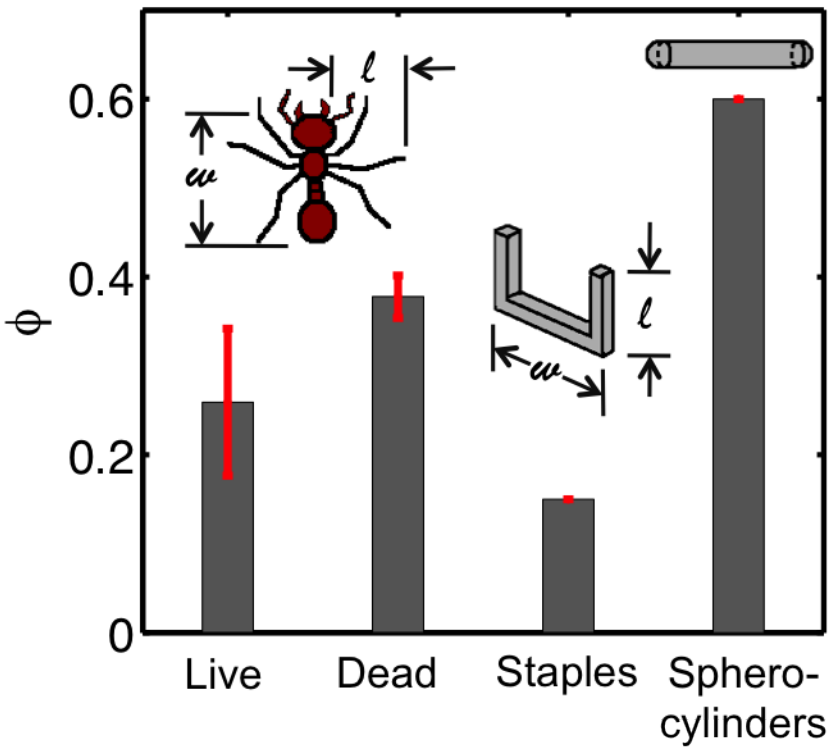

Figure 15: Packing fraction ϕ mean and standard deviation for live and dead ants from this study, staples from Gravish's study [1], and spherocylinders from Wouterse's study [2]. All values are at $\alpha = 4$. Ants halve their packing fraction by using legs to increase nearest neighbor spacing NND.

To measure local variability of packing fraction ϕ within our samples, we digitally divide each sample into 8 parts at the principle planes. This procedure yeilds a total of 32 parts for live samples and 16 for dead samples. We find marked differences in packing fraction range between live and dead samples. Live samples yield local packing fraction ϕ values ranging from 0.12 to 0.37, but we don't find this spread for dead ant samples, whose packing fraction is relatively homogeneous, ranging from 0.37 to 0.4. The spread in live ant samples is likely due in part to large ants pushing harder against neighbors than small ants, resulting in large voids and small voids respectively.

To compare packing of ants to those of other granular particles, we characterize ants

using their body aspect ratio $\alpha = 3.9 \pm 0.17$, defined as the ratio of ant length to head width. We compare ant packing fractions to those of packings of spherocylinders with $\alpha = 4$ [2]. Wouterse's simulations of packing spherocylinder with aspect ratio α=4 yield a packing fraction ϕ of around 0.6, or more than twice that of ants [2]. Thus, particles without legs pack more than twice as densely as live ants. Again, this result shows the effect of ant legs on packing fraction.

Studies of entangled granular particles also provide insight into the mechanism underlying the decreased packing fraction of live ants. Gravish *et al* studied the geometrically-induced cohesion of granular u-shaped particles, or staples [1]. The authors consider a dimensionless number to describe the barbs, a ratio of barb length ℓ to spine length w (shown in **Fig.15**). Despite ants having six legs, the analogous dimensionless number for ants is the ratio of leg length to body length, which is $\ell/w = 0.73$ (shown in **Fig.15**). Staples of this barb length have $\phi = 0.13$, a packing fraction half that of the ants. This disparity occurs primarily because Gravish *et al* considers thin-barbed staples, whose spines are much thinner than ant bodies.

One of the key results of their study is that staples with longer barbs occlude their neighbors, which decreases packing fraction. Specifically, ant-shaped staples with barbs pack at $\phi = 0.13$, half that of staples without barbs ($\phi = 0.28$). This paradigm is also clear in our ant experiments. Specifically, live ants pack at $\phi = 0.25$, more than half the packing fraction ($\phi = 0.6$) of spherocylinders, which can be considered as leg-less ants. From this comparison, we can conclude that ants use their legs to effectively cut their packing fraction in half.

4.3.2 Highly inter-connected networks

Ants can increase the strength of a structure by increasing their connectivity. **Fig.11**c shows a funnel extruding a hanging column of ants with radius 12 mm supporting the weight of thousands of ants. Given an ant mass of 1 mg and a planar packing density of 34 ants/cm^2, we calculate that 150 ants at the exit of the funnel support 2,000 of their neighbors hanging below them, indicating that each of the 150 ants is supporting the weight of 13 of their neighbors. They can remain in this configuration for 10 minutes or more. Such strength is needed in more natural situations as well. For example, consider a floating ant raft docking to a river bank to escape a flooded river; these linked ants are able to withstand being torn apart by the pull of turbulent currents. In this section, we visualize and measure the connectivity of the ant network that allows for such feats of strength.

Fig.16 illustrates the mechanisms whereby ants connect to one another in an assemblage. We employ SEM imaging because its magnification and resolution is much higher than CT-scan, making it useful in ascertaining the types of connections. SEM permits only ants on the surface of a self-aggregation to be observed, limiting the technique to small

sample sizes. Thus, to obtain quantitative data on the connection types, we will later turn to CT-scanning.

Connection is maintained mostly by the tarsal segment of the ant, shown in isolation in **Fig.16**a. Attachment is achieved through dual use of both the claws, clearly seen, and the adhesive pad, visible in **Fig.16**d between the claws. The most common attachment between ants is a tarsal connection seen in **Fig.16**b and **Fig.16**d. Here, the adhesive pad is used to adhere both to smooth ant body parts as well as rough hairy surfaces. A simple experiment illustrates the importance of the adhesive pad relative to the claw in maintaining these connections. Coating ants in talc powder dries out the sticky pad while still permit hooking by claws. Consequently, talc-coated ants can neither climb smooth surfaces nor form self-aggregations, behaviors for which the adhesive pad is needed.

The least common attachment type is the use of mandibles to grasp neighbors as shown in **Fig.16**c. Roughly 1 in 10 ants uses their mandibles to grasp a neighboring ant's leg, accounting for 1 of every 60 connections. Though rare, mandible connections provide high strength many times the force provided by a tarsal connection. In the context of granular materials, active attachment mechanisms such as adhesive pads and mandibles allow for compressive and tensile forces to be applied, providing a larger range of interactions than most granular materials.

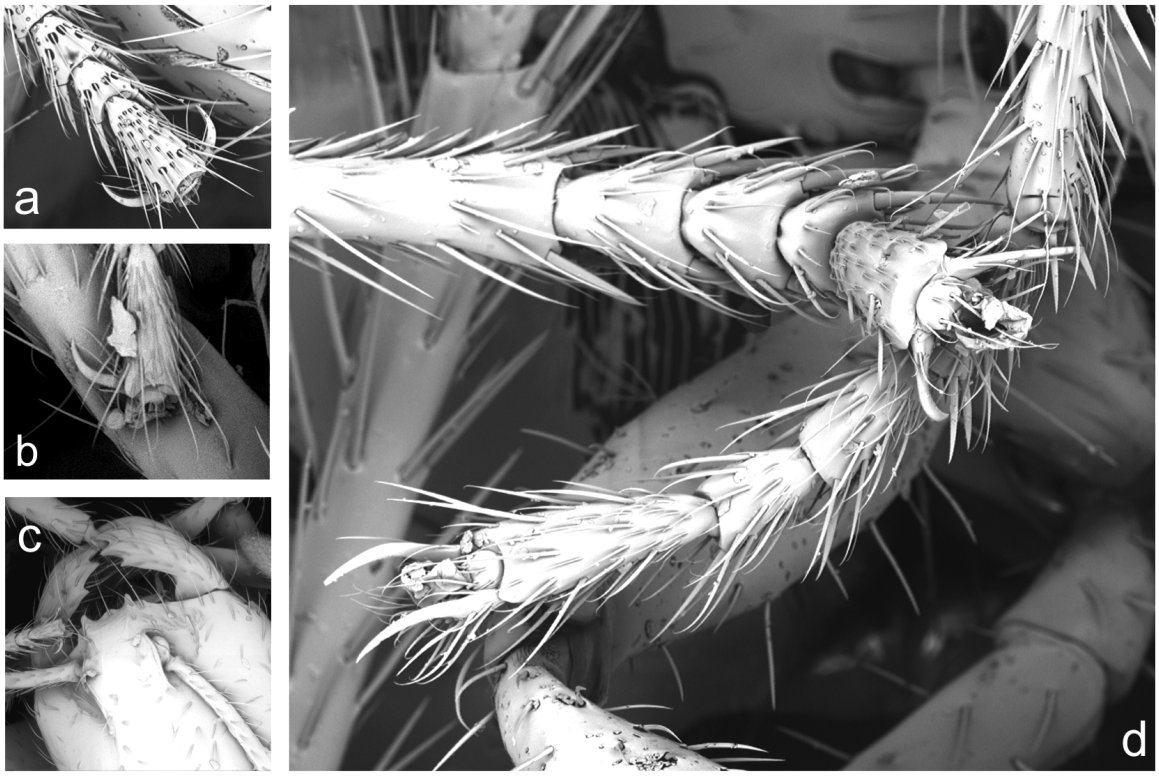

Figure 16: Ants use legs and mandibles to form connections with neighbors. Here we have scanning electron microscopy images of (a) a single ant tarsus, (b) an adhesive pad to leg connection, (c) a mandible to leg connection, and (d) a combination of claw-to-leg and adhesive pad-to-leg connections.

In the context of granular media, connectivity is described by contact number c, defined as the number of neighbors adjoining a particle. For granular packings of most particles such as cylinders, contact results in compressive or frictional forces that support neighboring cylinders. Granular contacts cannot retain tensile stresses, as those achieved by the ant network using tarsal pads. Through simulation, Philipse showed the contact number of packed spherocylinders asymptotically reaches $c = 10$ as aspect ratio α is increased. The expected contact number of spherocylinders for an α matching our ants is 9 [113].

Presenting results for the connectivity of ants will require new definitions because ants have both outgoing connections made by their own six legs and mandibles and incoming connections made by their neighbors' legs and mandibles. Because mandible connections are rare, we neglect them and consider only leg connections, illustrated schematically in **Fig.14**. We define c_{in} and c_{out} to be the number of incoming and outgoing connections, respectively, for a given ant. Their sum c_{total} is equal to the contact number c:

$$c_{\text{out}} + c_{\text{in}} = c_{\text{total}}. \tag{6}$$

Fig.17a and supplementary movie *single ant spin.mov* show views of a single ant digitally isolated from the network. An ant is connected to its neighbors both by its own outgoing legs c_{out} highlighted in blue and incoming legs c_{in} highlighted in red. **Fig.17**b is the distribution of number of neighbors each ant shares, where the term *neighbor* is limited to ants with a structural connection, rather than just body contact. We find that on average each ant is connected to 4.8 neighbors.

Since every ant has six legs, we define the number of outgoing connections as $c_{\text{out}} = 6$, assuming every leg contacts a neighbor. We measure the number of incoming connections as $c_{\text{in}} = 8.25 \pm 3.09$. Thus each ant contacts its neighbors a total of $c_{total} \approx 14$ times. This number of connections is 40% higher than the maximum number connections made for granular particles. Ants are able to exceed this theoretical limit for spherocylinders because their legs are used to reach out to other neighbors.

Fig.17b shows the histogram of incoming connections c_{in}. We find that the number of connections can range rather widely, from 4 to 21. The minimum number of connections occurs likely because ants on the outside of the cluster are connected to fewer ants than those in the center. As we discuss in the next section, this spread is also due in large part to the colony's polymorphism.

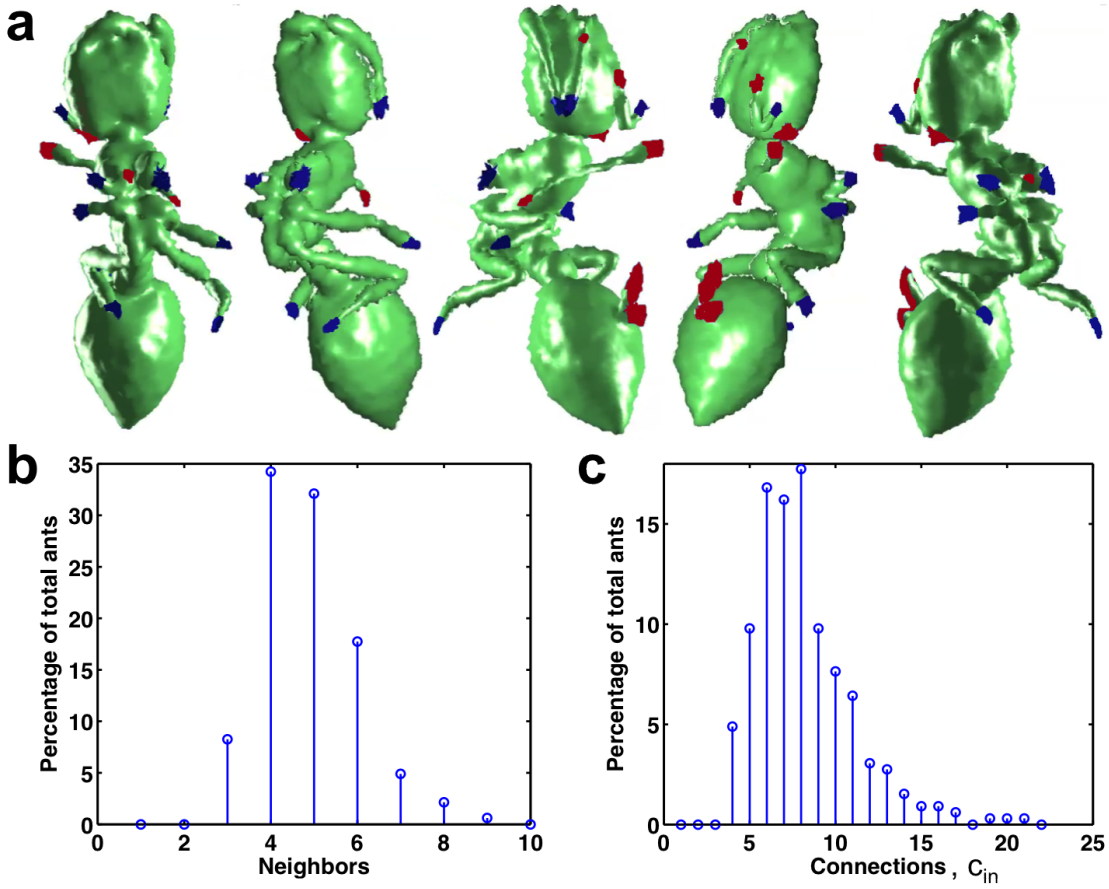

Figure 17: (a) Five views of a single ant in an assemblage. Blue highlights indicate outgoing connections (i.e. the ants own legs), and red highlights indicate incident connecting legs from neighboring ants. (b) Distribution of incident neighbor connections for a single ant within a self-assemblage. The data is from 4 clusters each containing approximately 110 ants. (c) Distribution of neighboring ants that a single ant is connected to.

4.3.3 Polymorphism of the colony increases connectivity and packing fraction

We show in this section that polymorphism in a colony results in more connections and tighter packing. Polymorphism refers to the large size distribution within a single fire ant colony, shown in **Fig.18**c_{inset}, where size is typically described by head width. A study by Wood and Tschinkel found 45 % of fire ant workers in a mature colony are small (head width up to 0.8 mm), 42 % are medium (head width 0.8 - 1.0 mm), and 16 % are large (head width greater than 1.0 mm) [114]. Despite this polymorphism, with some ants more than three times larger than others, the aspect ratio $\alpha = 3.9 \pm 0.17$ is preserved across scale. Another example of polymophism is shown by our CT scan in **Fig.18**a of ants with legs digitally removed, where a large ant is surrounded by and connected to several small and medium sized ants.

Fig.18d shows that the relation between ant body surface area and incoming connections for one of our samples is a power law with an exponent of 0.35 and R^2 value of 0.53. The largest ant is one of the most well connected to its neighbors at 19 incoming connections, with more than 4 times the connections seen by some of the smallest ants. **Fig.18**b illustrates this point by comparing a large and small ant with both incoming and outgoing connections highlighted in blue. The large ant has many incoming connections all over it's body and head, while the small ant has much fewer incoming connections.

In addition to having more connections, large ants have more neighbors than small ants. **Fig.18**c shows that the relation between ant body surface area and number of neighbors is a power law function with exponent of 0.41 and R^2 of 0.44. This indicates that number of neighbors does not scale linearly with ant size. We shed some light on this finding by performing a 3D simulation of N small spheres of radius r packing around a larger sphere of radius R. We limit $1 < R/r < 3$ because ants only vary in length by a factor of 3. We then find the relation between N and the surface area of the larger sphere: the best fit to our simulation results is a power law with exponent of 0.6 and R^2 of 0.99, as seen in **Fig.18** in red. The exponent for spheres is higher than for ants because a large ant is not always surrounded by the same size ant. Also, ant neighbors are counted by leg connections, not simply contacts as with spheres.

Ants in an assemblage see anywhere from 3 to 9 neighbors with the smallest ants seeing the least neighbors. The largest ant connected to 9 different neighbors also sees 19 incoming connections, indicating that each neighbors is connected to it by two leg connections. The large size variation in a self-assemblage permits ants to fit closer together and see more connections, increasing the strength of the structure.

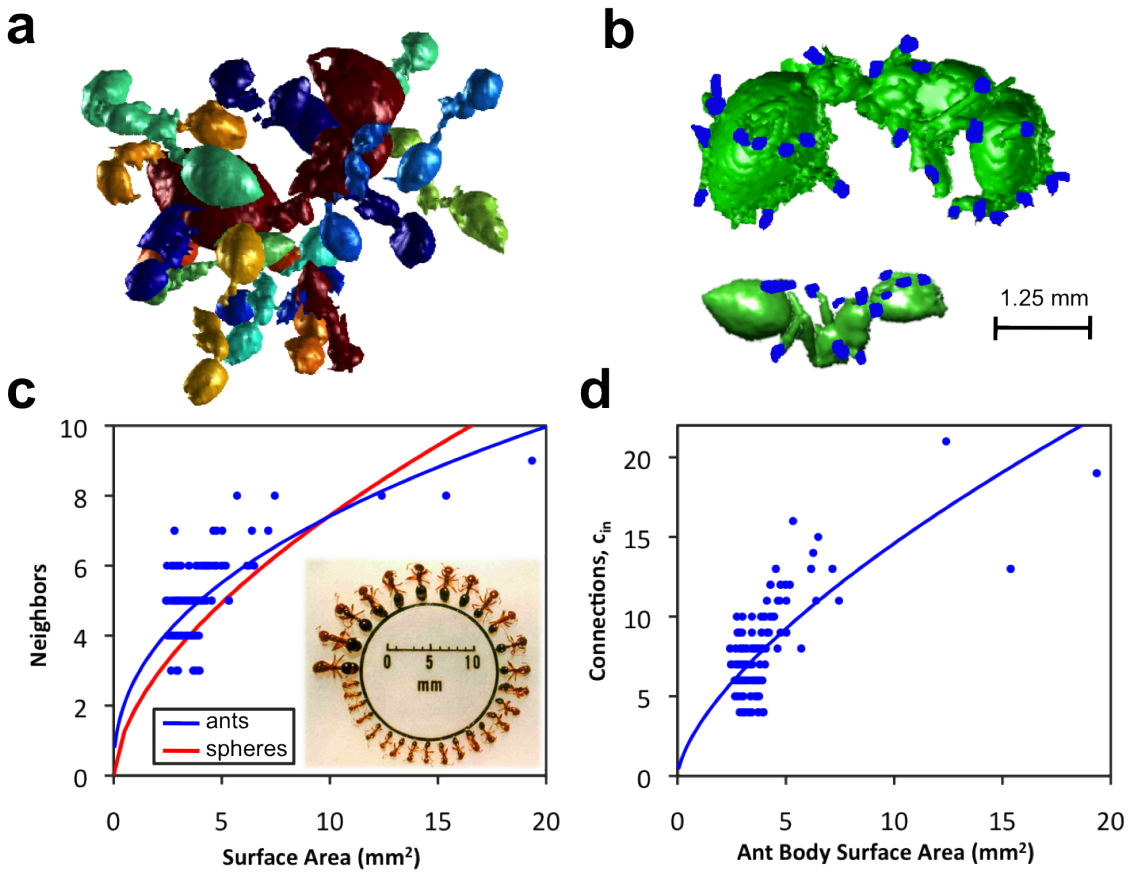

Figure 18: (a) A large ant surrounded by and connected to many small ants. (b) Large and small single ants showing the high and low number of connections respectively. (c) Relation between an ant's body surface area and the number of neighbors it is connected to. Best fit is a power law function with exponent of 0.41 and R^2=0.44. Inset is a display showing polymorphism range within a single fire ant colony (Image from Tschinkel's book *The Fire Ants* [3]) (d) Relation between an ant's body surface area and the number of incident connections it sees. Best fit is a power law function with exponent of 0.35 and R^2=0.53.

4.3.4 Ants orient themselves normal to each other

In this section we introduce a metric for relative ant orientation. We begin with the orientation of a single ant, which may be described by a unit vector $\mathbf{P_1}$ pointing along the ant body's first principal moment of inertia as shown in **Fig.19**a and b. Its first nearest neighbor has orientation vector **P2**. We define a relative orientation correlation as the component of **P2** in **P1**'s direction,

$$\Psi = \mathbf{P1} \cdot \mathbf{P2} = \cos\theta \,, \tag{7}$$

where θ is the angle between the two principal axis vectors. The angle θ between the P vectors is limited to $0^\circ < \theta < 90^\circ$ because we are unable to distinguish posterior from anterior of the ants in the scans; therefore the limits of Ψ are 0 and 1. As Ψ nears zero, the ants are oriented more perpendicular; approaching one indicates more alignment. A group of randomly oriented ants has an expected Ψ value of 0.5.

Fig.19c shows orientation correlation Ψ for live ants, dead ants and cylinders. For live ants, $\Psi_{live} = 0.44 \pm 0.27$ indicating a slight tendency towards normal alignment, but a random packing of dead ants yields $\Psi_{dead} = 0.6 \pm 0.28$ showing a greater tendency towards parallel alignment. We verified the significance of this result by comparing live and dead ants using a t-test, finding a p-value ≤ 0.0001.

The orientation correlation of dead ants is similar to numerical findings by Stokely *et al* for cylinder packings [4], verifying our experimental protocol indeed has generated a random packing. They found closer spaced particles are more aligned: specifically, cylinders half a body length apart orient with a correlation $\Psi_{cyl} \approx 0.6$. Similarly, ants with a nearest neighbor distance of half an ant length have an orientation correlation Ψ_{cyl}=0.6. This similarity is evidence that dead ants pack as expected for similarly dimensioned cylinders. For cylinders much further than one body length apart, the expected Ψ_{cyl} approaches 0.5, perfectly randomly oriented.

We now compare relative orientation of live ants to the findings of Stokely *et al*. They provide a relation between cylinder relative orientation correlation Ψ_{cyl} and spacing. Cylinders a quarter of a body length apart have strong parallel orientation with Ψ_{cyl}=0.9. In light of their findings, we expect long neighboring particles, such as ants, to line up with one another; indeed we find this is the case for dead ants. However, live ants a quarter of a body length apart tend towards slight normal alignment with relative orientation correlation Ψ_{live}=0.44. From these results, we reason that live ants actively use their legs to orient themselves.

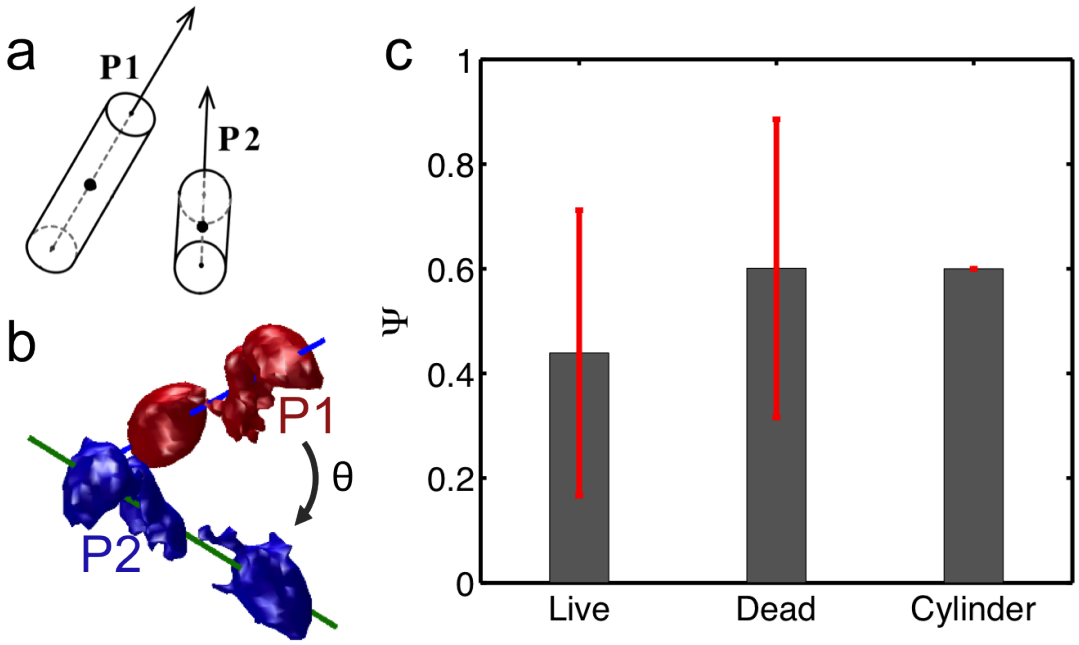

Figure 19: (a) Schematic showing the P vector, the axis running along an ant's principle moment of inertia. (b) Two neighboring ants with P vectors shown. θ is the angle between the P vectors. (c) Orientation correlation Ψ mean and standard deviation for live and dead ants from this study, and cylinders from a previously published study by Stokely [4]. Data is from 4 ant clusters with a total of 440 ants. Overall live ants arrange themselves more perpendicular to neighbors when compared to our control group of ants. We conducted a t-test to verify this claim, and it is supported by a p-value ≤ 0.0001. Published orientation correlation results also show cylinders with $\alpha > 1$ prefer parallel orientation.

4.4 Discussion

In this study, we find evidence that ants actively control their arrangement within self-aggregations. This ability gives ant aggregations an intelligence and reacting ability greater than previously credited to them. To control their arrangement, ants would require some level of cooperation, whose level still remains unknown. Further investigation of ants actively rearranging their network may yield discovery of mechanisms for controlling arrangement and further inspiration for the development of biomimetic self-healing materials [115]

Since fire ant connections are made actively, one can define a connective efficiency. Fire ants are remarkably good at finding connections with each other. Out of the 440 ants studied, 99% of them had all their legs completely attached to their neighbors. Only 26 legs remained dangling and unconnected, a very small percent of the over 2,600 legs. Since ants naturally try to keep all legs in contact with a surface when not moving, it is not surprising that the static interior of the network is so well connected. We attribute the unconnected legs we found to either ants on the exterior of the assemblage or to connections that may have been broken during sample preparation.

The high proportion of successful connections suggests ants are indeed intent on maintaining grip with one another. The high connectivity adds strength to the aggregation, and is likely to be a common attribute between other insects such as bees and army ants able to form self-aggregations. Moreover, species of ants unable to form aggregations would likely have a lower connective efficiency.

This study also shows fire ant aggregations share commonalities with well-known biomaterials. Namely, ant aggregations are porous, enabling them to be both lightweight and strong. Using porous materials has long been effective in making materials lighter without sacrificing strength. Porous aggregate concrete is known as a satisfactory substitute for lighter building material [116]. Cancellous, or highly porous, bone is an excellent example of a naturally occurring porous network that is very strong. Cancellous bone with volume fractions as low as 0.03 and as high as 0.5 can withstand 1000 kPa pressures and 100 MPa respectively [117]. Indeed, the ability to create porous structures in building materials is a trait common across scales and across species.

The effect of distribution of particle sizes has been studied in the context of granular media. In industrial applications where space is an important packing parameter, an increase in packing fraction means less wasted space. Granular studies have found polydisperse packings have higher packing fraction than monodisperse packings [118]. It is likely that a similar phenomenon occurs within ant aggregations as a result of colony polymorphism. We find in many instances, small ants tend to fill in spaces around large ants. While a lower packing fraction helps the colony stay afloat while rafting, efficient packing is equally important both to keep water from seeping in and to prevent weak spots in the raft.

Our study made use of a state-of-the-art 3-D CT scanner which may not be available to other investigators. Nevertheless, methods such as visual inspection can yield important characteristics, such as ant spacing, which are consistent with those found using CT-scanning. Using the ratio of the number of ants and their interpolated volume from our CT-scans, we calculate an ant concentration of 164 ants/cm^3. Assuming a cubic lattice, the associated ant center-to-center spacing is 1.8 mm. Previously, by visual inspection of frozen ants in a raft, we found a planar concentration of 34 ants in a cm^2 [17], and a spacing of 1.7mm, a value quite close to our current findings based on CT scans. Thus, visual inspection of a the surface of a self-aggregation can give a good indication of properties on the interior.

Future workers may also be able to exceed certain limitation in our study based on the state of current technology. The size limitations in our CT-scanning equipment set an upper bound of scans at 150 ants. Such numbers are small compared to the size of most insect self-assemblages; for instance, fire ant rafts may number from 10,000 to 100,000 individuals[119]. Thus, it seems at first our methods provide a poor representation of the aggregation. In fact, our small samples are justified by our choice of species. Anderson

rates insect self-assemblages in terms of complexity, rating fire ants as the least complex self-assemblages, far less complex than weaver ant pulling chains and army ant tunnels and walls [32]. Thus, compared to other ant species, the arrangement of fire ants is less crucial to function. His view of assemblages suggests that our samples of fire ant self-assemblage are good representations of the overall structure, despite their small size. Applying our CT-scan technique to more sophisticated species such as army ants would require a CT machine capable of scanning a higher volume of individuals.

The resolution of our CT-scan prevents us from distinguishing an ant's anterior end from its posterior. Improvements to the technology will enable future workers to determine if polarity is an important characeristic of the ant network. We are also unable to distinguish antennas from legs; since our algorithm accounts for all outgoing legs and antennae, we have simply removed the 2 antennae from our count leaving outgoing ant connections restricted to legs only: $c_{\text{out}} = 6$. Antennas have no role in providing tensile strength, but may be important in providing resistance to compressive stresses, as shown by the ability of ants to arrest falling in tunnels by extending their antenna [120].

4.5 Conclusion

We measure the connectivity and arrangement of a three-dimensional linked network of fire ants with results summarized in **Table 5**. We find ant aggregations are highly interconnected networks, possessing as much porosity as known biomaterials such as bone. We identify key ant behaviors that facilitate forming of such porous, sensing and responsive self-aggregations. First, ants use tensile forces applied by their legs to extend distance between neighbors. Increasing of distance between the ants keep the raft porous and so buoyant, permitting fire ant raft to stay afloat and buoy back to the surface when submerged by strong river currents. Ants also use their legs to arrange themselves into more perpendicular arrangements than would be expected for particles with a similar aspect ratio. Configurations in mutually perpendicular directions add to the adaptability of the structure, improving its ability to contract and expand in response to environmental forces. Lastly, we find an important role in polymorphism of the colony, previously known to facilitate the colony in performing different tasks such as foraging, carrying for the brood, and defense. Here, such polymorphism plays an important role in increasing connectivity of the self-aggregation.

Together, these properties make ant self-assemblages highly versatile tools enabling the colony to function successfully in a variety of situations. For example, local control of spacing allows ants in a raft to keep water out even when submerged. Controlling orientation allows ants to build bridges and towers anisotropically, with greater strength in the direction of highest load. The high connectivity of the network evenly distributes forces among an ant's appendages, enabling an assemblage to statically support self-weight for long periods.

Table 5: Geometric and packing properties of ants in this study. Both live and dead ants are provided for comparison. Results from studies of cylinders are provided to give perspective. Packing fraction ϕ is averaged from 4 live samples and from 2 dead samples. NND, c, and Ψ are all averaged from 440 live ants and 220 dead ants.

	Number of ants, n	Packing fraction, φ	Average of 3 nearest neighbors distance, $NND_{1,2,\&3}$	Total Connections, c_{total}	Orientation correlation, Ψ
Live sample	440	0.25 ± 0.10	1.82 ± 0.31	14 ± 3.09	0.44 ± 0.27
Dead sample	220	0.38 ± 0.02	1.23 ± 0.26	NA	0.60 ± 0.28
Cylinder		0.60		9.00	0.66 ± 0.05
Staples		0.13 ± 0.01		8.70	

CHAPTER V

THE ANT TOWER

5.1 What is an ant tower?

A fast growing interdisciplinary field is the study of the phenomenal ability of social insect colonies to cooperate effectively without central command and with individual capabilities that come no where near the complexity of the overall group capabilities. Such studies require collaboration between mathematicians, physicist, engineers, and biologists in an effort to understand this swarm intelligence. Often such studies require understanding the individual's role in the big picture since each individual is acting on the same set of behavioral rules.

There have been few studies on the collective structures built by insect societies, and most of these are qualitative. Much remains to be understood about what drives the formation of these structures, how they are formed, and how to effectively model the construction and deconstruction phases. Since these structures often occur under specific environmental conditions and in remote areas it can be difficult to produce controlled studies. Also, because there are thousands or even hundreds of thousands of individuals participating and cooperating as a group, understanding the construction dynamics of the constantly moving mass of insects can be a difficult task, but uncovering the mechanisms that drive structured insect self-assemblages is an important piece of the swarm intelligence puzzle. Such studies also bring us one step closer to developing a physical, robotic recreation of the functional principles that govern decentralized intelligence of social insect societies.

A study by Bonabeau and Theraulaz observed and modeled the droplet formations of the ant Linepithema humile showing that the time between droplets likely results from low-dimensional, nonlinear dynamics [21, 107]. Through behavioral assays and mathematical modeling, Zirbes showed that the probability of an earthworm joining a self-assembly increased with group size while at the same time probability of leaving decreased [121]. Previously, we presented a predictive model for the rate and size of fire ant raft construction based on observations of ant dynamics atop the raft [17]. While modeling insect self-assemblages is an understudied field, these studies are examples of successful modeling that leads to a better understanding of what drives emergence of group behavior.

Fire ants are experts at forming aggregations with their own bodies by linking limbs together [10]. In a lab containment bin, where there is no soil for them to dig in, they resort to forming temporary structures using their own bodies as the building block as shown in **Fig.20**a. While fire ant bivouac formation has never been documented, several

other ant species are well-known for their bivouac formations. Army ants are a nomadic species and therefore have no permanent residence. During colony rest periods, army ants quickly gather together around the queen and brood to form a protective nest composed of living ants joined together by mandibles and legs. When the colony is ready to move on, the colony members just as quickly dismantle the structure and continue marching in search of food. These temporary shelters termed bivouacs use natural support such as a fallen log or dense brush as a kind of skeletal support for the ants to build on. Studies have shown that the arrangement of army ants within a bivouac is actually quite structured, with ants generally linked vertically "head-to-toe" and larger ants on the outside wall. Tunnels leading from the outside allow ants to tend to the queen inside.

We observe fire ants building bivouacs in the lab as seen in **Fig.20**a & c. While fire ants typically reside in a system of underground tunnels, when removed from their natural environment and placed into one with no shelter, they provide their own, just like the army ants. They link together using jaws and legs and build a temporary shelter up against a support. Fire ant arrangement within a bivouac is much less organized than that of army ants, but there is still a general trend to vertical orientation. The shape of the structure actively built by live ants is qualitatively and quantitatively different than the structure formed by a pile of dead ants as seen in **Fig.20**b. The forces holding a live tower in its configuration are the active adhesion and spacing control of neighboring ants using their legs, but in a pile of dead ants, the angle of repose is set only by friction between incidental contacts.

It is unclear exactly why fire ants build bivouacs. Walter Tschinkel says that fire ant aggregation into bivouacs is a natural thygmatic response to ants being removed from their underground environment [3]. Ants use a variety of cues to form bivouac aggregations. Neighboring ant contact frequency provides ants with aggregation concentration information [104]. Pheromone cues signal the onset of colony aggregation so that other ants will follow suit [51]. Stimuli from the local environment, such as colony inundation or ambient lighting changes, can also trigger aggregation to occur. Anderson claims about ant bivouacs in general that they have four functions [32]. First a bivouac serves as a center of operations. Second it offers shelter for the queen and brood from the elements and intruders. Third it acts as a thermoregulator as shown by temperatures within a bivouac several degrees higher than ambient [12, 122, 123]. Lastly a bivouac serves as a population reservoir and a situation for ants to be gathered closely near other colony members when they are not carrying out tasks.

Fire ants can stick to smooth surfaces using a retractable adhesive pad located on the end of their legs between two claws as seen in **Fig.20**a$_{inset}$. This pad secretes an emulsion with both oily and watery substances that contributes to insect adhesion [124]. Despite many focused studies, the exact mechanism ants use to sustain static friction is unknown

[125]. One study by Federle revealed that the most significant role of the pad's secretion was increased contact area on surfaces with rough micro-topography, which translated to increased friction forces and resistance to shear as illustrated in **Fig.22**c [126]. These rough surfaces are still smooth in the general sense in that they appear smooth to the unaided eye and even feel smooth to the touch. Upon closer inspection, and especially relative to the size of an ant's foot, the surfaces are actually quite rough with peaks to valley heights about 1/4th the width of a fire ant adhesive pad.

This chapter discusses our findings on the tower-shaped bivouacs fire ants build against a wall or rod. The current chapter begins with our methods for controlling fire ant tower construction. We then briefly look at the affect of roughening smooth surfaces on fire ant adhesion and tower-construction. We then dive into the process that ants use to construct towers around thin Teflon rods. We use time-lapse methods to observe construction rates, tower shapes, and individual trajectory patterns, and present a justification for the bivouac shape and a model to explain the building rate. We also present new findings on dynamics and structure of fire ant bivouacs. Lastly, we discuss the implications of our findings on ant self-assemblages.

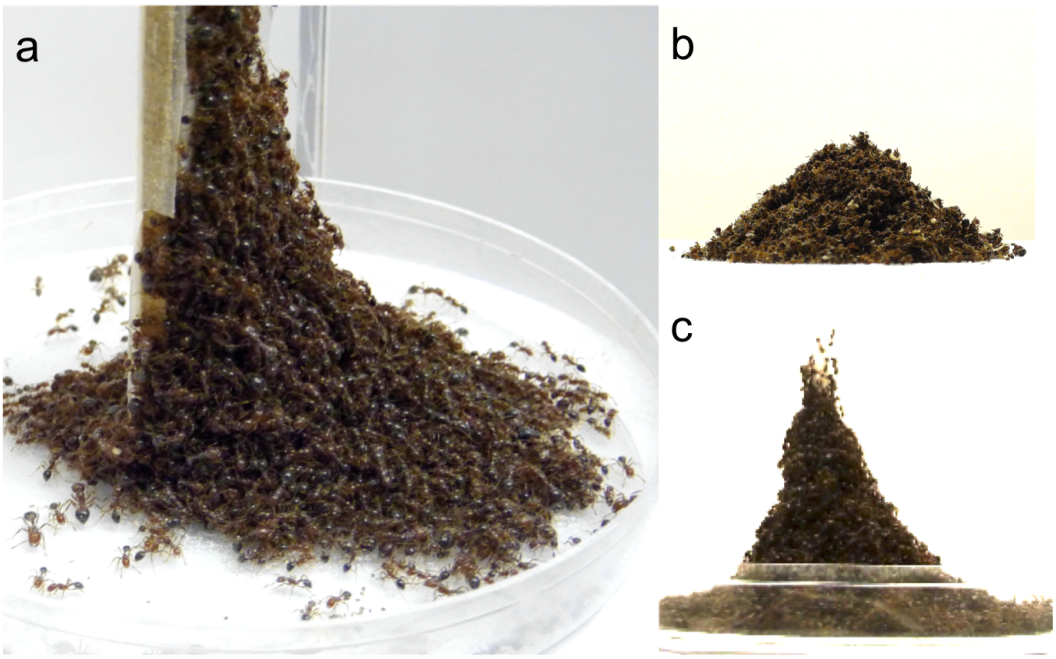

Figure 20: When confined with no escape route, fire ants assemble to construct towers with their bodies. They build against (a) flat walls or (c) circular rods that prevent tower buckling. When viewed from the side, the tower profile is clearly nonlinear; whereas, (b) a pile of dead ants has an angle of repose approximately 40°.

5.2 Experimental methods

5.2.1 Teflon strip preparation

Four Teflon strips measuring 1 inch by 6 inches were used for as a supporting substrate for ants to build towers on. Three strips were sanded using 60, 320, and 400 grit sandpaper to alter surface roughness according to the methods outlined by Nilsson to create super-hydrophobic surfaces [127]. One strip was left unaltered. The sandpaper grit sizes used were 60 grit, 320 grit, and 400 grit where 60 grit had the roughest surface and 400 was the smoothest of the three. The surface roughness of the unaltered strip fell between 400 and 320. First, the Teflon strips were sanded in random directions with even pressure to avoid patterns. After sanding thoroughly, any extra dust and pieces of Teflon were removed from the surface. Next the 1 x 6 inch Teflon strips were attached to hard wooden boards of the same size using superglue so that the Teflon strips remained rigid. The procedure was repeated for the other two strips.

5.2.2 Ant strength on Teflon

Strength is tested using two methods. The first method is to harness a single 1.5 mg ant with a rubber string and measure the deflection as the string is pulled to remove an ant adhering to a Teflon plate as seen in **Fig.21**d. The second method is subjecting an ant on a Teflon plate to centrifugal forces until it releases. We record the mass of the ant, angular velocity, and radius from the center of rotation to find ant holding force just before release.

5.2.3 Tower building

Fig.23a and **Fig.22**b show our experimental setup and methods for initializing ant tower construction on rods and plates respectively. 10 grams of ants are collected in a beaker. The ants are swirled to produce a sphere of ants and are subsequently placed as a group in the center of a 100 x 15 mm petri dish. The ants are allowed to settle into the dish for 5 minutes before a Teflon rod or plate lightly dusted with talc powder is lowered into the center of the sea of ants filling the petri dish. Ants are prevented from escaping the sides of the petri dish by heavily coating the sides with talc powder. Within a few minutes ants begin to form a tower centered around the Teflon rod or against the plate. Within about an hour, all of the ants have formed a stable tower in equilibrium. The process is filmed horizontally to capture the tower profile.

5.2.4 Tower sinking

To observe ant movement within the tower, 5 g of fire ants are doped with iodine by mixing with their drinking water, and allowing the ants to drink for at least 2 days before tower building. Immediately before tower building beings, 5 g of doped ants are mixed thoroughly

with 2.5 g of undoped ants from the same colony. The ants are placed in a 100 x 15 mm petri dish around a 55 mm tall and 6.2 diameter Teflon rod located in the center of the dish. Ants are allowed to build a tower with the process captured using an imaging system that includes the following: Spelman XRB502 Monoblock X-Ray source and Amorphous Silicon Digital X-Ray Detector PaxScan 2020+ (Varian Medical Systems). We operate the x-ray at a current of 2.5 mA and a voltage of 100 keV. In the resulting images, doped ants show as dark spots, and paths are traced frame-by-frame using Tracker.

5.3 Results

5.3.1 Controlling ant adhesion and tower height

Fire ants building a tower bivouac must have a vertical substrate to support their structure. Initially we discovered that substrate surface properties affect tower shape, size, and rate of construction. Ant towers built on a high friction surface such as sandpaper have a thinner base and generally reach higher than a tower built on a low friction surface such as Teflon. We investigate the role of surface roughness on tower height by observing tower heights on Teflon plates with customized roughness shown in **Fig.21**a & b. We test ant adhesion on four Teflon plates with peak to valley roughness heights ranging from 5 to 20 µm, finding that ant adhesion in shear and normal on rough Teflon is higher than smooth Teflon by a factor of two as seen in **Fig.21**c.

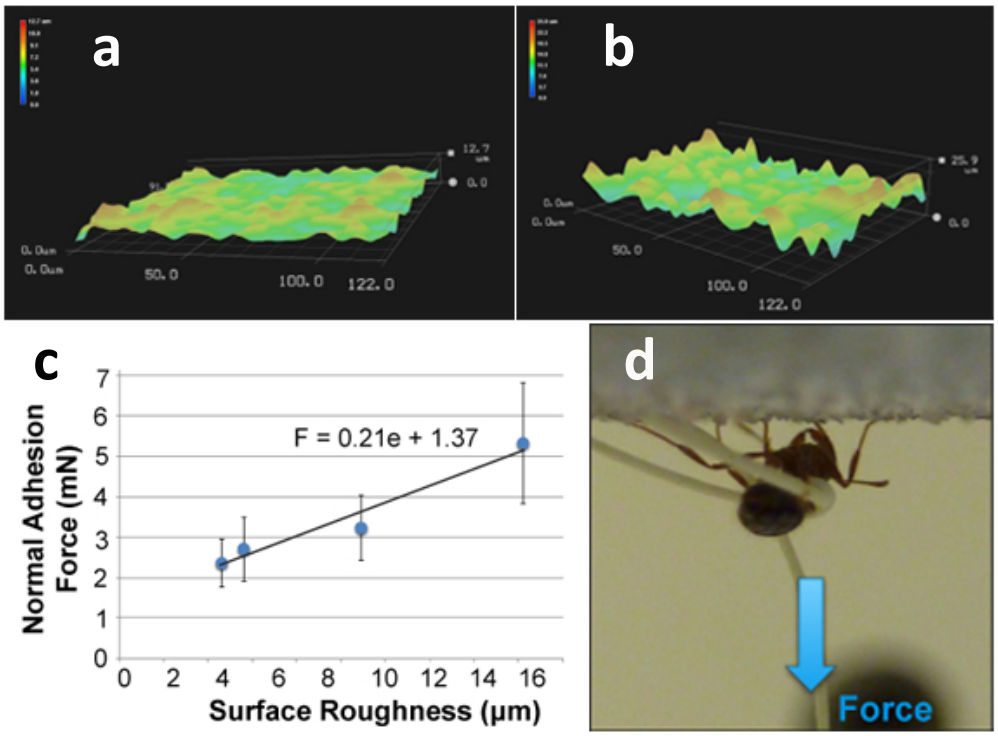

Figure 21: (a) Unaltered Teflon surface topography (b) Teflon surface topography after being roughened with 60 grit sandpaper (c) The relation between Teflon surface roughness and force required to remove an ant with normal pulling. (d) An ant harnessed with a thin rubber string is pulled normally to a Teflon surface upon which it rests inverted. The deflection of the string before the ant is pulled off is used to measure ant adhesion force to the Teflon.

Fig.22a shows the relation between Teflon surface roughness and measured tower height. When ants build towers against the roughest Teflon plates, tower height is increased by a factor of 1.8 as compared to the smoothest Teflon plates. Because ant connection strength to neighbors is much higher than to the supporting substrate, we find that the surface properties are an important part of determining tower size. The exact relationship between surface roughness and tower height remains unclear at this time, but because ants directly in contact with the substrate are supporting some normal forces, strong adhesion to the substrate will prolong tower buckling when compared to weak adhesion where ants may "peel" away from the substrate as seen in **Fig.23**b due to overloading.

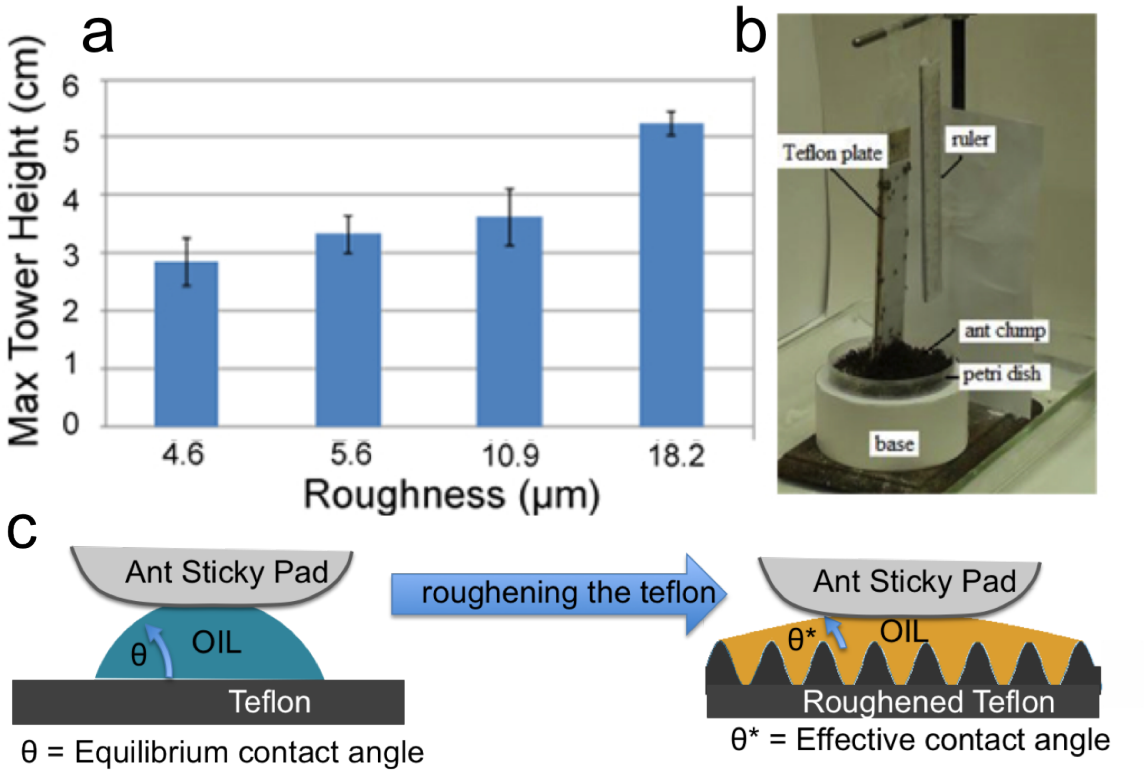

Figure 22: (a) When Teflon is roughened, ants build taller towers. The relation between Teflon roughness and tower height for 4 roughness values is shown here. (b) Several thousand ants are placed in a petri dish and allowed to build a tower against a flat Teflon strip as shown here. (c) We posit that increasing surface roughness of the Teflon acts to increase the adhesive capabilities of fire ants as explained by the Wenzel law in this schematic. According to the Wenzel law, contact area is increased for the ant's adhesive pad fluid when the surface is roughened, thus increasing the force necessary to remove the ant.

5.3.2 Tower construction

We move our focus from controlling tower height to analyzing tower shape in more detail. A Teflon rod is used as the supporting surface for ants to build a tower on. We choose a rod for ease of analysis and repeatability since the resulting structure is generally axisymmetric and independent of the viewing angle. We experimented with many different shapes and materials for the supporting substrate, but found that Teflon rods provided the most repeatable and analyzable results. We also chose Teflon rods lightly coated in talc powder because it provides a low friction surface that ants do not grip well on. This ensures that ants in the tower cannot get a secure grip on the rod, and are thus supported only by their neighbors beneath them and not by adhering to the support. This becomes important when comparing our results to our model.

A single ant can support in tension only its own weight or less on Teflon lightly powdered with talc, while on clean Teflon, an ant can support no more than ten of it's own body

weights. When Teflon is roughened or sandpaper is used, the tensile ant strength increases to around 50 ant weights or less. For comparison we test ant strengths to neighboring ants and find that for connections made with claws, the ants can support no more than 50 ant weights, but only temporarily. When jaws are used, an ant can easily support 1000 of its neighbors.

The tower building process begins when a large cluster of ants is placed into a petri dish. The ants settle into the dish spreading out to fill the volume of the container. Only ants on the outer layer are mobile, while all other ants remain stationary and are free to move only when not pinned by an ant on top of it. When the Teflon rod is lowered into the center of the tower, ants on the top layer of the group attempt to climb rod, making little headway. Although a single ant has trouble making its way up the rod, a ring of ants soon begins to form around the rod with all ants heading upwards attempting to climb. These ants are now approximately a body length higher than the "sea of ants" around them. Nearby exploring ants then begin to climb on top of the initial ring of ants around the rod, thus rendering that initial ring immobile. More ants explore the newly formed raised tower area and climb on top, pinning the ants beneath them and adding to the height of the tower at the same time. The process can be seen in the time-lapse images shown in **Fig.23**b. The ants continue until an equilibrium height and shape is reached. At this point, a mobile layer of ants remains, and the ants beneath remain a fixed part of the structure. Although exchanges do occasionally occur between ants on the outer layer and pinned ants beneath, the shape of the tower remains in equilibrium.

We repeat the experiment with different rod diameters to see the affect on tower growth rate or shape. We find no significant increase in time to build the tower or rates at various times. We gather from this that the limiting process in tower construction is not a gathering of ants around the rod, but rather a gathering of enough ants to support the rings forming around the rod. Without this gathering, the rings forming around the rod would buckle and collapse. When ants gather to support the growing tower, the shape also does not appreciably vary with different rod diameters. Across all towers, there is an exponential shape profile.

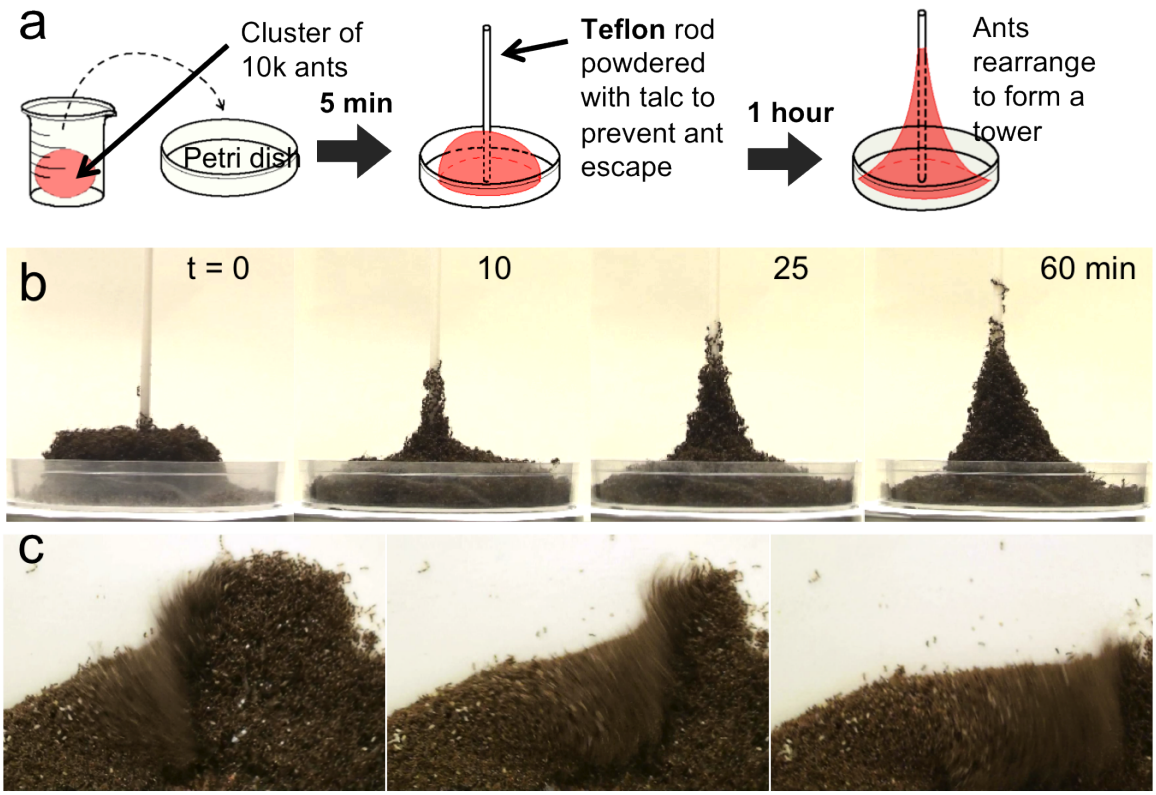

Figure 23: (a) Schematic showing our experimental setup and methods. Ants are collected in a beaker, placed in a petri dish and allowed to settle for 5 minutes. A Teflon rod is lowered into the center of the "sea of ants." In one hour the ants rearrange themselves into a tower around the rod. The ants will hold this equilibrium shape for at least a day. (b) Fire ants also build long walls on flat surfaces. When loading is unstable on one side, the wall will buckle, causing the tower to fold and collapse. The collapse propagates down the wall, pulling all of the ants down like a crashing wave. (c) Fire ants build their towers around Teflon rods. Ants collect and form rings around the rod, recruiting other ants to do the same until a stable equilibrium shape has been reached.

5.3.3 Defining tower shape parameters

During the construction process we observe the tower emerges out of a "sea of ants" with a roughly horizontal free surface. To measure tower shape during construction we made a quantitative distinction between the emerging tower and the sea of ants beneath. This distinction between the tower body and sea of ants can be seen in **Fig.23**b as the steep sides of the tower emerge from the near horizontal bed of ants beneath. **Fig.24**c provides an illustration of our definitions for tower height and width. Tower height $h(t)$, a function of elapsed time t, is measured between the highest visible ant attached to the tower and the free surface of the sea of ants. Tower width $w(h,t)$ is defined as half the distance across the tower at a specific time and tower height. Time t begins when the tower first emerges from the sea.

Tower h and w are tracked for 12 towers. For every time t that a measurement is taken, 5 random images are selected from within a 30 second bound on either side of t. The h and w are measured for each of these images and then averaged to represent the shape profile of the tower. Measurements of the tower's shape are made roughly every 5 minutes of construction. **Fig.24**a shows the tower growth rate on 5 different rod diameters. For rod diameters ranging from 3.1 to 11.2 mm we found the time to reach equilibrium is increased as rod diameter increases. In addition, the tower growth is linear, but is divided into two linear regimes divided at approximately 15 minutes. We will revisit the linear growth and two regimes in the tower dynamics section.

When the ants have reached an equilibrium point, and construction on the tower has halted, we observe that the profile is exponentially shaped as plotted in **Fig.24**b. **Fig.24**c shows that at equilibrium, the sea of ants has "evaporated" because all of the ants that made up the sea are now part of the tower. The area where the sea used to be, is now partially covered by mobile scout ants. This moving reference frame is the reason why tower height cannot simply be measured from the top of the tower to the bottom of the containing dish. Equilibrium is defined as the point in time when the height and width of the tower reach a value that does not change on long time scales relative to the growth rate during construction.

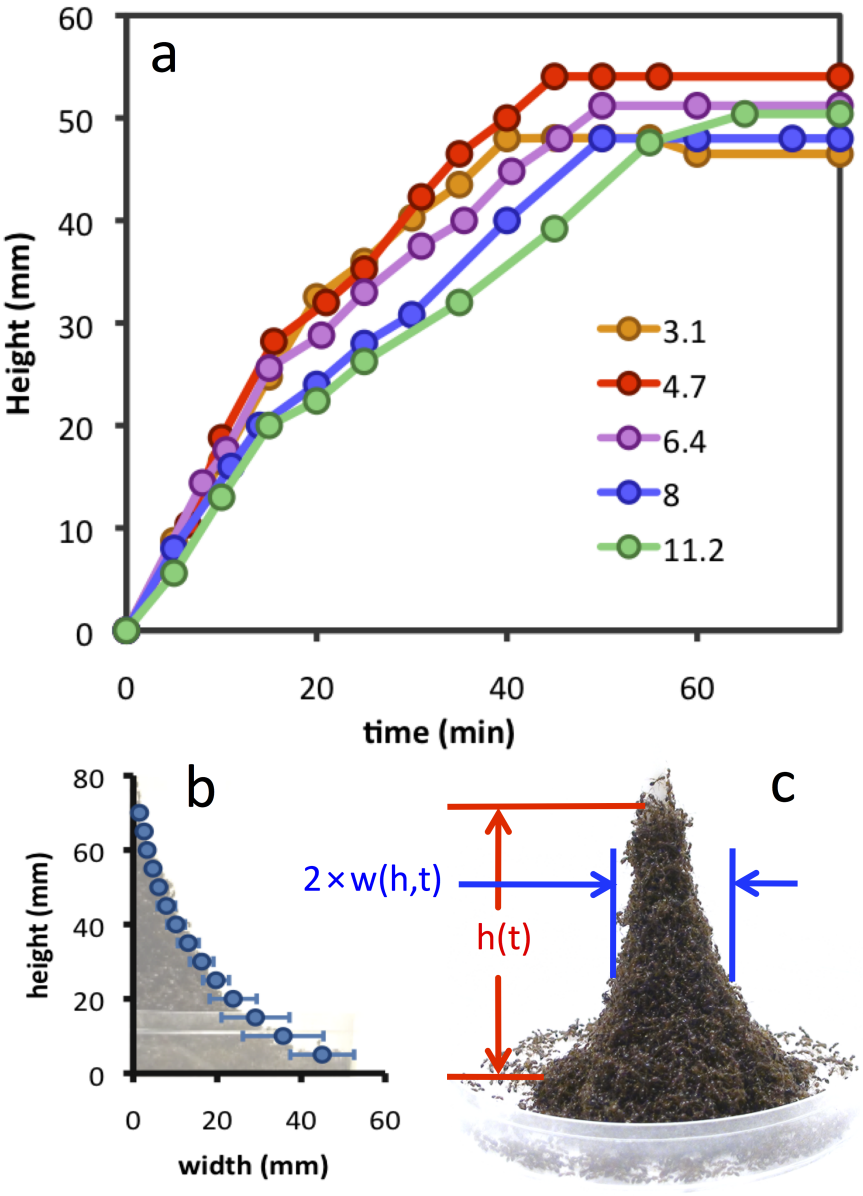

Figure 24: (a) We make the assumption that ant towers are axisymmetric and describe the shape by defining parameters height, a function of time, and width, a function of time and height. Height is the vertical distance from the sea of ants to the last ant that is connected to the tower. This does not include disconnected scout ants higher up on the rod. (b) We average tower height as a function of time for 12 towers. The growth rate is almost linear for the first 40 minutes and then slows down to reach an equilibrium shape after an hour. (c) We average tower height and width at equilibrium and plot on top of a representative tower profile. (d) At equilibrium, the sea of ants is all but "dried" up leaving only a thin layer of scout ants outside the tower perimeter.

5.3.4 Developing a model to explain tower shape

We now use the tower parameters and data gathered on the shape of the tower built by ants to explain the observed exponential shape profile. We develop a model for tower building based on uniform strength throughout the tower, meaning that every ant is supporting the same weight as its neighbors. To begin, we approximate the tower as axisymmetric. We idealize the tower as consisting of discrete horizontal layers of equal sized ants oriented vertically with a 4:1 aspect ratio. **Fig.25**a shows that Layer 1 is the top layer and Layer N is the bottom layer. Layer $n+1$ is the layer directly below layer n, where layer n contains X_n ants. We assume constant strength in the tower, meaning that the combined weight of the ants $\sum_{i=1}^{n} X_i$ in Layers 1 through n is uniformly distributed and supported fully by the X_{n+1} ants in Layer $n+1$. Furthermore, we define ant strength α as the weight, measured in number of ants, that a single ant is supporting in the tower, where α is not necessarily an integer. Therefore

$$\alpha X_{n+1} \geq \sum_{i=1}^{n} X_i. \tag{8}$$

This result depends on the assumption of a slowly varying tower profile such that every ant in layer $n+1$ is active in supporting the ants in layer n. Another way to say this is to assume that the entire weight of layers n through 1 is uniformly distributed to each ant in layer $n+1$. Furthermore, assuming α is consistent for all ants, then equation 8 holds with equality as a good approximation for every level of the tower. We can rearrange this equation to find an approximation for the number of ants X_n at each level n for a tower of constant ant strength:

$$X_n = \frac{1}{\alpha} \sum_{i=2}^{n-1} X_i. \tag{9}$$

This is an approximation because X_n is restricted to integers only because each layer is composed of ants. A simple example of $\alpha = 3$ to test our relation reveals that layers 1 through 4 will have 1 ant each, where layer 4 is supporting exactly 3 ants. Layer 5 requires 2 ants because a single ant is not strong enough to support the 4 above it, X_5=2. At layer 6, there must be enough ants to support the 6 ants in layers 1 through 5; therefore X_6=2. Continuing with this logic we find X_7=3, X_8=4, and so forth to X_N.

We recognize that when α >1, equation 9 is not valid for $n \leq \alpha$, but only holds as an approximation for $n > \alpha$. Because X_n must be an integer, there is no closed-form expression for X_n as a function of α; thus we approximate X_n by the piece-wise formula

$$f(n) = \begin{cases} 1, & \text{if } n \leq \alpha \\ \alpha(1 + \frac{1}{\alpha})^{n-\alpha}, & \text{if } n > \alpha \end{cases} \tag{10}$$

This model for ant tower building provides a prediction for shape. If the fit is good at any α value then we can propose that strength in the tower is uniform at all heights and α is the strength each ant supports. In **Fig.25**b we show the tower shape at equilibrium and fit the model using three different values for α. We find that at larger values of n the model fit is very sensitive to changes in α. For example, when α=2, the model predicts that tower width increases much faster with n than our experiments show. Also, when α=6 is plotted, we see a profile that appears almost linear when limited by the N in our experiments. Plotting the model with α=3.5, we max out R^2 at 0.98 and yield an exponential profile that matches very well with the average equilibrium profile found experimentally. We also find that when the model is compared individually to all tower instances at equilibrium that α only ranges from 3.2 to 3.9.

We also investigate tower shape during the process of construction and decide if the model is a good fit and if so at what ant strength value α. This will reveal whether ants maintain the same shape throughout the construction process. In **Fig.25**c we compare the model to experimental findings at two different time instances before equilibrium, choosing 10 min and 25 min, the times that tower height reaches roughly a third and two-thirds of its equilibrium height respectively. After 25 min of construction, an α of 2.7 yields the highest R^2 value at 0.99, and after 10 min of construction, an α of 2 gives a max R^2 value of 0.99 as well. We find that during the construction process, the ants do build towers such that the load is distributed uniformly to each ant, but that as the process continues, each ant is taking on more load. But when we plot experimental results at 10 and 25 minutes against the model using the same α found at equilibrium, we find R^2 values are only reduced to 0.98 and 0.75. This is because α is not very sensitive to change for low n. We therefore conclude that an ant strength α=3.5 is a good indicator of ant strength through the building process.

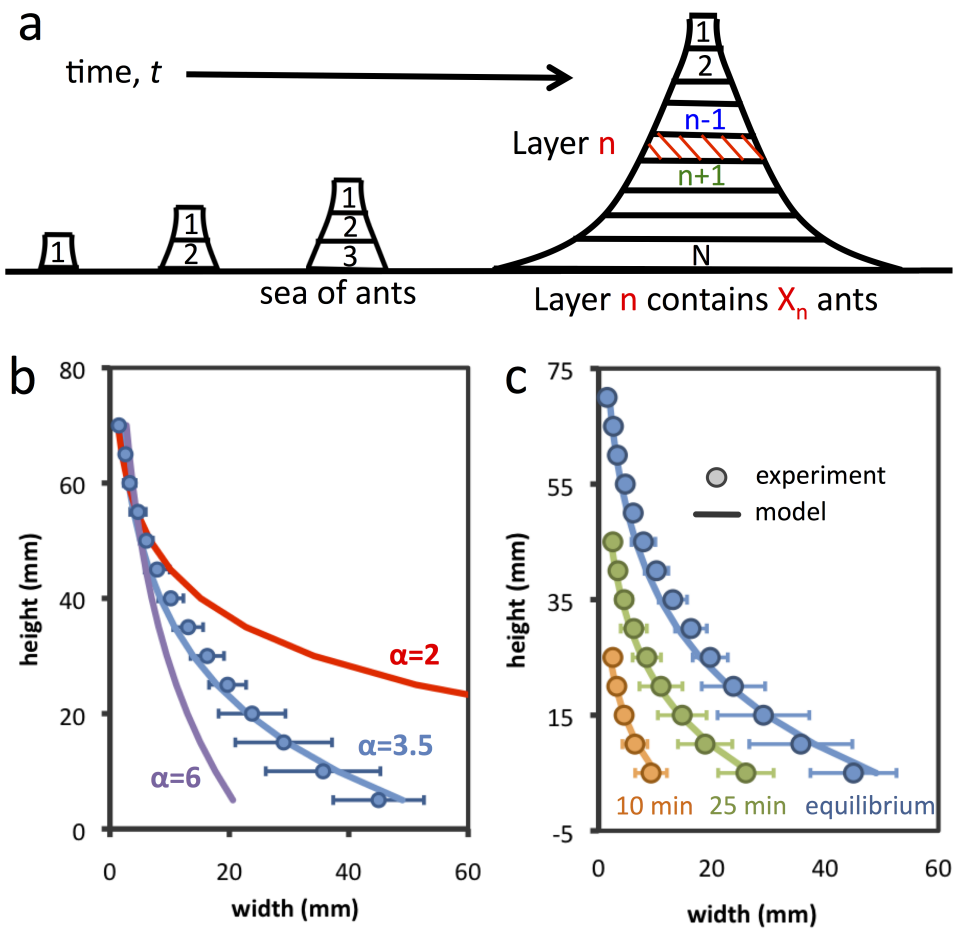

Figure 25: (a) Schematic illustrating our model of tower growth. Layer 1 is the top layer, and Layer N is the bottom. Layer $n+1$ supports Layers 1 through n. (b) Here we see the effect of changing α on the model fit. When α=2 (red), the width increases much too fast with increasing n, and when we choose α=6 (purple), the model is almost linear for moderate values of n. (c) Tower shape at 10 min, 25 min, and equilibrium. The model fits best at equilibrium with an ant strength α=3.5 (blue). At 25 and 10 min α=2.7 and $\alpha = 2$ respectively provide the best model fit.

5.3.5 Tower dynamics

In our experiments on shape, tower height is limited by fixing the number of ants in the experiment. We now limit tower height by fixing rod height such that ants build the tower all the way to the top of the rod as seen in **Fig.26**b. A time lapse of the ensuing footage as seen by supplementary movie *Ant Tower Side Time Lapse.mov* reveals a surprising finding: the stationary ants in the tower beneath the mobile surface layer are actually slowly "sinking" or "flowing" downward both during construction and at equilibrium. We call this phenomenon the tower waterfall. Discovery of the tower waterfall proved that our initial assumption, that ants joining the tower remained in the same position indefinitely, was incorrect. The

discovery of a "flowing" tower also raised some important questions such as "what does the flow velocity field look like, what is the mechanism that initiates flow, and what happens to the ants flowing down when they get to the bottom of the containment dish?"

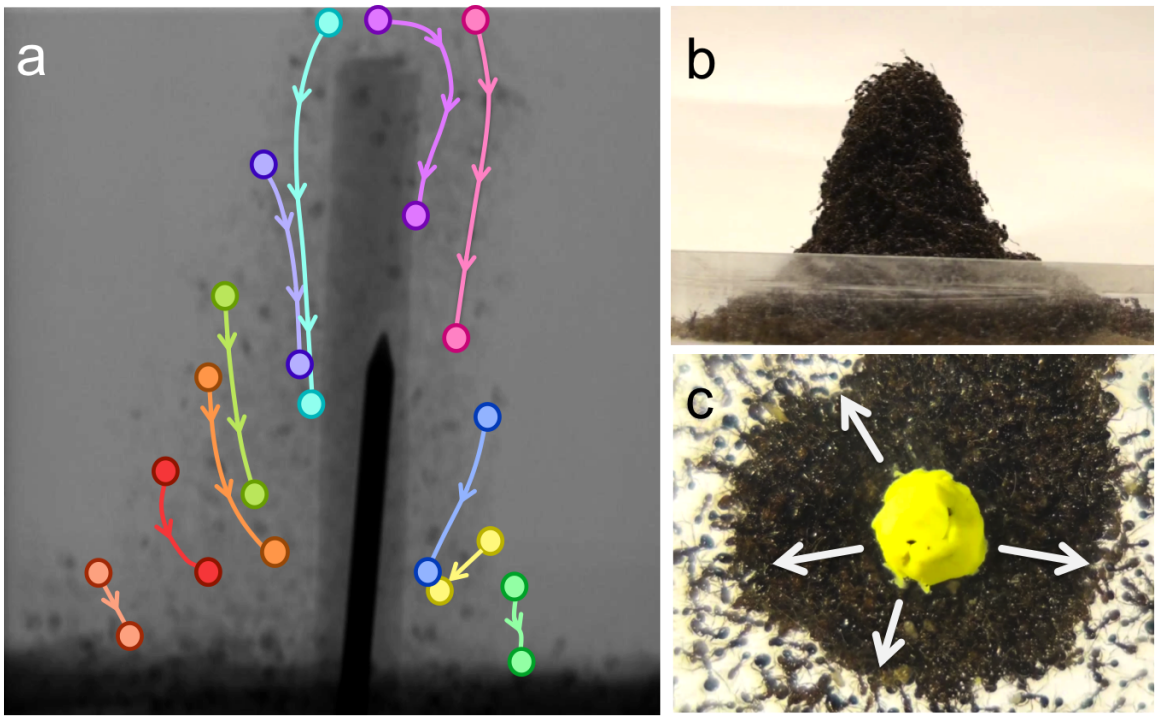

Figure 26: Ants are doped with iodine (according the methods shared by Dan Goldman and Darya Monaenkova) and tower building is observed with x-ray image capture, allowing us to track individual ants. We observe that ants in the tower "flow" down slowly over the entire process of construction. A single ant may sink the entire length of the tower in 40 - 60 minutes. (a) Here we show several representative ant pathlines from a 2.5 hour construction time as they sink in the tower. As ants sink they trend radially in toward the rod and join the central tunnel located around the rod. (b) Ants are allowed to climb a short rod until their tower covers the top. (c) A view from underneath this tower at equilibrium reveals that ants excavate tunnels in and out of the tower. White arrows show ant tunnels connecting the central tunnel around the rod to the outside of the tower. Ants walk in and out of the tower via the tunnels, but the net movement is out of the tower.

Because the tower is opaque, looking at the mobile surface layer of ants on the tower will reveal very little about how the tower is sinking inside. Using x-ray imaging, we can track individual ants inside the tower to answer our questions about where the ants are sinking. Iodine doped ants appear as dark spots in the tower, and tracking them during tower construction reveals the bulk downward flow rate of the tower. A time lapse of the x-ray can be seen in supplementary movie *Ant Tower X-ray Time Lapse* on Youtube. **Fig.26**a shows an x-ray image with sample ant pathlines overlaid from throughout the entire construction process and equilibrium. X-ray imaging confirms that all the ants beneath the

mobile surface layer flow slowly down at a rate of approximately 1 ant body length per minute. In addition, we found ants flow toward the rod as they sink.

While x-ray confirms the sinking of the tower, it doesn't answer the question of where ants go when they flow down. Because tower height doesn't change at equilibrium and we observe the tower still sinks, the ants must somehow be leaving the tower and climbing back up on the surface and joining the bulk of the tower again. Ants recirculate in a tower: they walk up the surface of the tower, become a fixed part of the tower at the top, sink down in the tower to the bottom, and leave the tower to start the cycle over again. At this point it was unclear how ants were leaving the tower. Also, we didn't know what was causing the tower to sink.

To investigate this phenomenon further, we filmed the tower from beneath. This revealed surprising behavior. Ants physically excavate tunnels beneath the tower, allowing ants access in and out of the tower. **Fig.26**c shows a view from beneath the tower at equilibrium with white arrows representing tunnels leading in and out of the tower. This behavior can be seen clearly in supplementary movie *Ant Tower Underneath Time Lapse* on Youtube, which is 130 minutes of footage time lapsed. The video reveals activity beneath the tower during the 60 minutes of construction and 70 minutes of tower equilibrium. During the tower construction phase, the height is constantly increasing. When the tower reaches the equilibrium phase, the height doesn't change, but there is still a lot of ant movement: ants on the tower surface are walking up and down, ants underneath the tower are walking in ant out via the excavated tunnels, and there is bulk flow downward within the body of the tower. The tower has reached an equilibrium, but is still full of activity.

Ants travel in and out of the tunnels, but we observe the net movement is leaving the tower. Similarly, ants travel up and down the tower, but the net movement is always up the tower. This is what contributes to the circulation. An ant that has added to the tower will eventually sink down towards the bustling tunnels at the bottom of the tower. At some point after it comes into contact with a tunnel, the ant will join a tunnel, transitioning from a stationary to a mobile ant, and is free to move about the tunnel system.

For further clarification **Fig.27** and **Fig.28** are two schematics illustrating the tunnel system that exists in the bottom of an ant tower. **Fig.27** shows side and top section views of the ant tower at three points during construction. The views at t=0 show the stationary sea of ants with mobile layer of ants on top. During construction, the ants begin to excavate tunnels in the center of the tower headed radially outward. By at least 20 minutes into the construction process, ants are able to move relatively freely in the bottom center of the tower as illustrated by the middle two views. By the time the tower reaches it's equilibrium height, the tunnel system is fully established, and ants are moving in and out of the tower and around the rod. Ants are still walking up and down the tower with net movement up. Ants that become fixed to the top of the tower, slowly sink down with the rest of the ants in

the bulk of the tower and eventually join with the ants moving in the tunnels. **Fig.28** is a pictorial view that illustrates the same concept as **Fig.27**, but provides further clarification.

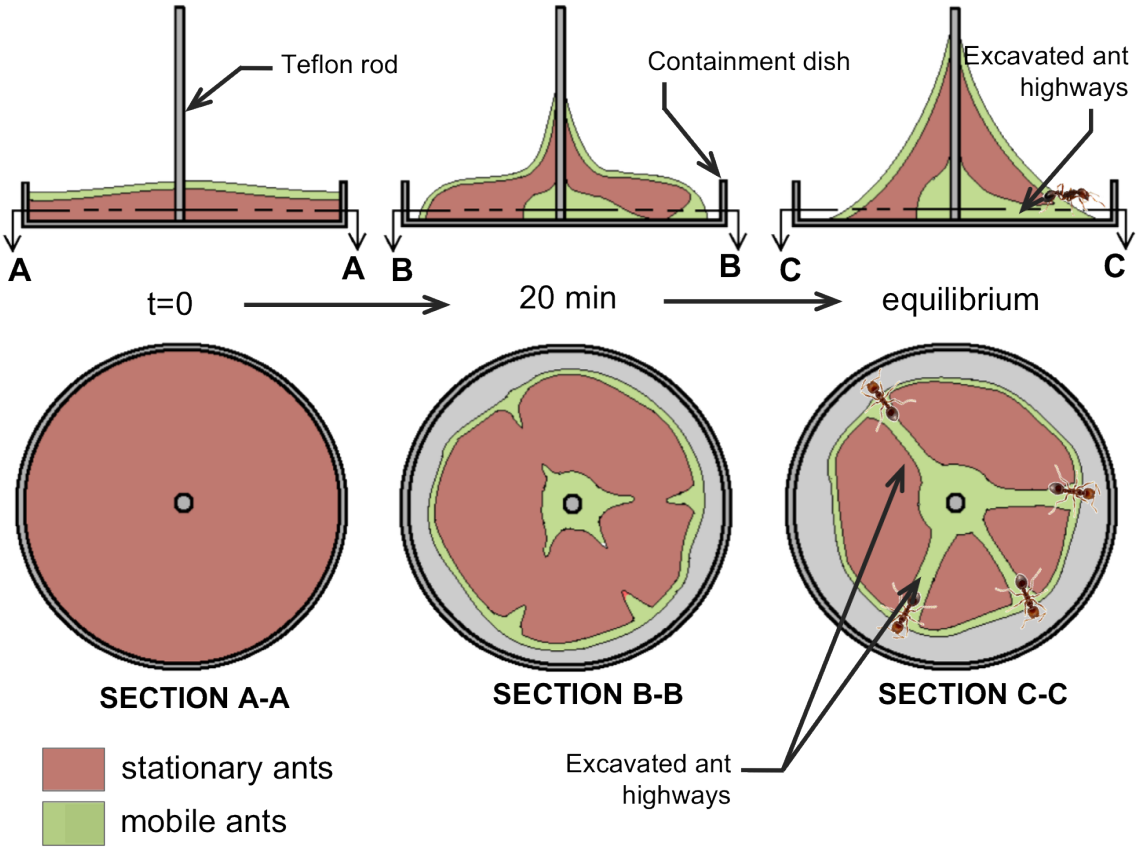

Figure 27: During the process of tower construction, ants excavate tunnels radially outward between neighboring ant bodies. At equilibrium, the tunnels are established and traffic flows in and out of the tower. The top row of schematics shows a side section view time progression of the tower and tunnel construction. The bottom row shows the corresponding top section views. The red regions represents "stationary" ants that do not actively move but rather slowly "flow" toward the central tunnel as a results of ants below joining the ant tunnel regions shown in green. The green regions represent mobile ants that actively move inside the tower and on the tower's surface.

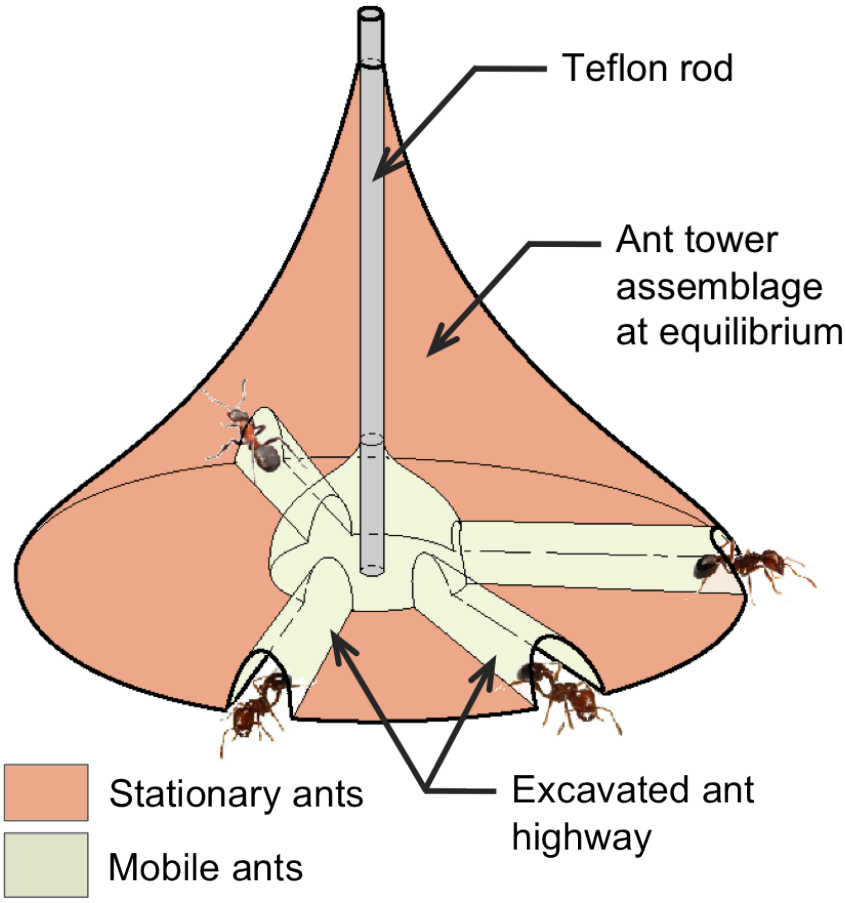

Figure 28: Shown here is a 3D wireframe schematic of an ant tower at equilibrium. During the construction process, ants excavate a region around the bottom of the rod. Ants then construct tunnels branching out radially from this central chamber allowing ants access in and out of the tower.

Furthermore, the tunnel excavation provides an excellent explanation for the two linear growth regimes as seen clearly in **Fig.24**a. The two regimes of linear growth are split at approximately 15 minutes of construction time. This is also when the tunnels are opened up and ants begin leaving the tower. In addition, this is also the time when the waterfall begins. Completion of the tunnels cut the tower growth rate by more than half.

5.3.6 A model to explain the linear growth rate

We begin by defining several parameters based on observations of the tower:

ρ density of moving ants on the surface of the tower in ants per cm^2.

v speed of moving ant on tower surface in cm/sec.

p probability an ant approaching the rod sticks versus bouncing off ant returning down the tower.

d distance ant travels before changing direction if it does not bump into another ant or reach the boundary first, in cm.

α number of ants an ant supports.

χ density of ants in tower in $ants/cm^3$.

ψ thickness of an ant layer, in cm.

s downward speed of ant waterfall in $cm/minute$.

g growth rate of tower height due to filling in empty space on rod in cm/sec.

T time at which waterfall starts in sec.

D diameter of the rod in cm.

R number of available spaces for ants to fill a ring around the rod.

Next we idealize ants in the tower as existing in one of two states: 1) *mobile* ants on the tower surface or in the tunnels at the base of the tower or 2) *stationary* ants that occupy the bulk of the tower but do not move relative to one another and slowly sink as a result of ants joining the tunnels. Ants in the tower attach to each other with tarsal claws and mandibles. Their locations relative to each other do not change (unless they depart the tower via a tunnel at the tower base as described below).

Ants on the surface of the tower move at speed v for distance d or until they bump into another surface ant or they reach the top of the tower. If they reach the top of the tower they stick with probability p and bounce with probability $1 - p$. If they bump into another surface ant they stick to it with some probability, thus forming clumps of relatively immobile surface ants. If the clumps violate the shape law by having more than w ants per ant, there is a small local collapse of the tower that reinstates the shape. When a surface ant stops moving, it rests for r seconds, then moves again in a random direction. If a mobile surface ant is on a part of the tower surface that is nearly vertical, its direction of movement is extremely likely to be either up or down. If the ant is on a roughly horizontal surface, as with the ant raft, its direction of movement is random, equally likely in all directions, as in the ant raft. It is much easier for an ant to stick to other ants than to the pole.

The ants have no idea that they are building a tower higher and higher. All they are doing is occupying the ring of empty spaces on the pole adjacent to the top of the tower. When that ring is occupied, there is a new ring available for occupation. Since it is relatively more difficult for an ant to stick to the pole than to other ants, the bottleneck in the growth of the tower is the occupation of empty spaces on the pole. The filling in of the rest of the tower is faster and not a bottleneck.

The shape law says that there are $n(i)$ ants at level i where $i = 0$ is the top level and $n(i+1) = n(i) + \frac{1}{w}n(i)$ because the ants on level $i+1$ must support levels 1 to $i-1$ which requires $n(i)$ ants by definition, plus supporting level i which requires $n(i)/w$ by definition. So if $n(0) = 1$ then $n(i) = (4/3)^i \approx e^{.29i}$. The key thing about the shape law is that once the tower reaches a height of k cm, the top k cm of the tower will from then on always have the same shape. This is true for all k. In particular it is true for $k \approx d$. Only ants within d cm of the tower top have a chance of filling in an empty space on the pole. So once the tower reaches a height of d the rate of growth of the tower height will be a constant. What happens more than d away from the top is irrelevant. Let g denote the growth rate caused by this behavior.

After T seconds ants start to leave the base of the tower via tunnels. The growth rate then decreases from g cm/sec to $g - s$ cm/sec. The prediction of the model is linear growth at rate g for the first T seconds followed by slower linear growth at rate $g - s$ thereafter until there aren't enough ants to make the tower bigger. The rate of growth is predicted to be independent of the number of ants, until growth stops. That is, if 5000 ants build an 8cm tower in an hour, then 10000 ants are predicted to have formed a tower of height 8cm after one hour.

We idealize ant movement on the tower in the following manner: Recall that R is the number of ants in a ring. R is proportional to the diameter of the pole. Partition the tower into R segments radially divided with R radial planes. The top layer of each segment has one ant, the ant in the ring on the pole at the top of the ant tower. The idealization is that ants stay within their segment. This is an approximation for what the ants actually do. Real ants mostly move radially but do a small amount of azimuthal (horizontal) movement. The number of ants in each segment follows the shape law.

For an estimation of g using values for other parameters see Appendix D. At this point, we have an explanation for why tower growth is linear and why it is broken into two regimes. Further work is required to verify the growth rates predicted by the model and the rates found experimentally.

5.3.7 Fitting our shape model to human towers

The activity of building human towers or pyramids has existed for hundreds of years. Human towers have been used in siege tactics, a competitive event, rituals for festivals, acrobatics in entertainment, or for bonding between friends. The Casteller groups in the Spanish Catalonia region are the most well known human tower builders, and have been around for centuries [128]. Other notable human tower traditions lie are those of the Chinese Bun Festival and the Hindu festival Krishna Janmashtami in Maharashtra, India where young men attempt to reach pots filled with curd and butter suspended high above the ground. The common threads that runs through all human towers are the structural tactic

of building a wide stable base, an inverse relationship between tower height and width, and placement of the strongest humans on the bottom of the tower. We investigate the shape of human towers and compare our results to our constant strength model.

We scour Google Image and wikipedia for any images we can find displaying human tower feats. We present tower shape results averaged from 30 different tower images with a representative showing seen in **Fig.29**. Tower shape is characterized by number of human layers high and half the number of humans wide in each layer. Our data includes towers of 3 to 10 layers high. To compare these towers of different height, we treat the top layer as layer 1, and the bottom as layer N_h. For all of the towers, we average the width for the corresponding layers. **Fig.30** shows the relationship for tower width and tower layer plotted against the model for two different α_h values. Here, α_h is the number of humans each human in the tower is supporting.

Figure 29: Human tower building traditions date back at least several hundred years. Human towers have been used for group bonding, festival performances, competition, and even siege tactics. Our model based on uniform stress in each layer provides a good explanation for the shape of human towers.

The results in **Fig.30** show that the model is a good fit and can explain the shape of human towers. On average each human in a tower is supporting α_h=2 other humans except when the tower reaches 9 and 10 layers at which point each human is supporting α_h 2.5 other humans. The strongest humans are put on the bottom of the tower and are supporting

more weight than the humans in the layers above them. Our assumption of slowly varying layers reaches its limit for a specific α_h value below layer n_h=8. To continue building such that load is distributed evenly throughout the layer, the bottom layers must take on more load than the top, thus explaining the "jump" in fit between α_h=2 to 2.5.

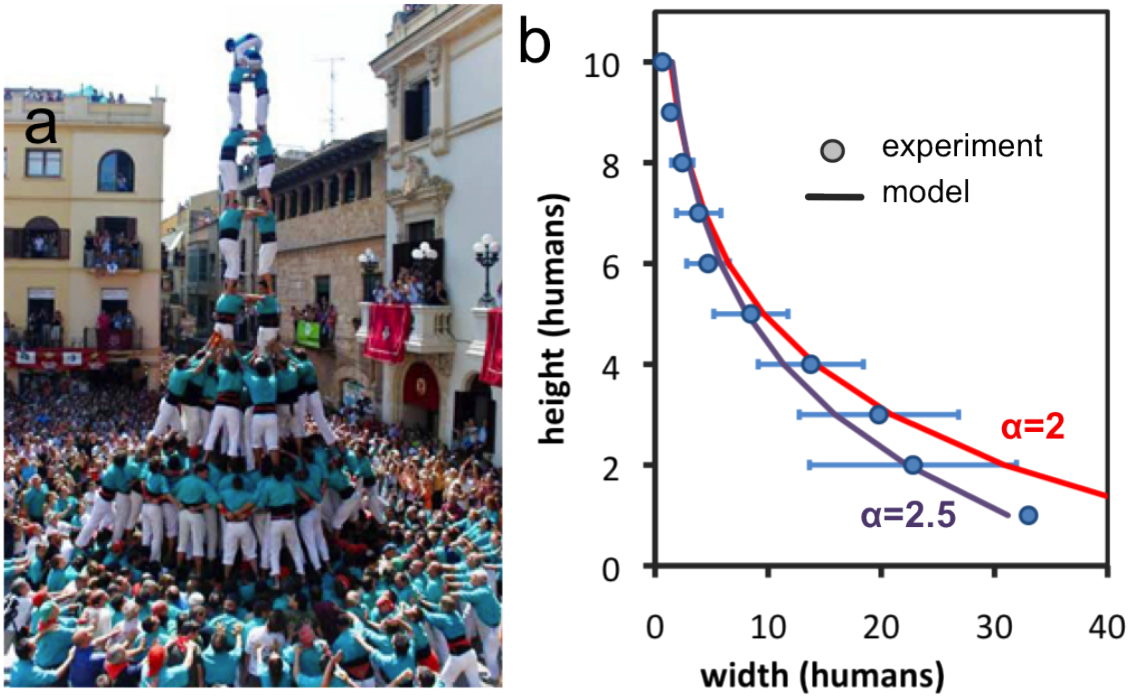

Figure 30: (a) Castellers de vilafranca from the Catalonia region in Spain have been building human towers for competition and entertainment. Formally founded in 1948, but having roots back to the 18th century, the Castellers are dedicated to preserving and promoting popular Catalan culture and history. (b) Here we compare the shape of human towers to our model using two alpha values. For towers less than 8 layers, each human supports α=2 other participants. For larger towers, α=2.5 fits the lower levels best, indicating that humans put the strongest on the bottom of the tower.

5.4 Discussion

A common thread throughout all stable towers is a wide base tapering with increases in height. A measure of this taper is of importance because it provides insight into how stresses are distributed throughout the tower. We find that on average ants build towers such that the stress at each horizontal cross section is the same. This means that the strength of each ant in the tower is the same as it's neighbors, and at equilibrium each ant supports 3.5 others.

If the tower profile were linear, then each ant in a layer would be supporting more load than each ant in the layers above. This is the case for any pile of granular media such as

sand, medical pills, or even dead ants. These substances have a maximum angle of the liner profile at which the material is stable called the angle of repose; if material is added to increase this angle beyond the repose, then material in the pile collapses and settles back to equilibrium. Dry sand has an angle of repose of 34°. Piles of active granular material such fire ant self-assemblages will not have a constant angle of repose, rather one that a function of height. We found profile ants for ant towers to range between 0 and 90°. We have discovered the relation between tower angle and height indicates equal load sharing among ants in the tower throughout the building process.

Prior to our studies on the ant raft we believed that ants in the raft must be circulating to allow the ones on the bottom to survive. Contrary to this initial assumption, our findings revealed that once an ant joined the bottom layer, it remained in position until the ants no longer needed to raft. Similarly, our initial assumptions about the ant tower were revealed to be faulty after a thorough investigation. Initially, we believed that ants in a tower remained in position, until the tower was disassembled. However, observing a time-lapse of the tower construction from the side and the bottom reveal ants excavate tunnels radially outward from the rod at the base of the tower. This results in the waterfall effect and a circulation of ants in the tower.

To further compare our current findings on fire ant tower construction to our previous findings on raft construction [17], we observe that tower growth rate is always linear. Conversely, the growth rate of the raft is never linear, but is rather a complex function that depends on the number of mobile ants atop the raft. The raft does not grow linearly because the frontier where ants add to the raft edges is always growing. On the other hand, the tower growth rate is linear because the frontier where ants add to the top of the tower around the rod stays the same shape.

We now know that the function of ant towers is to act as a bivouac for the colony– providing shelter for the colony when no other option is available. While we did not include a queen in the experiments, we believe that the chamber around the rod as seen in **Fig.28** would serve as housing for the queen. Most of the other ants in the tower compose the bulk of the tower. The excavation of tunnels at the base of the tower sheds light on an important observation that ants next to a solid surface are able to move with respect to one another even if they are beneath other ants.

Besides offering shelter to ants that have an affinity for covered, dark areas, we find that ant towers are very water-repellant. Extrapolating from our previous findings on the hydrophobicity of linked ants [17], we test tower water-repellency by water droplet impingement. Falling over 24 inches, a drop splashes on the side of the tower, coalesces on the surfaces, and rolls off. While the tower clearly keeps water out, it is also possible that the tower may aid in reducing moisture loss by frustrating evaporation and by providing the ants a place to remain still. Desiccation is a serious concern for ants, and we have

observed that static ants remain alive much longer than highly active ants when removed from a water source.

When the experiment begins, the mobile ants begin to explore their limited environment, finding that the rod in the middle is the only new explorable area. During the first few minutes of the experiment, as the ants discover the rod in the middle, some begin to explore the walls of the petri dish as potential escape routes. We prevent the ants from building towers up the walls by manually knocking down the mini ant towers that form on the dish walls. This is only required for the first one or two minutes of the hour long process until the ants establish a tower on the rod, at which point the ants no longer attempt to escape up the walls of the dish.

We observe periodic collapses and rebuilding of the tower that may help maintain the shape and limit the rate during building process. These collapses are caused by uneven weight distribution when ants hurriedly crawl to the top of the tower; a process analogous to sand running down a pile while being poured. Often collapses that occur near the top of the tower will propagate down like a wave. All of these observations play a role in regulating the building process so that equal strength is an emergent property.

In our approach we have made several assumptions for ease of analysis. One assumption is that the tower is composed of discrete layers, but in a real ant tower this is not the case. While we do see the majority of ants faced vertically as they add to the tower, there is no way to make a clear distinction between one layer and the next. To carry out the analysis using the model, we discretize the tower into layers of one ant height. This does not create a problem, because even in the limiting case in which the tower is viewed as a continuum with material property density ρ, we find that for uniform stress distribution, tower cross-sectional area should increase exponentially from the top down. This is exactly what we find for the ant tower, and the uniform stress model still holds.

Our model also holds for towers humans build by self-assembling. While we find that humans place the strongest on the bottom of the tower, as backed by our data for the tallest human towers, we don't find the same behavior in ant colonies. While the largest ants are indeed several orders stronger than the smallest ants, large and small ants do not have location preference in a tower.

Our findings for human and ant strength in a tower do have biological significance in explaining strength tolerance. The strongest humans in the tallest towers can temporarily support the weight of 2.5 neighbors above them; while in shorter towers, each participant in level $n < \alpha$ can temporarily support the weight of 2 other humans. This temporary strength constant is close to the maximum strength in humans and provides insight into the limits and tolerance of human strength and endurance levels when working toward a common goal. On the other hand, the strength of each ant in the tower is many times less the maximum strength of an ant both in tension and compression. Ants in an assemblage

will support near their maximum strength on short time scales, but will rearrange to lessen the load. We propose then that α=3.5 at equilibrium is the maximum value that fire ants will support indefinitely in a tower assemblage without rearranging. In addition, ants do not exercise their maximum strength because the function of the tower as suggested by the tunnels is to provide temporary shelter for the colony.

Gravity may be the ultimate force at work to regulate ant behavior and in turn tower shape. Ants were the subjects of gravity altering tests when a small group of harvester ants were sent above the earth's atmosphere aboard a shuttle. The project aimed to see how ants behave in zero G, and counter to predictions, the ants "tunneled like crazy" and were hyper active. We expand upon this idea by manipulating gravity in our lab. We subject the entire tower building process to increased gravity and observe the results.

A tower is attached to a centrifugal device that can be ramped up to exert ten times earth's gravity. We calculate g force on the tower by observing the deflected angle while spinning. When subjected to 6g, the ants don't build a tower at all, but rather remain motionless and the entire cluster is flattened uniformly to the bottom of the petri dish. We cut back down to a 10% increase in gravity and find that ants do build towers that fit our model, with α lower than 3.5 as expected. With a 10% increase in gravity, we expect to find a 10% decrease, but instead we observe a drastic drop down to α=1.2.

5.5 Conclusion

The most important finding of this study is that ants repeatedly build towers such that load is uniformly shared by each ant. The process takes places without centralized intelligence; none of the ants have an overall plan for the tower, but are rather only responding to local cues. Out of these fine-tuned behavioral algorithms emerges a versatile and adaptable superorganism. Individuals act alone, but behaviors compound to carry out group tasks or build a larger functional structure.

We compare the shape of the ant tower at equilibrium with a constant strength model finding the fit is excellent with an ant strength of α=3.5 neighbors. We also find *during* the construction process the ants maintain a shape that uniformly distributes stress, but the load carried by each ant increases during the construction process until the tower reaches its equilibrium point of each ant supporting 3.5 neighbors. We propose that α is the biological limit that fire ants will support indefinitely in a tower assemblage.

The tower structure we observe is a fully operational bivouac, much like the bivouacs built by army ants. The center of tower acts as a holding chamber for brood, and tunnels lead radially away offering a path in and out of the bivouac. X-ray and observation from beneath reveal the tower is far more dynamic that simple observation of the surface can reveal.

We have provided a model that explains the linear growth observed in the tower. The

bottleneck process in the tower is filling in the space around the rod at the top of the tower. Because the rod does not change diameter, and the top of the tower never changes shape as it grows, the observed growth is linear. We have defined parameters and a model to predict growth rate, but have yet to compare the values to the observed tower growth rate.

CHAPTER VI

ANT RHEOLOGY

6.1 Introduction

Rheology is the study of the flow of complex and non-Newtonian fluids [129]. Such fluids have a complex molecular structure that results in a coexistence of fluid and solid properties– referred to as viscoelastic [130]. These substances respond to stresses with a mixture of stored (or elastic) energy and lost (or viscous) energy [131]. Some everyday examples of these substances are shaving cream, silly putty, ketchup, paint, or a corn-starch and water mixture. Other examples include some polymeric liquids, solutions, emulsions, biological gels, and body fluids. Rheology has direct applications in materials science engineering, geophysics, physiology, biology, and pharmaceutics. The characterization of viscoelastic properties in the production and use of polymeric materials has been important in the manufacture of many products used in both the industrial and military sectors.

The study of the linear and nonlinear rheological response of these complex fluids is of great interest to researchers because complex fluids are prevalent in consumer products, military research, and medical practice. While the flow of Newtonian fluids is generally understood, Newton's law of viscosity is inadequate for describing macromolecular (or polymeric) liquids [132]. While various isothermal flow experiments performed on a Newtonian fluid yield a single viscosity, these same kinds of experiments performed on a complex fluid will result in a host of material functions that depend on shear rate, frequency, and time. Some of these material functions include viscosity, normal stress coefficients, stress ratio, elastic and storage moduli, and creep compliance. To solve flow problems involving a complex fluid such as a polymeric liquid, rheologists may adapt the generalized Newtonian constitutive equations for a solution. More effective though has been the use of models developed empirically.

Rheologists perform stress-strain experiments on complex fluids using a device called a rheometer as shown in **Fig.31**a. A rheometer transfers torque to a fluid using plate-plate, cone-plate, or Couette geometries. These torques are converted to measurable strains using a transducer. Typical protocol for investigating new substances involves determining the limits of the linear viscoelastic regime and critical stress/strain values using amplitude and frequency sweeps with oscillatory torques [133]. Often times, during a stress/strain sweep, results show that the substance responds in a nonlinear manner. These nonlinearities often arise from inhomogeneities in the substance, or rearrangement of particles during shearing, and demand a different set of experimental procedures and results analysis.

Within the past 15 years, a few rheologists have begun to express an interest in the rheology of a highly nonlinear rheological material called active matter. Active matter consists of particles that convert energy into movement [47, 48]. Most of the rheological studies of active matter involve particles on the scale of bacteria or proteins in a fluid [134–136]. A theoretical study by Hatwalne *et al* investigated the activity, order, and flow of active, energy dissipating particles. Using a set of coarse-grained hydrodynamic equations, the authors make predictions for the rheology of these systems that can be tested using bacterial suspensions, cell motors, or even artificial machines in a fluid [136]. In 2002 a study by Coussot *et al* found that when typical yield stress fluids are stressed, they begin to flow like avalanching granular materials [137], a behavior we have clearly observed in fire ants.

We approach our rheology studies on groups of live linked ants with the perspective that they are an active material with bulk continuum properties. Ants have been observed to push and pull, as well as reverse their direction for short spurts. We perform rheological measurements to determine if fire ant assemblages can be classified as a viscoelastic behavior, and if so what kind of model best describes their viscoelastic response.

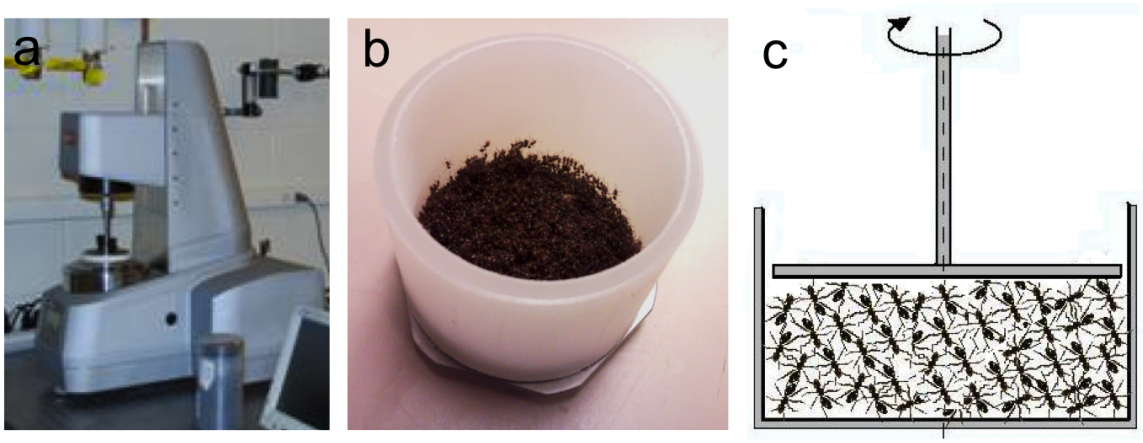

Figure 31: (a) Plate-Plate schematic showing ants between the plates and annulus barrier to prevent escape. (b) Ants are placed inside the annulus wall and on top of the bottom plate. Both plates are covered in velcro to ensure no-slip condition at the plate walls. (c) A rheometer is typically used to measure rheological properties of non-Newtonian and complex fluids. We adapt a rheomter to measure a novel complex fluid: linked live ants.

6.2 Methods

6.2.1 Setup

We adapt an Anton Paar 501 rheometer using a 50 mm diameter plate-plate configuration for use with fire ants as illustrated by a schematic in **Fig.31**b. Both top and bottom plate are covered with velcro to ensure a no-slip condition at each plate. We test this by measuring

ant adhesion to velcro and to neighboring ants, finding that ant adhesion to velcro is an order of magnitude larger. A thin walled annulus with inner diameter 50.4 mm is placed around the bottom plate to keep the ants contained as seen in **Fig.31**c. 5 mg of ants are collected and placed into the container, and the top plate is subsequently lowered to reach a gap size such that normal force against the top plate is 0.18 N. During tests, ants may "settle" and lower the normal force. We then lower the top plate until normal force is restored to 0.18 N.

6.2.2 Controlled shear rate (CSR) test

Shear rate $\dot{\gamma}$ of the top plate is specified and maintained, while viscosity and shear stress response of the ants are recorded during the test. We perform the following two sets of CSR tests: (1) shear rate $\dot{\gamma}$ increases from 0.01 s^{-1} to 10 s^{-1} then decreases back to 0.01 s^{-1} and (2) shear rate $\dot{\gamma}$ increases from 0.001 s^{-1} to 100 s^{-1}.

6.2.3 Yield stress test

A shear stress τ slowly increasing from 0.01 Pa to 500 Pa is applied to the ant assemblage, while the shear strain γ of the top plate is recorded as measured by displacement of a point on the top plate perimeter.

6.2.4 Strain relaxation test

A stress relaxation test abruptly applies a constant strain rate for a set time and measures the material's corresponding stress response. We conduct five sets of tests with strain γ=2, 5, 10, 20, and 40 % for 1200 sec. Strain is measured as a percent of plate gap and we apply a strain uniformly for the duration of the test.

6.2.5 Oscillatory strain amplitude sweep (OSAS) test

A strain amplitude sweep test sweeps through a range of strain rates $\dot{\gamma}$ [s^{-1}] while oscillating a fixed frequency ω [rad/s]. Strain rate is defined as the displacement of a point on the top plate perimeter given as a percentage of the gap between the top and bottom plates. We run the following two OSAS tests: (1) strain rate $\dot{\gamma}$ is ramped from 0.01% to 10% at frequencies ω = 0.1, 1, and 10 rad/s; (2) strain rate $\dot{\gamma}$ is ramped from 0.01% to 100% at frequencies ω = 0.1 rad/s. We exclude a frequency of ω = 10 rad/s here because the high strain rate combined with the oscillation rate will kill the ants.

6.2.6 Oscillatory frequency sweep (OFS) test

A frequency sweep test sweeps through a range of oscillation frequencies while at a fixed strain amplitude γ. We perform the following OFS test: frequency ω ranges from 0.1 to 100 rad/s at strain amplitude γ = 0.1, 1, and 10%.

6.2.7 Creep recovery (CR) test

A constant torque T or shear stress τ is applied to the ants for a specified time followed by zero torque, while shear strain is measured throughout. We record 3600 seconds of zero shear stress creep initially as a reference. We follow this with the following two CR tests: (1) constant torque $T = 0.1$ mNm or shear stress $\tau = 4$ Pa is applied for 600 seconds followed by zero torque for 1200 seconds and (2) constant torque $T = 1$ mNm or shear stress $\tau = 41$ Pa is applied for 150 seconds followed by zero torque for 450 seconds.

6.2.8 Preparing tests with dead ants

We freeze 3.5 g of ants with liquid nitrogen and gently untangle any incident connections. We allow ants to thaw, but not to desiccate. The dead ants are placed between rheometer top and bottom plates with normal force felt by the top plate of 0.18 N.

6.3 Results

Ants in an assemblage can *flow* and are physically entangled much like polymer chains in a polymeric liquid or solution (**Fig.32**). Polymeric liquids are composed of chains of two or more carbon structural units, and they can exist naturally or synthetically. Ants in an aggregation link to one another using claws at the ends of their legs. Similarly, polymer chains often branch at the ends creating a hook that can resist shear when linked to nearby chains [132]. Entanglement of both chains in polymeric liquids and legs in ant assemblages result in non-linear responses when sheared.

The single most important characteristic of polymeric liquids is that viscosity is dependent on shear-rate. These fluids can be categorized as either shear-thinning of -thickening depending on the sign of the relationship. Most polymeric liquids are shear-thinning, meaning that as shear-rate increases, the viscosity of the fluid drops, and the inverse relationship for shear-thickening. Almost all polymeric liquids are shear-thinning, and there are only a few reported examples of polymer solutions that exhibit shear-thickening behavior. These are characterized by concentrated suspensions of very small particles.

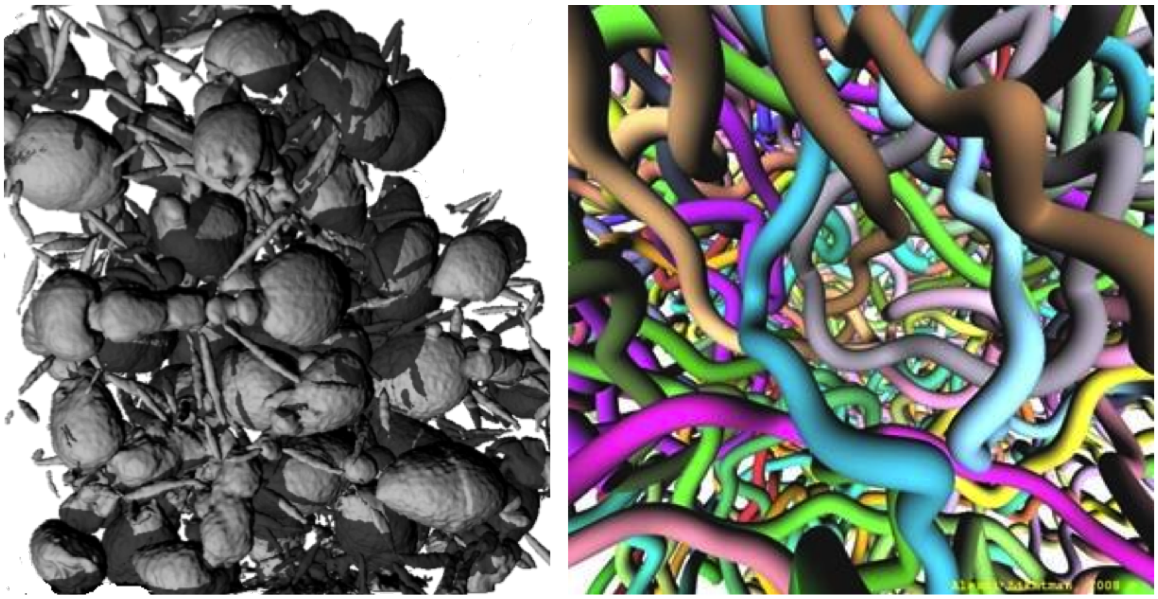

Figure 32: Ants and polymeric liquids can both be categorized as rheological fluids. Polymer chains and ant legs physically entangle when grouped together, resulting in non-newtonian flow characteristics when sheared. Ants also actively attach to one another using their legs. The polymer chain image is borrowed from Alexei Likhtman's website, professor of mathematical physics at the University of Reading.

6.3.1 Controlled shear rate test

We subject fire ant assemblages to controlled shear rate (CSR) tests to reveal if there is a clear thinning or thickening response. We run two experiments. The first increases shear rate $\dot{\gamma}$ from 0.01 s^{-1} to 10 s^{-1} and then back to 0.01 s^{-1}. In the second we increase shear from 0.001 s^{-1} to 100 s^{-1}. The results are shown in **Fig.33**. In both tests, viscosity decreases and shear stress increases with increasing shear rate. Viscosity drops several orders of magnitude during the test, which is not unusual as the decrease in viscosity for polymeric liquids can often be dramatic, spanning several orders of magnitude as well. We find that the trends are the same for increasing and decreasing shear rate, indicating that ant viscosity is time-independent.

The Otswald-de Waele model or "Power Law" model is a useful empiricism for non-Newtonian viscosity, and is given by

$$\eta = m\dot{\gamma}^{n-1} \tag{11}$$

where η [Pa·s] is fluid viscosity and shear rate $\dot{\gamma}$ [s^{-1}] is defined by the ratio of distance traveled by a point on the upper plate perimeter and plate gap per second. The two parameters in the model are m, sometimes referred to as the "consistency index," and n, the "power-law exponent" since it describes the slop of η. When fit to our experimental data, we find m=151 and n=0.14 with R^2=0.99. These values are comparable to aqueous

solutions of hydroxyethylcellulose polymer chains with $m \approx 100$ and $n \approx 0.18$ [132].

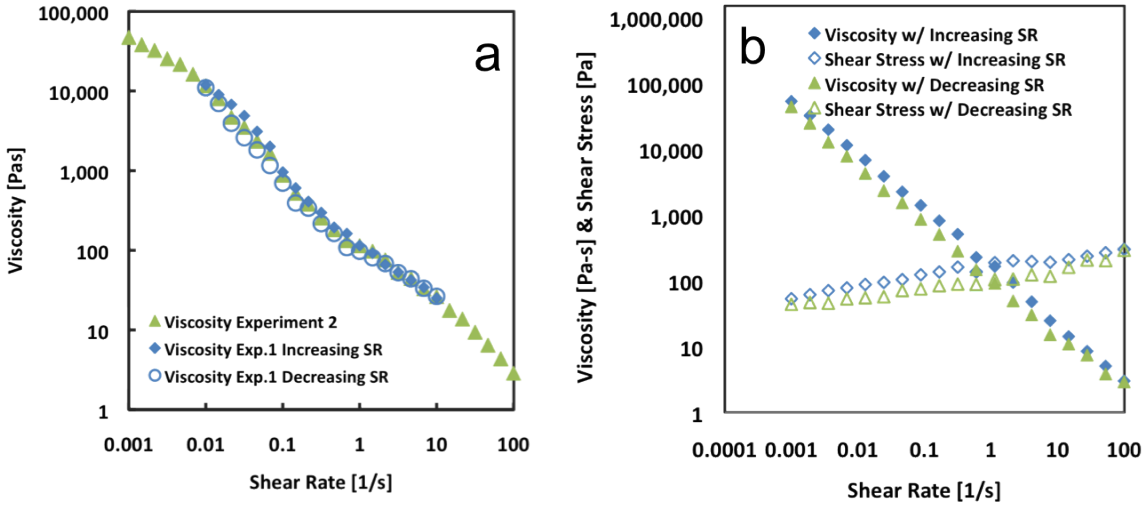

Figure 33: (a) Live ant assemblages are shear-thinning: as shear-rate increases, the viscosity increases. The viscosity's shear-rate dependence is time independent as seen by the matching increasing and decreasing shear rate data. Viscosity spans several orders of magnitudes, which is not uncommon for shear-thinning rheological fluids such as polymeric solutions. (b) Dead ants span a similar range as live ants, but the results are more uniform. In addition, the shear stress increases as shear rate increases.

6.3.2 Yield stress test

The active rearrangement and active applied stresses of fire ants can be seen clearly in the yield stress results shown in **Fig.34**. Negative shear strain results for low applied shear stress because ants are actively rearranging between the plates and actually "reverse" the direction of the top plate. This activity accounts for the highly nonlinear results for stress less than 10 Pa, indicating that at stresses this low, ants are virtually "unaffected". This is extremely unusual behavior for a rheological fluid. In theory, shear strain should stay at zero, until the applied shear stress exceeds the yield stress of the testing material.

It isn't until stress reaches 10 Pa that the strain response is more ordered, increasing slowly, indicating a yield stress $\tau_y \approx 10$ Pa. The strain still increases slowly because of the viscous nature of linked ants. At an applied shear stress of around 500 Pa, we see a spike in the strain, indicating that the ants can longer hold the plate, and little resistance is seen in the plate. This can be compared to material failure such as breaking or cracking because at this point, linkages between ants begin to break, and ant the applied forces are more than the ants can resist.

In the yield stress tests we found $\tau_y \approx 10$ Pa. Our creep recovery tests support this yield stress value with independent tests showing yield stress between 4 and 40 Pa. Ants begin to "flow" under relatively low shear stresses as most solid materials have yield stress

hundreds of orders of magnitude higher, and even relatively "soft" materials such as clay or toothpaste with yield stress an order of magnitude higher.

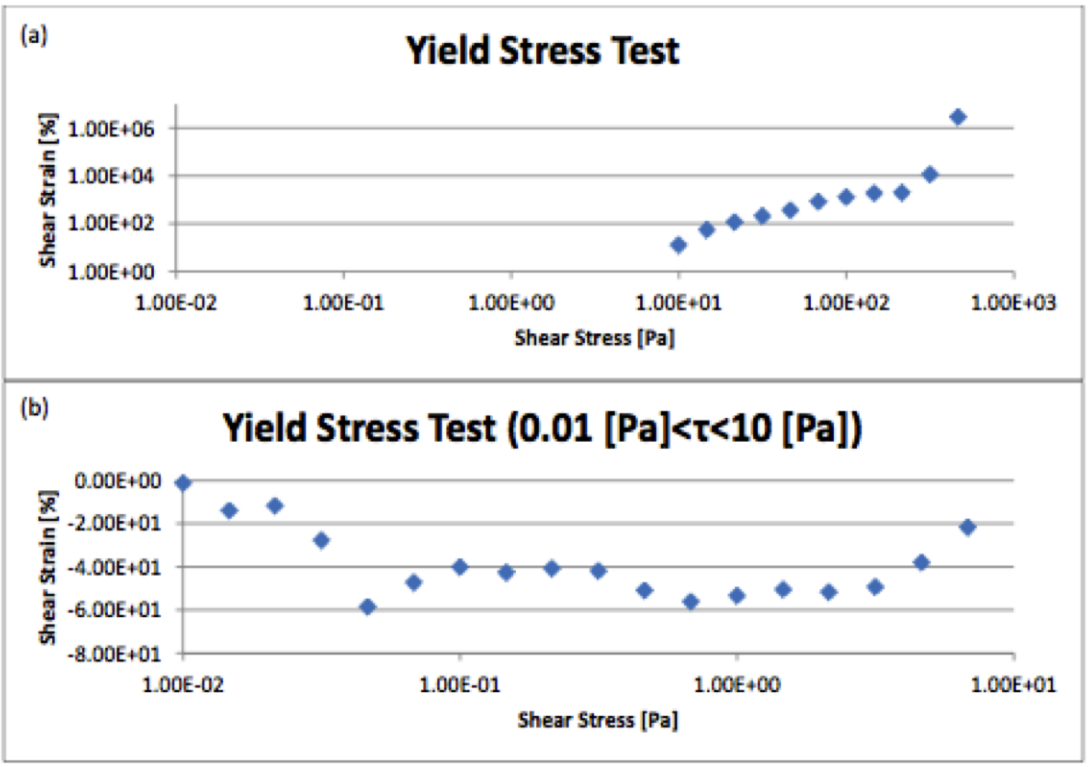

Figure 34: A cluster of over a thousand linked ants is sheared with shear stress τ and the resulting shear strain of the top plate γ is recorded. At low shear stress, ants are virtually unaffected. In fact the results show negative shear strain because the ants actually reverse the direction of the applied shear stress: a sign of active rearrangement despite the confinement of the plates. The yield stress for the ants is approximately 10 Pa. At this point, the ants begin to flow. At approximately 50 Pa the ants are torn from their neighbors.

6.3.3 Strain relaxation test

When a constrain strain rate $\dot{\gamma}$ is applied over a time interval Δt, the result is a total strain $\gamma_0 = \dot{\gamma}\Delta t$. We vary total strain γ_0 from 2 to 40 %, finding that the results are very similar to characterizations of some high concentration polymeric solutions and melts. Shear stress jumps up quickly and then slowly relaxes back to a low value. We find that even after the time interval Δt has ended and the top plate is no longer sheared, the shear stress applied by the ants is not zero, but rather maintains the same value as just before the shear was removed. This is to be expected and actually confirms that the ants did relax back to their steady state value during the test. Given a long enough time interval, most polymeric solutions would relax back to a state of zero stress, thus also the top plate would experience no change in stress measured. Further, we find that when increasing total shear γ_0, the

resulting shear stress function can be superimposed by vertical shifting to match the general shape of the shear stress functions at lower total shear. This is also a characteristic of some concentrated polymer solutions and melts [132].

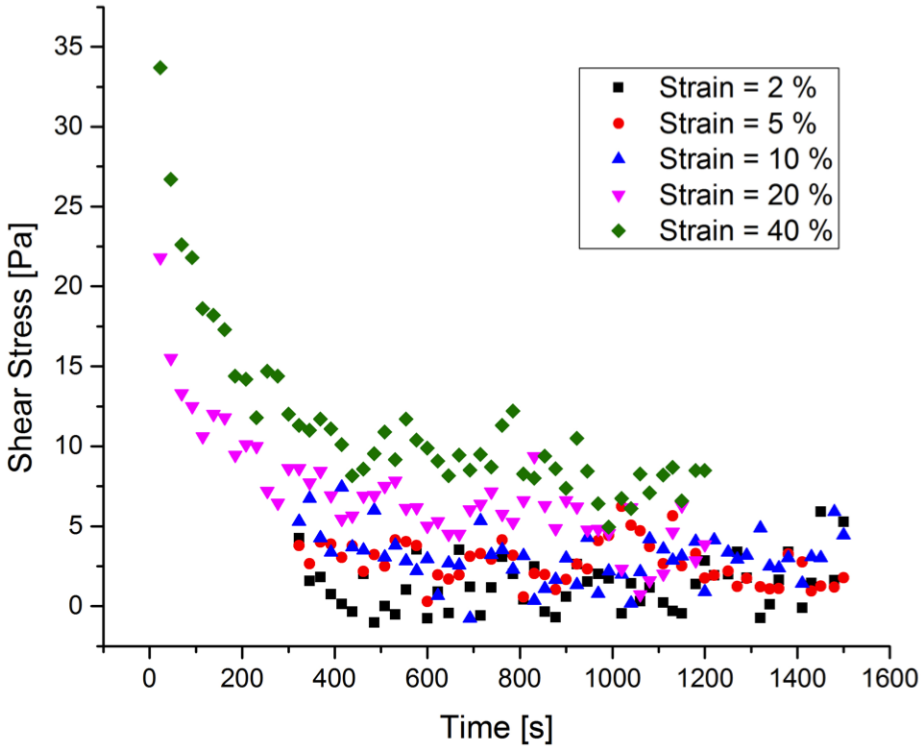

Figure 35: During a strain relaxation test, ants respond much like some polymeric liquids would. When a strain of 40% plate gap is applied over 1600 seconds, the stress response of the ants is high initially, but quickly drops and levels off to a lower constant value, indicating constant shear responses much like the stress response from a fluid in shear. When total strain is lowered below 5% the ants do not respond.

6.3.4 Oscillatory tests

We perform two types of oscillatory tests on the linked fire ants to probe the limits under which liquid or solid properties are evident. Results are seen in **Fig.36**. When frequency or strain is small, then the resulting storage (G') and loss (G") moduli are highly nonlinear because the ants do not respond to such small perturbations. But as frequency and strain are increased in each test, the moduli responses become more ordered around frequency ω=10 rad/s and shear strain γ of 1%. After frequency and strain cross these thresholds, the two moduli have almost equal value, a type of behavior that is extremely rare. This means that the ants are storing and dissipating the same energy values during all oscillation conditions. Typically, a storage modulus that is larger than a loss modulus means the material is behaving as a solid under the particular test conditions by storing more energy than it dissipates, and in the reverse situation, the material is behaving as a fluid and

dissipating more energy than it stores. For the fire ants we see that they are behaving no more like a viscoelastic solid than they are a viscoelastic fluid.

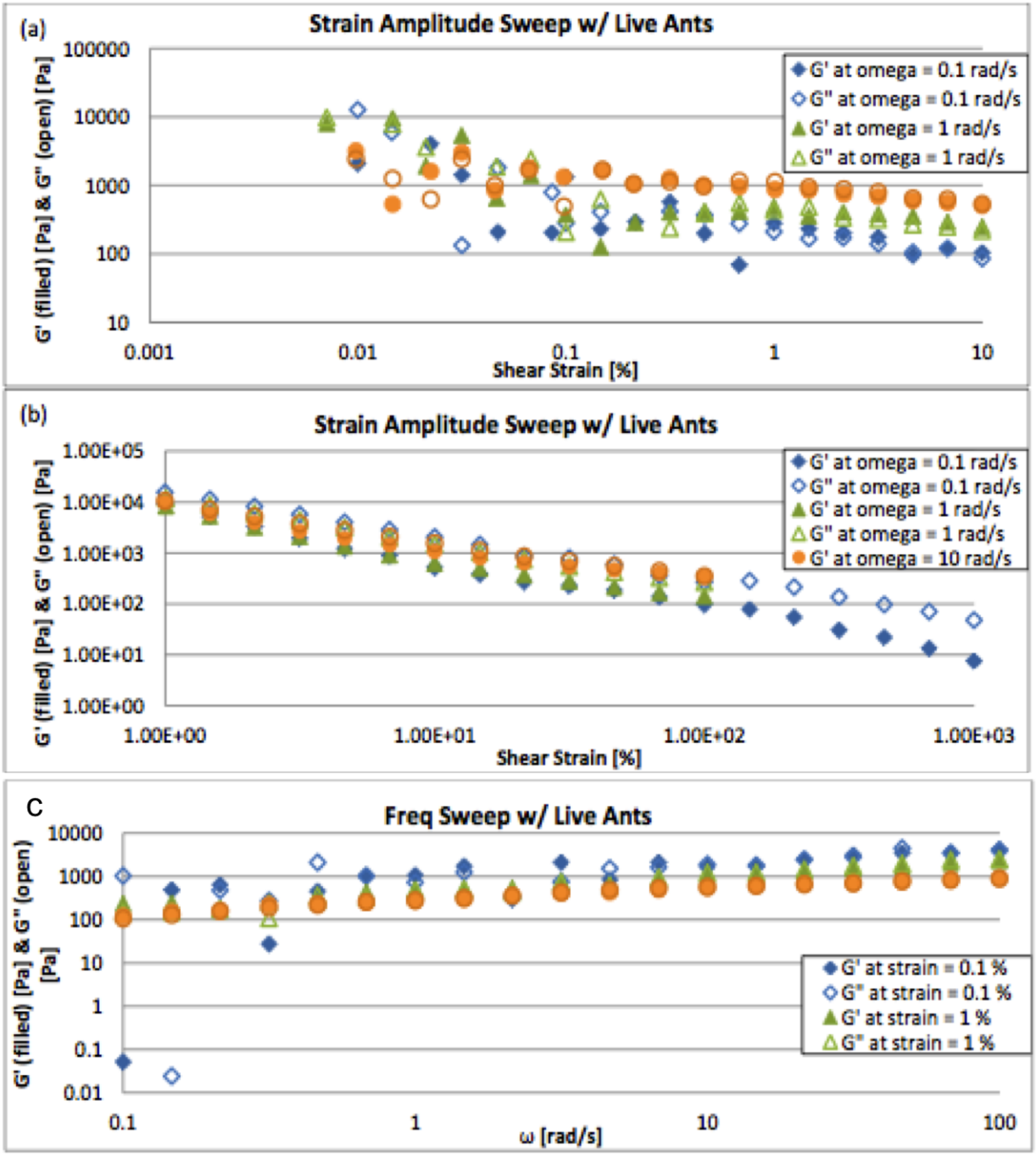

Figure 36: Using (a & b) amplitude and (c) frequency sweeps, the limits of the viscous and elastic responses of linked fire ants are probed. Live ants exhibit a rare behavior in which their storage modulus (G') and loss modulus (G") have approximately the same value over three orders of magnitudes of frequency and two orders of magnitude of strain, indicating that the ants are neither fluid nor solid.

6.3.5 Creep recovery test

Creep and creep recovery tests are useful for determining yield stresses and measuring energy stored by a material when it is sheared. As a reference we measure the deflection of the top plate under a zero stress condition as seen in **Fig.37**a. Typically a non-active rheological fluid would not deflect the top plate, but in our case, because they ants are actively rearranging between the plates, we see deflection of the top plate around 8 degrees in 1000 seconds. Since the radius of the top plate is 2.5 cm, this means a max deflection of only about 1 ant body length. This results is still surprising since we would expect a net zero deflection if the ants are moving randomly.

Fig.37b shows a similar behavior to zero stress when we actually apply a small 0.1 mNm torque or 4 Pa shear stress. Because the results are so similar we can conclude that the such a small stress is negligible and the ants do not respond. In fact, just as in the zero stress condition, ants in the 4 Pa condition occasionally reverse the direction of the top plate. Additionally there is no recovery deflection when the stress is removed, indicating that the ants were not storing any energy, but that it was lost during their movement between the plates. This further indicates that such low shear stresses have a negligible effect on the ants.

This is further supported by the results seen in **Fig.37**c when we apply a larger 1mNm torque or 40 Pa shear stress to the ants. In this result, we clearly see a more typical strain response characterized by an initial "glassy" response followed by a brief nonlinear strain increase at a decreasing rate. A "glassy" response is a quick initial jump in the deflection angle due to reaching the yield stress of the complex material. This is then followed by a linear deflection increase. The "noise" in the data is gone, and there are no reverse deflections showing the ants are flowing under the applied stress. Furthermore, when the stress is removed, there is an immediate and distinct recovery deflection showing an elastic response due to the energy stored by the ants during shearing.

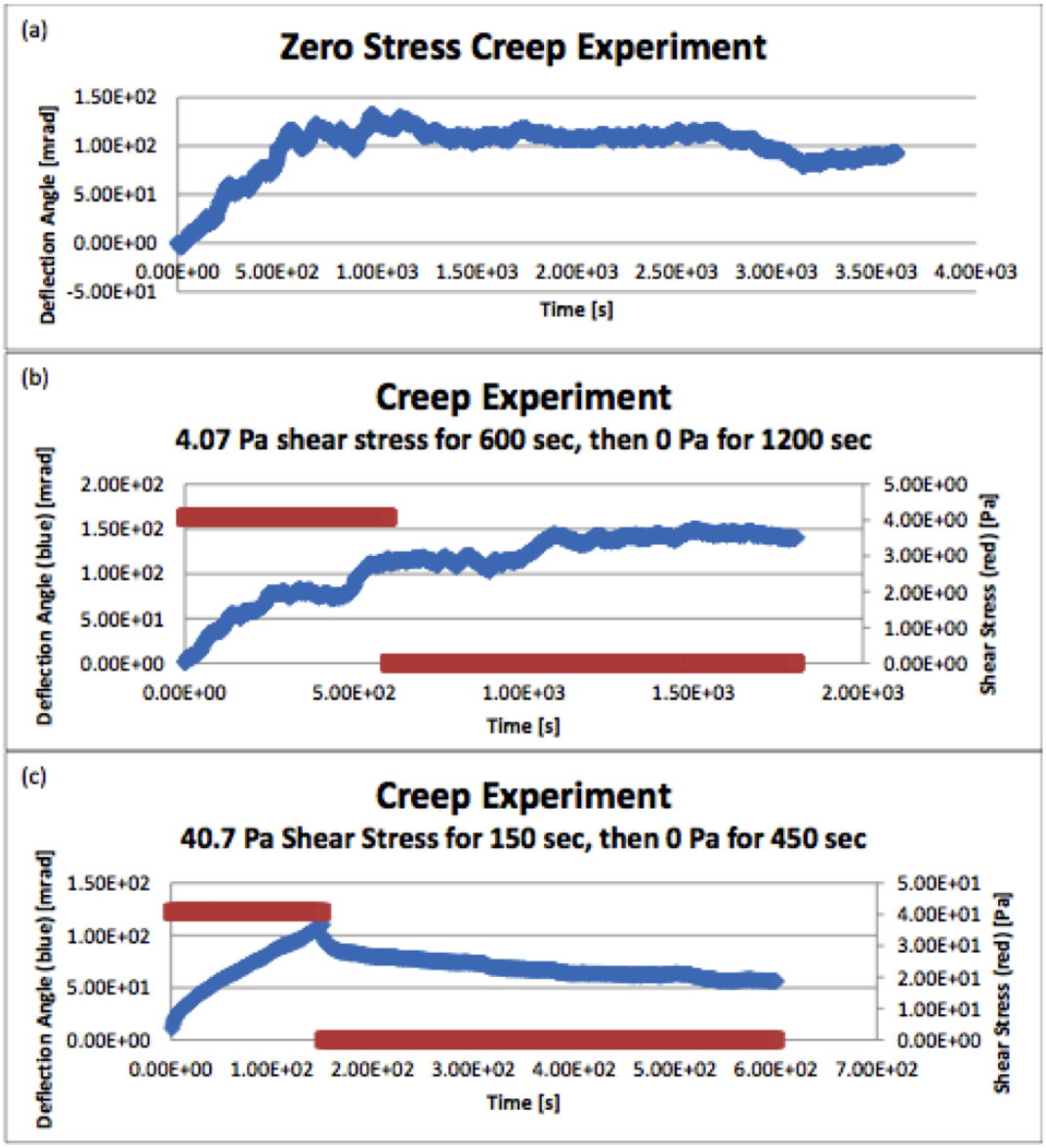

Figure 37: (a) The deflection response of the top plate when zero stress is applied is tested. Surprisingly, the ants move the plate 8 degrees or a maximum arc length of around an ant body length. This provides a good reference and reveals that at a small applied shear stress of 4 Pa (b) the ants are unaffected. We find that by 40 Pa of stress (c), the ants are sheared and even recover some deflection because of stored energy.

6.3.6 Comparing rheology of live and dead ants

We compare the viscoelastic response of live to dead ants, and find that dead ants behave more like a viscoelastic solid for the entire range of oscillation in the frequency sweep as seen in **Fig.38**. G' is well above G" for all strains tested as well. Bonds between individual ants are only incidental and result from occasional leg and body entanglements. Despite this, the bonds are weak, and cannot be actively reformed as in live ants. As such dead ant

aggregations can be treated as granular solids rather than a viscoelastic fluid. While live ants cannot clearly be modeled as a viscoelastic fluid, they also cannot be classified as a viscoelastic solid as we illustrated previously.

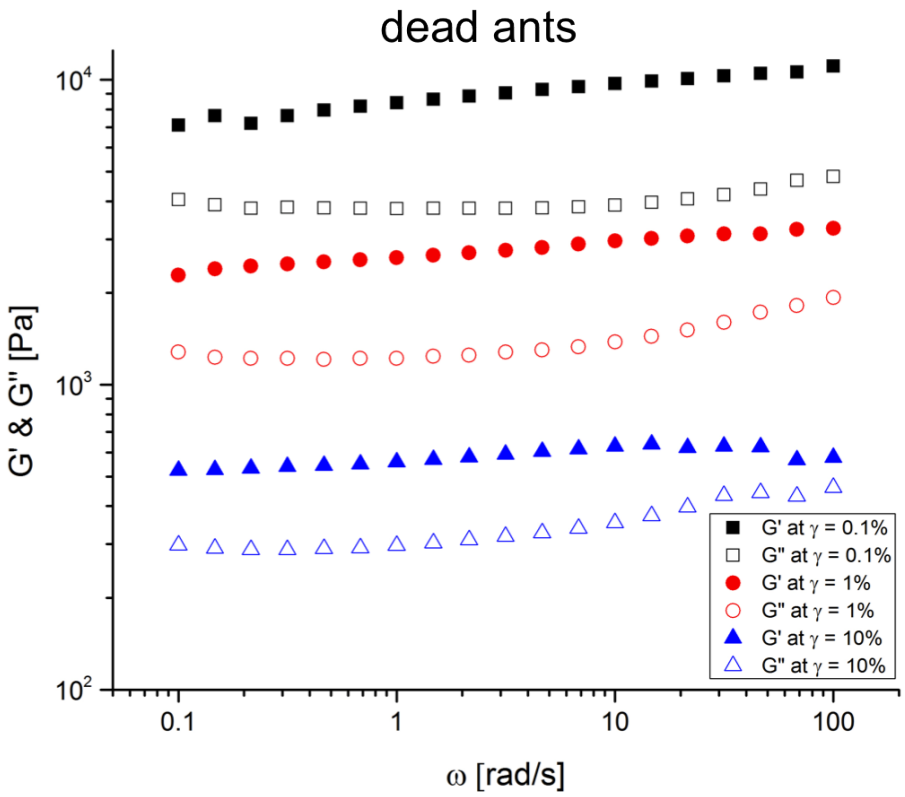

Figure 38: A frequency sweep is performed on the dead ants as the working medium. The storage modulus G' is always higher than G", indicating a dominance of solid like behavior. Bonds between individuals ants are only incidental leg and body entanglements, but as expected the bonds are too weak to cause cohesion, and rather the bulk of ants behaves as solid granular particles rather than a viscoelastic fluid.

Live ants behave differently from dead ants when shear rates are low as seen in **Fig.39** and **Fig.40**. **Fig.39** shows the relation between the difference between live and dead ant shear stress τ and viscosity η values and applied shear strain γ. When shear rates are low, the viscosity and shear stress for live ants are disordered, but for dead ants, the results are very uniform. As shear rate increases, live ants begin responding more and more like a pile of dead ants because they are unable to actively rearrange under the time scale of the shearing. At low shears, live ants are able to rearrange even while being sheared.

By looking at the shear rate at which the difference between dead and live ant shear stress approaches zero in **Fig.39**, we find live ants stop actively rearranging at around a shear rate $\dot{\gamma}$ of 10 s^{-1}. We can also verify this finding by looking at **Fig.40** a & b and noting that when shear rate is increasing, the results also become uniform at a shear rate $\dot{\gamma}$ of 10

s^{-1}. Typically for a polymeric fluid, when shear rate is increased above a critical value, the shear stress response levels out. We find that for ants, this leveling out only occurs when ants are sheared to they point that ants start dying.

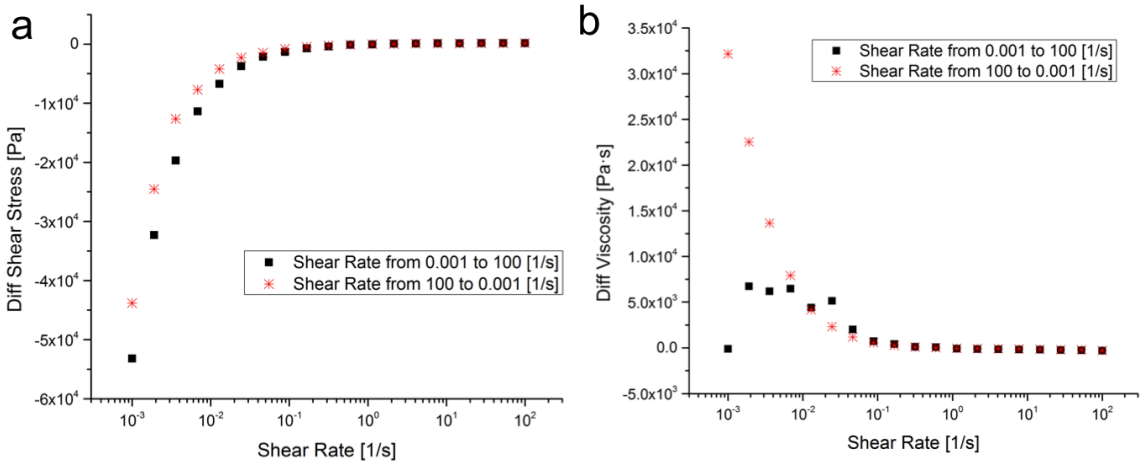

Figure 39: The rheological response of live and dead ants are compared by looking at the difference between their respective shear stress and viscosities while shearing at an increasing rate. The difference between the live and dead shear stresses approaches zero at a shear rate approximately 10% of the plate gap per second. This is the shear rate value at which live ants are unable to actively resist. However at low shears, the live ants actively rearrange, resulting in large differences between the two data sets.

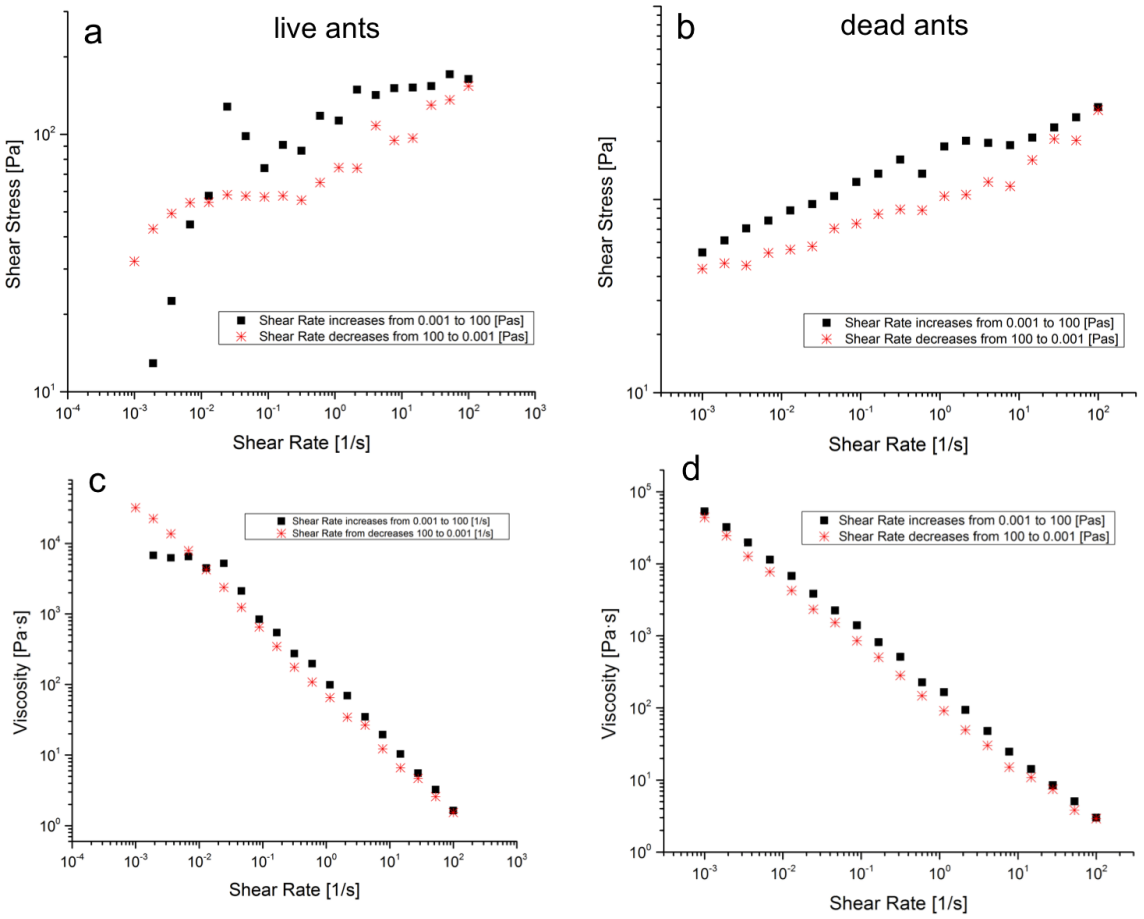

Figure 40: Here we plot shear stress and viscosity individually for live and dead ants. The nonlinearities in the results of the live ants at low shear rates are due to the active rearrangement of ants between the rheometer plates. Comparitively the dead ant results are uniform and show more defined trends. As shear rates are increased the live ants become more ordered as they are responding to applied stresses.

6.4 Discussion

With typical fluids in steady shear flow, energy is transferred layer by layer through moving particles dragging nearby particles along. This also how energy is lost as friction in the flow. When shearing ants, we ensured a no slip condition at the top plate by using velcro, but we don't yet have much insight into how the applied stress of the top plate propagates down through the bulk of the ants. Prior to shear experiments we test our no-slip condition of ants on velcro by testing whether two layers of ants shear easier than a layer of ants and velcro. Some ants tend to become embedded in the velcro creating the effect we want: a layer of ants fixed to the top plate while it is shearing the layers beneath. Future efforts include using a transparent containment wall to observe some ant movement on the outsides. In addition, a significant improvement but difficult collaboration would combine our x-ray techniques with rheometer techniques to track individuals between the plates.

In some self-assemblages such as rafts or bivouacs fire ants remain statically linked to their neighbors while supporting a load for hours, days, or even weeks at a time. Before conducting rheometer experiments we hypothesized that linked ants would be able to indefinitely resist small applied shear stresses. We found that ants either actively rearrange or flow under any magnitude of applied stress, but they didn't hold the plate still. This was perplexing as we have seen ants do this in many different more natural assemblage conditions.

We are currently unsure what triggers ants to indefinitely hold loads, but we believe it is either externally or internally generated high frequency excitations. We have tested this with observing fire ant bridge construction with and without high frequency excitation. Ants reinforce bridges when excited, but the bridge fails when excitations are stopped, supporting our theory that high frequency excitations elicits fire ants to hold tight to neighbors. We plan to test this theory with the rheometer by superimposing a small amplitude oscillation with a constant shear. By tuning the variables we may be able to further probe the limits at which the ants will create static self-assemblages that don't flow unless sheared beyond the ultimate yield stress.

We compare our findings from the CSR test to a power law model for $\eta(\dot{\gamma})$ because it is the most well-known and widely-used empiricism in engineering work; a wide variety of flow problems have been solved analytically for it [132]. However, the model does have its shortcomings: it often fails in the low shear rate region often leading to large errors. This is especially the case with ants as they are actively rearranging and stresses felt by the top plate are not indicative of the stress being applied to the ants. In addition the values m and n are difficult to relate to other key parameters such as characteristic time λ [132].

Characteristic time of the fluid flow t_{flow} and λ are used in the key dimensionless group for viscoelastic fluids, *Deborah number* defined as De=λ/t_{flow}. It is often interpreted as the ratio of the magnitude of the elastic forces to that of the viscous forces. Characteristic molecular time of the fluid λ is often taken to be the largest time constant describing the slowest molecular motions [132].

With fire ants, we interpret the characteristic molecular time λ as the time to reform a broken bond with a neighbor while being sheared. When shear rate exceeds this time, we find that viscosity decreases because ants can no longer make connections with neighbors after being torn apart. We don't however see a drastic drop-off in the viscosity after λ is exceeded because ant bodies and legs still experience physical entanglement and jamming, much like polymer chains experiencing shear. In addition while ants closest to the top plate may not be able to reform bonds, ants at the bottom that are moving slower may be able to.

There are several helpful tests that can be run to explore rheological properties without using a rheometer. We have begun to explore some of these options including recovery rate

after quick compression of a fire ant ball, falling rate of a rod placed vertically in a sea of ants, and settling rate of a ball or a disc in a sea of ants.

Most fluid properties exhibit a high dependence on temperature. Exploring the effect of temperature on fire ant viscosity may provide insight into how temperature can affect the assemblage construction process.

Previous to this study, no one has investigated the viscoelastic properties of fire ants. We were inspired to conduct this study by observing the unique bulk properties fire ants exhibit when linked. The properties are appealing from many perspectives. Ants are able to flow freely over one another much like snow in an avalanche. They naturally stick to one another giving them viscous properties, yet they have strength enough to support one another statically and for long periods. The system is strong, yet bonds break easy enough such that the particles are not damaged when broken. When broken, the material can readily self-heal. The entire system is flexible and adaptable. The system can readily absorb impact, yet remain cohesive. A viscoelastic model can only account for a small part of the bulk behavior we observe in fire ants because viscoelasticity is only one part of the array of unique properties exhibited by fire ants.

Despite the shortcomings of a viscoelastic model to holistically capture fire ant bulk dynamics, rheological studies offer much insight into the physical interactions between ants when subjected to a variety of stress conditions. In particular, we find that ants cushion applied stresses through active rearrangement and storage and dissipation of energy with the ants' muscles. This behavior of individual fire ants acting cohesively as a collective provides an excellent case study for the growing field of active matter.

6.5 Conclusion

From this novel study on fire ant rheology, we find that ants are able to able to rearrange even when loaded. This supports our previous findings that ants build tunnels in and out of stationary bivouacs built into a high energy equilibrium state. It isn't until applied stresses reach a critical value that ants begin to flow much like a viscoelastic fluid, yet they retain equal characteristics of a viscoelastic solid at the same time. In contrast dead ants behave like a solid granular material with a storage modulus twice as large as their loss modulus. Also we find that ants use active rearrangement to cushion applied loads and dissipate energy throughout the assemblage by using their muscles.

CHAPTER VII

WORKS IN PROGRESS

7.1 Agent-based simulation of ant assemblage deconstruction

Agent-based models (ABMs) are particularly attractive for studying the collective, emergent behavior of individuals operating in a complex and stochastic environment. Prevalent examples include the simulation of markets or economies, traffic congestion, warfare, population dynamics and disease spread. In each of these scenarios, the simulation embodies a collection of mobile, autonomous agents operating on a uniformly gridded, or celled, landscape. This can be viewed as cellular automata with the inclusion of mobile agents, where both the cells and the agents store a set of states [138]. The autonomous agents make decisions about their next position based on a set of rules that account for the agents state, its neighboring agents states and the states of the cellular landscape in close proximity to the agent. Time therefore flows in an explicitly stepped manner in which each agent evaluates its next move before the simulation proceeds to the next time step. Along with updates of agent positions, there are updates to the agents state variables during each step. An in-depth review of agent-based modeling is given by Bonabeau [139].

Certain aspects of generic ant behavior have been successfully studied using agent-based modeling. Bruckstein detailed an early agent-based model whereby ants follow a leader toward a food source such that a smooth trail of ants emerges, closely resembling that seen in nature [140]. Resnick developed a compact model of ant foraging behavior, using only a few autonomous ant rules, which accurately captures the collective behavior of an ant colony in search of food [141]. In the model, ants initially perform a near-random walk (their heading changes at most by +/- 20 degrees at each time step) as they head out from the colony until they encounter a food source. They then release a spatially and temporally diffusing pheromone trail for other ants to follow as they head back to the colony. Resnick documented accurate emergent behavior using this simple scenario, to include (1) efficient identification of food sources and subsequent recruiting of peers to the source, (2) systematic and sequential foraging of food, as if informed by a central plan, nearest to the nest followed by foraging of food sources further away, and (3) the presence of stable, coherent pheromone trails leading from the colony to the food source.

Ants placed into a container with no place to take shelter will form their own shelter for the colony by linking together to form a bivouac. When shelter for the ants is then introduced into the container and discovered by scout ants, the ants in the bivouac begin to

disassemble and move as a colony to the new shelter. We have begun to investigate the disassembly process through time-lapse photography. We attempt to describe the disassembly process as a behavioral algorithm that we then use to fuel an agent-based simulation of the disassembly process.

The experiments consist of placing a clump of ants at the center of a storage container. A home was placed adjacent to their starting position near one side of the container. We observed from these experiments that while the ants dissipate from the initial clump, they form semi-persistent patches of new clumps when they attempt to move to the home. It is also observed that the more ants used in the experiment for a given container size, the more likely clumping occurs. We hypothesize that the new clumps emerge due to ant entanglement, and we set out to test this hypothesis using the agent-based model.

We also observe there is a relation between the time to relocate and the ratio between number of ants and container size. When the ratio is above a critical value, satellite clumps form at the edges of the main bivouac clump during disassembly as seen in **Fig.41**b. Below this value, satellite clumps do not form as seen in **Fig.41**a, and the disassembly process is much faster. We hypothesize that individual ants at the ball need to be stimulated to leave the ball by returning ants, and that satellite clump are caused by superseding a critical concentration of ants. These satellite clumps may prevent returning ants from communicating information about the shelter to the bivouac, and thus delay relocation.

This phenomenon presents an opportunity for a unique study with both experimental and simulation elements. The researcher can experimentally probe the bounds and parameters for the disassembly process, gathering both macro and micro level data. On the micro-level the ants can be tracked using an open-source tracking software called BioTrack developed by Andrew Quitmeyer in Tucker Balch's robotics group. Using this tracking software, one can gather statistics on ant trajectories including direction changes, time spent resting, and interaction responses. On the macro-level, one can adjust the starting position of the ant bivouac, home, container size, and number of ants. The researcher can then determine the effect of these parameters on the deconstruction process including the relation between bivouac size and time, total colony relocation time, and satellite clump formation.

We developed a preliminary agent-based model of fire ants, using the NetLogo simulation tool [142], to explore its ability to capture self-assemblages seen in our ant experiments. Similar to our live experiments, the simulator allows us to explore fire ant behavior when dissipating from a central aggregation. In large part the preliminary model is based on Resnicks model with additional rules governing ant behavior when ants meet, share a cell, or are unable to move to a free cell. The rules are based solely on the ants state, its neighbor ants states, and nearby cell states, and thus the ants operate autonomously without intervention from a global authority.

Based on the hypothesis and experimental observations, a minimal candidate rule set

was generated, and then tested in the simulator. The ants are modeled as being in either an initial state (home not found), or a state in which they have located the home. Depending on their state and the presence of ants sharing their space or neighbor spaces, and the pheromone state in cells around them, the ants make random or decisive movements (e.g., in the direction of highest pheromone). Additional rules govern physical interactions between ants, including a probability associated with ants entangling with each other when they meet.

Results collected from experiments and the agent-based simulator appear in **Fig.41** as time snapshots of the colony. For a given container, **Fig.41**a displays results from a small number of ants while **Fig.41**b displays similar results for a large number. A white region depicts the colony home in the simulation results (top row) while pheromone trails are depicted with high intensity (white) and low intensity (green). Both the experiments and the simulations document ant dissipation rates and probabilities of entanglement. With small populations **Fig.41**a, the ant dissipation rate is fast, resulting in almost immediate dispersion. Both the images from the experiment and simulations document little to no clumping in the small population case, and both evolve to a steady-state wherein a vast majority of ants reside within the home, leaving only a few isolated ants elsewhere in the container. When the population size is increased **Fig.41**b, the dissipation rate and the probability of entanglement increases. Both the experiments and simulation results document emergence of a large number of clumps after the initial dissipation. Similar to the study with a lower density of ants, a steady-state is achieved wherein the majority of the ant population resides in or around the home, leaving a smaller percentage elsewhere in the container.

Our NetLogo agent-based simulation has already captured much of the disassembly dynamics, including satellite clump formation. Our simulation is currently lacking in that it cannot capture the time-scale of the deconstruction process or the precise relocation dynamics. This research project has already received several months work, and with a few more months of work could capture the important dynamics at all time scales.

Future work on the project can build upon the preliminary agent-based model in several directions. In the first, physics-based modeling of ant aggregations will be integrated using lattice-spring type models [143]. Ants that share a space or neighbor one another will be modeled with stochastically interacting tarsal claws and adhesive pads (i.e., springs) that allow for transmission of forces. These connections will break at predetermined force levels informed by tarsal claw tensile tests. In addition, ants will be able to exert forces on substrates and external force modeling will be present (e.g., gravity body forces) which will result in tension/compression throughout the ant collections. Ultimately, this capability will allow us to compute continuum-level material properties (e.g., material strengths, Poisson ratios, etc.) that change spatially and temporally due to ant collective behavior, and due to

changes in the ants environment. It also allows us to probe which individual ant behaviors give rise to which material properties and to what degree.

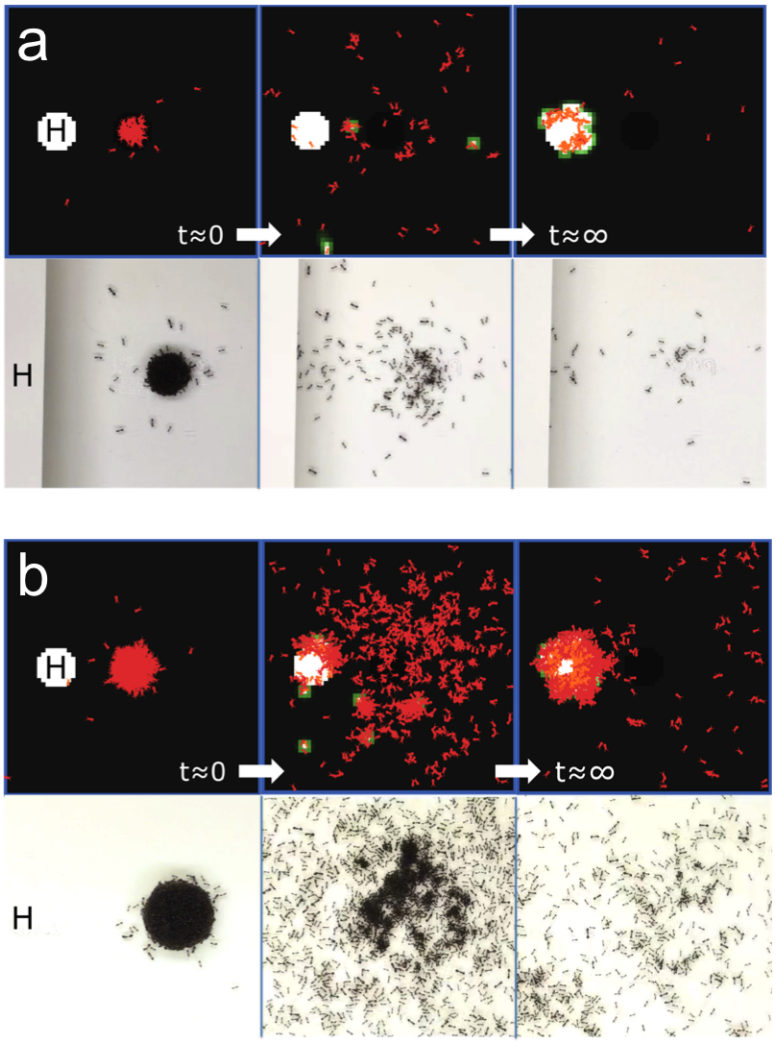

Figure 41: Ants in a container with no shelter will form a bivouac by linking together. When offered a shelter (marked by H), ants quickly disassemble and relocate to the shelter. How quickly the ants relocate depends on several parameters including number of ants in the container, size of the container, and relative locations of ant bivouac and shelter. We have developed a NetLogo simulation that captures the satellite clumping that is evident when the number of ants in the container is sufficiently high (bottom image time series).

7.2 A structural model for linked ants

Linked fire ants form a material with a low volume fraction, where volume fraction is defined by the ratio of solid material to total volume (air and solid material). This material is porous, lightweight, and strong much like material made up of random fiber networks. We make a comparison between linked fire ants and random fiber networks by attempting to quantify the network properties of the ants. Studies on random fiber networks show the structure is characterized by a number of parameters including density, filament orientation, nature of the cross-links, and fiber shape. Researchers show that the overall strength of such networks can be deduced by quantifying specific properties of the individual fibers such as their bending and axial stiffness. Such studies refer to fiber networks as a continuum with uniform properties emerging based on the nature of the individual fibers.

Research shows that the nature of the linkages between fibers determines the mechanical behavior of the network [144]. The compliance level of the cross-links plays a crucial role in how external forces are transferred within the network. Fire ants within an aggregation are held together by linkages with high compliance. This allows the structure to absorb applied forces without breaking individual linkages.

Often times, the mechanical behavior of a fiber network can be predicted through development of a model based on the properties of an individual fiber. In our studies, the analog is understanding the properties of a single ant. Our observation and understanding of ant networks has led us to model the aggregations as a series of nodes connected by springs. Such a model will allow us to predict how the network will respond to external forces.

Future research plans may use data gathered from CT scans to make theoretical predictions of the strength, buoyancy, and water-repellency of the ant cluster both using mathematical formulations and computer simulation. One can then verify these predictions through carefully designed and implemented experiments.

Predictions of strength of the network can be based primarily on connectivity of the network, where connectivity is defined as the number of connections per ant. Using our findings for ant-to-ant spacing and experimental results of the holding strength between individual ants, we can make predictions about the ultimate yield strength of the ant network. Similarly, a simulation that models each ant as a node with six connection points modeled as springs could provide predictions about the yield strength as well as how the structure will respond to shear forces. Such predictions will be verified through experiments in which the ultimate tensile force and shear force response will be measured.

A hanging column of ants can support itself **Fig.11**. When more ants are added to the structure, the stress at each cross section increases. At some critical stress, the column will break off. Knowing the mass of the broken off column and diameter of the column at pinch off will yield the tensile stress. Our initial tests find yield stress of a hanging ant column around 100 Pa. This value is much less than the predicted value using maximum strength

for all ants at the cross section experiencing largest load. We believe this discrepancy is due to ant rearrangement, causing bonds to break and shock loading. Shear stress predictions can be verified with the use of a rheometer (see Ant rheology section for details).

A physical model of the ant entanglement network can be constructed by using the volumetric information attained in CT scans to 3D-print a scaled up replica of the soft-structure entanglement network using printing media of varied viscoelastic properties. Stress-strain measurements and fracture tests on the 3D-printed entanglement network can be employed to build an understanding of the passive rigidity properties of the ant-entanglement network. Furthermore, by reduction of the contact numbers (by deletion of randomly chosen limbs in the CT data) one could print models of ant-entanglement networks with reduced contact numbers and thus assess the rigidity networks robustness characteristics under perturbation.

7.3 Ants as an active granular material

7.3.1 Sedimentation within active soft-materials

Rheometric experiments will assess the viscoelastic properties of the ant material soft-structure. However in these experiments the role of ant activity is hard to ascertain because visualization is not easy. Thus here we propose an additional set of experiments to determine how the viscoelastic response of soft-structures is influenced by the activity level of the individuals. In a recent study of sheared granular materials, it was found that a sphere will sediment into the fluidized granular media as seen in **Fig.42** [145]. The activity level (i.e., fluid-like properties) of the granular media set the shear rate and it was found that this rate influenced the equilibrium sedimentation depth of the object. The study showed that the spheres followed an Archimedes-like law in which the density and shear-rate control the equilibrium depth of the spheres. Our studies on fire ant aggregations have shown that ants also have the ability to behave collectively as a complex-fluid. Ants within a soft-structure are active and typically moving and so we expect that similar sedimentation experiments will allow exploration through direct observation of how ant activity influences the viscoelastic properties of the bulk.

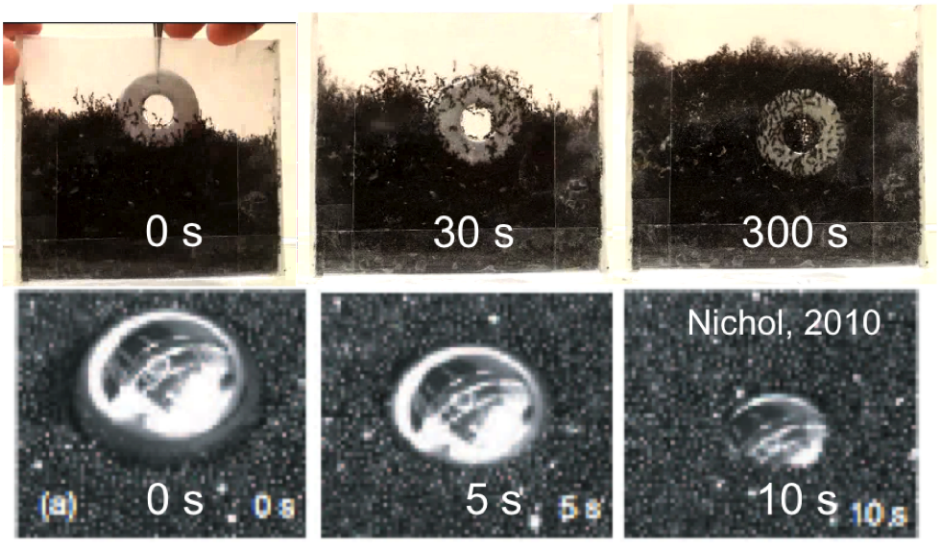

Figure 42: The first row of images shows a metal washer placed in a bed of ants with thickness of 5 ants. The ants begin to flow around the ants as it sinks into the bed. Similarly, the second row of images taken from a study by Nichol et al shows a large glass sphere sinking into a fluidized bed of glass beads. The density of the sphere effects the depth that it sinks.

We have observed that high-density spheres fall through a bed of ants similarly to a sphere falling through a viscous fluid. We have been able to make rough predictions of the viscosity of the ant material based on the time scales of sedimentation **Table 6** [17], but

close analysis of the flow patterns within the ant aggregation are extremely difficult because the ants are opaque. Visualization of ants within the cluster is impossible using traditional fluid visualization methods.

Table 6: Physical properties comparison of water, ant material, and fluidized granular glass beads.

	Density, g/mL	Dynamic Viscosity, cP	Surface tension, dyn/cm
Water	1.0	0.89	72
Ant Aggregations	≈ 0.2	$\sim 10^6$	$\sim 10^3$
Fluidized Glass Beads	1.92	$\sim 10^7 - 10^9$	~0 NATE –XX?

To resolve these issues of visualizing flow around an object sedimenting within an ant cluster, one can design 2-D sedimentation experiments in a hele-shaw cell several ant layers thick. We have already placed thin, high-density coins into the cell to sediment. **Fig.42**, frame 1, shows a metal coin placed into a bed of ants approximately 5 ants thick. Edge effects are minimized by lightly coating the glass walls with talc powder, preventing ants from adhering to the walls. By 30 seconds, ants have begun to flow around the coin. The coin displaces ants beneath it that then flow around the coin and fill in the area behind it much like a disc sinking into a high viscosity fluid or like a sphere sinking into a fluidized bed of glass beads [145]. By 4 minutes, the coin is fully immersed in the ant bed. The coin continues to sink until it reaches the bottom of the container after 30 minutes.

In these experiments one can induce different levels of ant activity during sedimentation by controlling the ambient temperature. Ant metabolic energy rate, like all insects, is highly sensitive to temperature. High-speed imaging can be used to measure the overall flow patterns of ants using particle-image velocimetry to monitor the rearrangement of individual ants. PIV measurements can be used to determine an effective granular temperature field of the soft-structure [146]. Performing this experiment with coins of different density will allow determination of the density of the ant fluid as well as the dependence of viscosity on the activity level and loading of the soft-structure.

7.3.2 Mechanical tests of active geometric cohesion and construction of active particles

Active particles such as ants or micro-activated devices are capable of having dramatically different properties from passive granular media. Active particles based off a simple mechanical design can be constructed from pager motors and a rotational interlock system.

These “simple” devices can be compared to more sophisticated “micro-robot” devices. One can further the analogy by experimentally varying the particles activation energy by varying the temperature for the ants and varying the motor torque for the micro-robots.

Vibro-fluidization.

Groups of ants, when subjected to vertical vibration, aggregate and form an induced spherical soft-structure. This ant sphere, unlike clusters of staples or rods, does not easily disassemble under vertical oscillation and instead preliminary data suggests that increasing the shaking intensity causes the sphere to increase in rigidity. Live ants form tight clusters by grabbing neighboring ants tarsi, with their own mandibles and tarsi as shown in **Fig.43**, thus cohering geometrically. When this tightly formed ball of ants is frozen in liquid nitrogen, however, subsequent shaking readily disassembles the structure similar to experiments with staples. The effect of the liquid nitrogen is to remove the active clinging behavior of the ants. Thus we have observed that active interlocking of limbs plays an important role in the strong cohesive properties of ant balls.

Shear and tensile tests. The tensile strength of live ant clusters has been measured using a load cell to measure tensile force while an actuator applied a strain. The resulting force-displacement curve exhibits three regions of yielding as shown in **Fig.43**. Initially there is an engagement region where the force increase is small. As the group is stretched further apart the force increases linearly with displacement indicative of an elastic response, which is then followed by a plastic yield event likely due to breaking limb entanglements. The ultimate tensile strength of the cluster is set by the strength of a single ant. An important feature that the ants possess, beyond that of passive particles, is their ability to re-connect and repair regions of the structure.

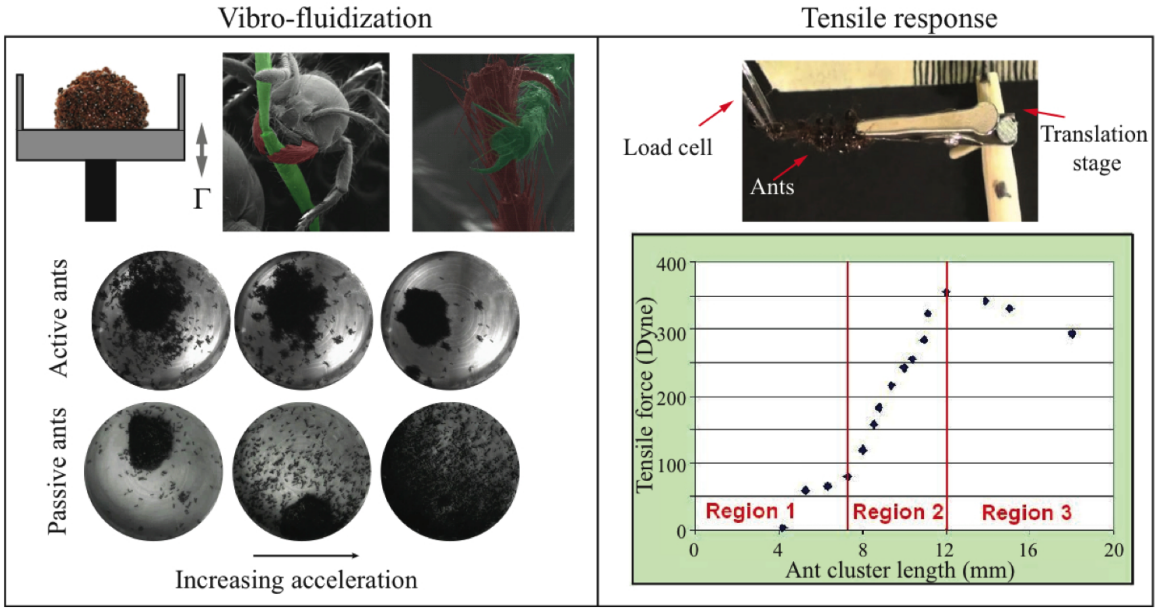

Figure 43: Vibro-fluidization experiments subjected cohesive balls of live and dead ants to vibration at increasing amplitude. Live ants formed tight balls that resisted breakup even at high amplitude, while dead ants exhibited a phase transition from solid to gaseous state as amplitude increased. This phase transition of dead ants is much like the response of a ball of staples when tested in the same manner.

Biological inspiration.

Subjecting ants to the same experiments performed on passive granular materials can achieve measurements of the influence of active grabbing on soft-structure cohesion. Ants possess 7 barbs they use to grab other ants (6 claws and 1 pair of mandibles): one can systematically reduce these degrees of freedom by applying wax to the claw tips and observing the resultant bulk cohesive ability. This experiment could provide an understanding of the degrees of freedom per ant required for cohesion, and in turn inform our experiments on active micro-robots.

High-speed video is a useful tool for investigating the differences between passive and active interlocking of individual ants (using dead and live ants, respectively). One could also use our data collected on average number of contacts between the ants to inform experiments on micro-robots and simulation.

Construction of active particles.

Based on insight we gain from the biological experiments, one can construct both simple and complex active particles and subject them to similar tests described above. In contrast to the passive experiments (such as 3D printing entanglement networks, using non-active particles), the construction and testing of active particle ensembles would provide insight into what level of control is employed in maintaining cohesion within a soft-structure.

The simple active particles seen in **Fig.44** consist of a rotational motor coupled to a grabbing mechanism that can capture and hold on to the interlocked barbs from neighboring particles. These particles should be made from durable "sticky" plastic and different strategies for particle robustness will be evaluated. The motor torque sets the strength and rotation rate, and thus tunes the effective interaction potential and timescale of the active geometric cohesion. The motor current driving the active particles can be regulated by a phototransistor mounted to the stationary disk surface. In this way the activity level of particle ensembles can be modulated spatio-temporally by varying the spatial intensity of light from an overhead projector. Thus through a simple rotational mechanism, researchers can construct actively cohesive particles on the size scale of a pager motor (1 cm, a few grams). Such particles would be light enough that a sufficient quantity can be driven using a powerful mechanical shaker (e.g., Dan Goldman's VTS shaker can drive loads of 500 lbs at 1 g).

To more closely model the grabbing behaviors and geometries of the ants we have developed a concept for a miniature cooperative ant robot **Fig.44**. These robots of length scale 3 cm are designed to link together to create vertical and horizontal assemblies composed entirely of identical robots, mimicking the active cohesion of fire ants. Each robot can be propelled by servos driving pronged gears to enable traction of the ant robots over each other. "Sticky" plastic or rubber on the linear actuator may enable inter-robot binding. Note that although modular robots have been built by others [44, 147], none can both actively link together and climb over their robot counterparts, as in our proposed design.

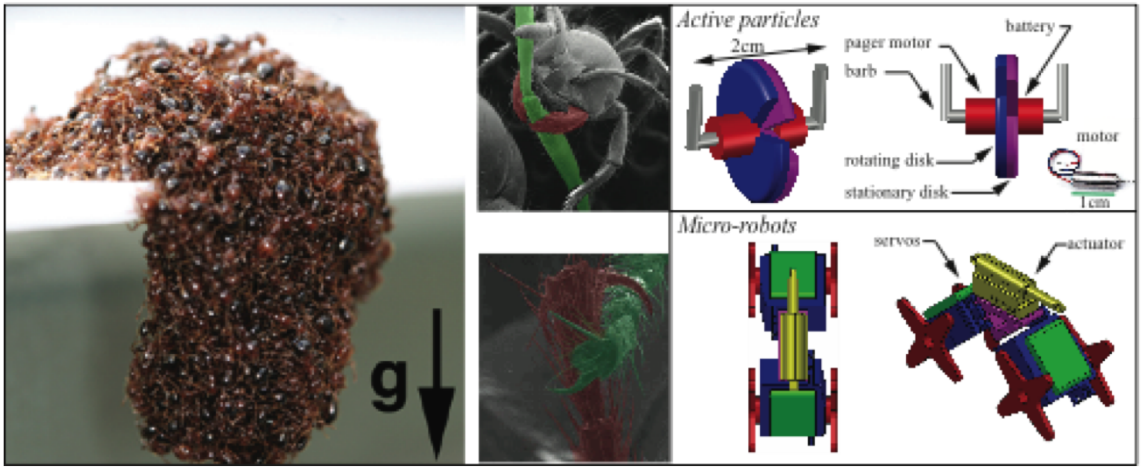

Figure 44: Groups of hundreds to hundreds of thousands of ants form tight spheres through mechanical interlocking. A sphere perched on an edge resists breaking apart due to cohesion, but deforms under gravity. Mechanical interlocking is achieved through gripping neighboring tarsi and mandibles as seen in SEM images of ant balls. Miniature active particles (right top) and micro-robots (right bottom) are based upon pager-motor Hexbots with magnetically controlled attachments. Active particles can consist of two rotating disks with quadrants cut out from them. One disk driven by a pager motor (shown in inset) could rotate about the other stationary disk. When the open quadrants of the disks align a neighboring particle's barb may fall into this region and as the motor turns link the particles together.

7.4 Ant bridges

Army ants *Eciton burchelli* participate in large colony-wide raiding marches. The colony stays connected to the nest by a large trail of ants extending hundreds of feet through the forests in South and Central American where they are found. Often the colony encounters "potholes" or holes in the terrain larger than a single ant can walk across. A recent study by Powell *et al* investigated the unique behavior of army ants to fill in these potholes by forming "living plugs" or bridges to span the pothole allowing other colony members to pass by with ease [148]. The researchers found that ants match their size to the hole they are filling and cooperate to fill larger holes. Their findings also show that the hole plugging process increases prey-intake for the colony during raids.

Other ants also build bridge self-assemblages to cross gaps several times the length of a single ant. A study by Hölldobler *et al* identified at least five distinct mechanisms the African Weaver Ant *Oecophylla longinoda* uses to recruit others for colony foraging [149]. The researchers placed a plant near the nest site and observed that several ants stretched their bodies out towards the plant holding them rigid for several minutes while nestmates clambered out over the bodies of their nestmates to assume a similar position. This continued until a bridge was formed to allow nestmates easy travel back and forth between plant ant nest.

Fire ants in nature build raft-like bridges across the water to traverse stagnant flooded areas as shown in **Fig.45**a, but fire ants bridge building between two suspended points such as observed in the army ant and African weaver ant has never been documented. We hypothesize that fire ants will build a strong bridge when subjected to high frequency vibrations. We test this hypothesis by developing an experimental setup to test fire ant bridge building while subjected to a range of vibration frequencies.

We initiate bridge building by filling two 10 mm diameter tip funnels with with fire ants. We hang these funnels side by side attached to a rod connected to a B & K vibration exciter type 4809 as shown in **Fig.45**b. When the exciter is activated the funnels vibrate at the designated frequency. Using a signal generator and amplifier, we modulate excitation frequency from 0 to 150 Hz at an amplitude less than 1 mm. The resulting bridge formation is filmed using a Sony HD Handycam.

When no excitation is applied, the ants begin to slowly "drip" out of the funnels in columns. This continues for 10-30 minutes until all the ants have fallen. The ants collect and fall in a manner similar to the droplets observed by Bonabeau *et al* in their study on ant droplet formation and dynamics [107].

If we vibrate the funnels at low frequency (<5 Hz) after they have begun to drip out, the ants begin to sway and the columns eventually swing into one another. The two columns stick together because an ant in one column adheres to an ant in the other column as shown in **Fig.45**c&d. The ants in each column are very active, walking up and down the columns

and back and forth once the columns adhere together. If the excitations are maintained below 20 Hz, then the bridge between the two columns will maintain at only an ant or two thick, but if the excitations are ceased, then the columns will soon break apart (<1 min) and continue dripping.

If two columns are bridged, and the excitation frequency is increased above 20 Hz, then ant activity decreases, and the ants begin to reinforce the weakest point in the bridge by adding links to the structure as shown in **Fig.45**d. This continues until the bridge is a uniform thickness. At very high excitation frequencies (>120 Hz), the ants stop moving altogether.

We can conclude that frequency of column vibration plays a large role in fire ant bridge formation. When ants are not vibrated, then a bridge will not be formed, and a previously formed bridge will soon collapse. The most important discovery that need further study is the relation between frequency and bridge reinforcement. We clearly observe that when vibration frequency is increased, that ants fill in weak spots in the bridge making it stronger.

Previously, it was not known that fire ants form bridges to span suspended gaps. We believe this behavior may exist in nature when ants in a floating raft form bridges to twigs suspended from dry land as shown in the bottom left image of **Fig.1**. The bridge may be reinforced by perturbations from the water or winds.

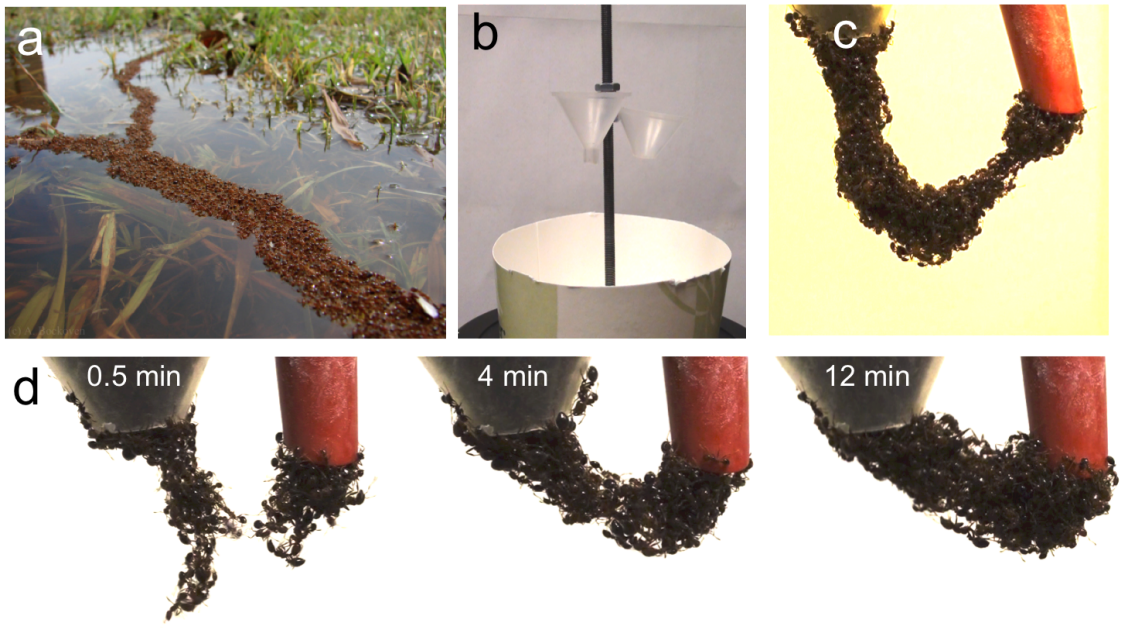

Figure 45: (a) Fire ants are known to link together and form a floating bridge for the rest of the colony to use to quickly cross flooded terrain. (b-c) We vibrate two ant-filled funnels to initiate suspended bridge construction between the funnels. (d) When vibrated, columns of fire ants hanging from each funnel begin to swing. The two columns join into a bridge when they come into contact. If the vibrations are stopped, the bridge breaks, but if the funnels are vibrated at a greater than 20 Hz, the ants begin to reinforce the bridge and fill in the weak points. The higher the excitation frequency the less the ant movement. As long as the excitations continue, the ants will hold the strong bridge indefinitely.

7.5 Other unique phenomena

Over the past five years of working hands with fire ants, we have observed several intriguing phenomena that may offer interesting future studies, or even just merit further investigation.

7.5.1 Air bubble capture

If a group of floating ants is submerged, the water's surface will wrap around them, trapping them in an air bubble underwater as seen in **Fig.4**e. If the submerged ant cluster with density a fifth that of water is then released, it will quickly buoy back to the surface. When a single floating ant is submerged and subsequently released, it too will also buoy back to the surface. This occurs at least in part because a thin layer of air is trapped against the single ant's body when submerged. The water surface wraps around the ant's body, but is kept at bay by the thousands of tiny hairs covering the ant.

When filming the construction of ant rafts, we often pin the raft in place using a pair of wires attached to a small piece of hardware. The two wires pierce the underside of the raft preventing it from translating or rotating. We occasionally observe ants breaking the surface tension and walking down the wires to the bottom of the flooded container. Sometimes these ants drag air bubbles down with them as shown in **Fig.46**, causing the ant to fight an even stronger restoring force than the one resulting from only the thin air layer trapped by its hairs.

We have also observed a unique "bubble collecting behavior" where an ant on the bottom of a flooded container will gather air bubbles and add them to the air already attached to it's body. When the air bubbles are sufficiently large, the ant will be carried back to the surface. This behavior has yet to be understood from a behavioral or functional perspective. In addition, it is unknown how ants are able to so easily adhere to smooth wet surfaces.

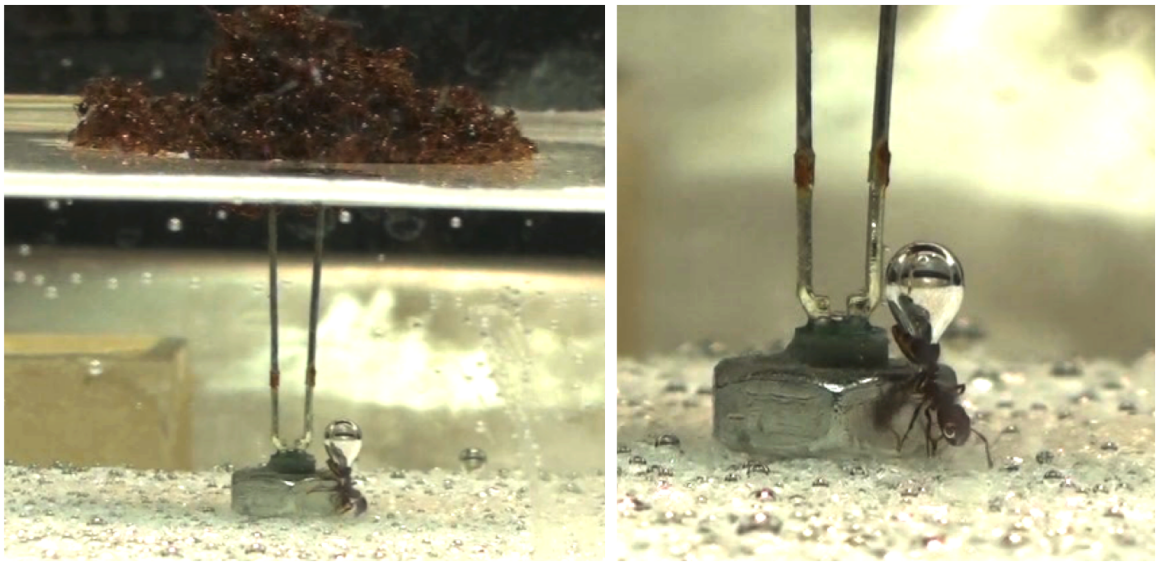

Figure 46: Ants can walk freely on submerged surfaces relatively unhindered. The large ant pictured under the water abandoned the raft above it and dragged underwater a large air bubble attached to its gastor. The bubble acts to buoy the ant back to the surface, yet the ant is able to grip the underwater surface and walk around. Eventually, the ant loses its grip, and is dragged quickly to the surface by the air bubble.

7.5.2 Ant avalanche and wall folding

If a handful of sand or other granular material is placed in a cup that is then turned on its side and gently spun in place, then the grains of sand at the front of the rotation direction will spill over and roll down the sand pile. This continues uniformly and steadily as long as the cup is turned. The same phenomenon is seen with a large cluster of dry ants in a spinning sideways cup (see supplementary video *Fire Ant Avalanche* on *Youtube.com*).

A related phenomenon is the buckling ant wall. Fire ants flooded in a container build a wall against the container side using their own bodies. The wall can be hundreds of ants wide and high as ants continue to add to the wall. If the wall becomes "top-heavy" in any area, and develops a torque large enough to peel the ants away from the wall, then the wall folds over on itself, taking the rest of the wall down in either direction like a wave. This can be seen both in **Fig.23**b, and in supplementary video *Fire Ant Wall Folding* on *Youtube.com*.

Both of these behaviors offer opportunity for a significant study of the system dynamics.

CHAPTER VIII

CONCLUDING REMARKS

8.1 Main Findings

This thesis represents the first quantitative studies of fire ant self-assemblages. While there have been a few studies on other insect self-assemblages, most are descriptive in nature and provide little analysis of structure, mechanics, or predictive models. We not only develop elegant models to explain assemblage construction rate, size, and shape, but we also provide beautiful and striking images displaying the variety of assemblage arrangements and functions. Our novel SEM and micro CT scanning preparation and analysis techniques allow us for the first time to peer into ant assemblages, revealing the degree of interconnectivity and mechanisms of ant attachment. We have also brought to light the viscoelastic nature of fire ants behaving collectively. Previously, it was not known that fire ants behave in this way. We have shown that the complex behavior of decentralized individuals acting as a collective can indeed be modeled by only describing the local behavior of an individual.

Our main contribution is the development of parsimonious mathematical models of how the behaviors of individuals result in the collective construction of fire ant assemblages. The models posit only simple observed behaviors based on local information, yet their mathematical analysis yields accurate predictions of assemblage shapes and construction rates for a wide range of ant colony sizes.

8.1.1 Rafts

Our initial study on floating fire ant rafts reveals that thousands of ants stay dry while linked together and floating. We find that even the ants on the bottom of the raft do not break surface tension, but rather sit atop the water while the surface deforms beneath the raft like a stretchy waterproof fabric. Although water repellency in nature has been previously viewed as a static property unique to plant and insect cuticles, we demonstrate a self-assembled active hydrophobic surface. While a single ant sticks to water, a group of linked ants repels water effectively.

Fire ants build rafts in response to flooding of their underground nests. We attempt to initiate the raft construction process in a repeatable, easily analyzable manner. We form 1,000 - 7,000 ants into spheres, place them on the water's surface, and record the subsequent rearrangement of ants into a flat pancake shaped raft. Observing and tracking individual ant motion atop the raft, we find ants travel using a stereotyped sequence of behaviors. We gather trajectory statistics to form a discrete model of raft construction. This model based

on individual behavior captures the overall raft dynamics extremely well for small rafts.

In naturally occurring floods, rafts can be quite large, exceeding 50,000 individuals. We notice that for larger rafts containing 10,000 or more ants, our model tends to over-predict the growth rate. Our previous model is based on experimental observations of randomly-directed linear ant trajectories atop the raft, but inspection of ant trajectories on rafts of up to 25,000 ants reveals anomalous behavior. As raft size increases, ant behavior approaches diffusion, which is in closer alignment with other studies on the foraging and scouting patterns of ants. We incorporate this ant behavior into our model, yielding predictions that more accurately reflect the growth rate of large rafts.

Our previous model also relies on an assumption of raft circularity. We show that this assumption is not necessary for large rafts because it follows from the random directionality of the ant trajectories. We perform a simulation of ants adding randomly to the edge of a raft to determine shape after all ants have added to the edge. Our predicted relationship between raft size and circularity closely fits our experimental data gathered from very large raft construction.

8.1.2 Strength, structure, and packing properties

Probing individual ant strength on different materials reveals a level of control over adhesion by modulating surface roughness. Because ant adhesive pads are believed to function by use of a non-Newtonian secreted emulsion, the contact area and thus adhesion can be regulated by increasing surface roughness. We demonstrate this property by observing ant adhesion on Teflon strips. We also find ants are much stronger when grasping with their mandibles or claws rather than sticking with adhesive pad. By pulling on a cluster of ants attached to a thin rubber string and measuring deflection, we find ants tend to use only a percentage of maximum attachment strength when connecting to neighboring ants as compared to other surfaces such as plant material or velcro.

Since ants are opaque, the arrangement of the ants within these three-dimensional networks was unknown prior to our work. We apply micro CT to visualize the connectivity, arrangement and orientation of ants within an assemblage. We identify both active and geometrical mechanisms ants use to obtain favorable packing properties with respect to well-studied packings of inert objects such as cylinders. Ants use their legs to push against their neighbors, doubling their spacing relative to random packings of cylinders.

These legs also permit active control of their orientation, an ability ants use to arrange themselves more perpendicular than parallel, which is not what we would expect when compared to similarly sized static particle packings. Lastly, we find an important role of ant polymorphism in promoting self-aggregation. A large distribution of ant sizes permits small ants to fit between the legs of larger ants, a phenomena that increases the number of average connections per ant. These combined mechanisms lead to low packing fraction and

high connectivity, which increase raft buoyancy and strength during flash floods.

8.1.3 Towers

A few ant species are known for their ability to build temporary housing encampments using their own bodies. These self-assemblages called bivouacs serve as shelter for a colony when none is available. For some nomadic ant species such as the army ant, bivouacs are a way of life since life is always "on the road." When fire ants are contained and faced with nowhere to take cover, they cooperate to build a bivouac against the container walls. Although never previously documented, a raft of fire ants display this behavior in nature when docking to establish their colony again.

In our study we investigate the shape and rate of fire ant bivouacs built around a supporting Teflon rod. We design an experiment to standardize the building process, and we film from the profile view to gather data about the tower shape and building rate. We find that both during construction and at equilibrium fire ants build an axisymmetric tower-shaped bivouac with an exponentially shaped profile. We rationalize the tower shape using a discretized tower model build one layer at a time. Our model stems from a constant ant strength assumption such that the tower load is uniformly shared among all ants. The shape predicted by our model matches closely to the ant tower shape, bringing to light the number of neighbors ants will support indefinitely.

8.1.4 Rheology

When fire ants like together they exhibit bulk behavior similar to a fluid or a solid; thus we can study assemblages as a continuum rather than containing discrete elements. We find that neither solid or fluid models match the ant behavior well, so we turn to a rheological approach. Rheology is the study of the flow of complex and non-Newtonian fluids: materials that exhibit solid and fluid properties. Some common examples include silly putty, paint, or shaving cream. Rheometers are used to measure elastic and viscous responses to applied stresses. We retrofit a rheometer to measure viscoelastic responses of live, linked ants. Ant material is shear-thinning with a shear-rate dependent viscosity spanning four orders of magnitude, a trait that can exist in shear-thinning polymeric fluids [132].

8.2 Perspective

This study on fire ant self-assemblages is a first of it's kind, but certainly not the last. The world of insect self-assemblages is an interesting and intriguing one; it is a never-ending source of inspiration and potential future research. While this world may seem overwhelming, especially when putting it in context of other related fields such as collective behavior, granular media, and active matter, one must keep the perspective that a study

such as this one can only unlock a small part of the whole puzzle, and the whole puzzle is far too grand and profound for any one scientists or group of researchers to unlock.

8.3 Further impacts

During research collaborations with a local artist, I was told that our work sometimes blurs the lines between science and art. Not only do we strive for significant scientific discoveries and intellectual merit, but we also strive for our work to be aesthetic, appealing to a general audience, and enjoyable to read. Through pursuing this goal we have been able to impact many outside our immediate scientific community. Not only have we collaborating with physicists, biologists, and mathematicians, but we have collaborated with film directors, multimedia artists, photographers, and magazine editors just to name a few.

The scientific impact of our work is clear: a strong publication, a follow up article, a paper under review, and one more on its way. I want to briefly take this space to highlight the impact of our research beyond the publications. Roughly once or twice a month for the last 2 years I have been contacted via email by someone who either stumbled across or was directed to my website asking me details about my research or requesting permission to use my images or videos on their website or publication. It brings me joy that others are ably to use our work to further interest in science.

We were awarded a grant in collaboration with Joseph Peragine, an artist at Georgia State University, for developing artwork inspired by ants. Joe has helped us see the *broader* impacts of our work we didn't know existed. Michael Watchulonis, established nature documentary producer, director, and writer, contacted me saying he was inspired to make his next film on fire ants by coming across our work. We worked closely with Michael to film much of the documentary that is now available on *Netflix*. BBC also filmed with us to produce a small segment for their hit nature documentary series entitled *Planet Ant*. One of my soundbites even made it into the opening sequence–"fire ant rafts are truly a force to be reckoned with." Media outlets such as National Geographic, The Washington Post, and Popular Science have given our work national and international attention through their online and print publications. Lastly, the world of Youtube seems to love that fire ants won't sink as evidenced by our video entitled *A floating fire ant raft is pushed down on the surface of water* with 2 million views.

APPENDIX A

PUBLICATIONS

Published manuscripts

Mlot NJ, Tovey CA and Hu DL. "Fire ants self-assemble into waterproof rafts to survive floods," Proceedings of the National Academy of Sciences. 108.19, 2011.

Mlot NJ, Tovey CA and Hu DL "Diffusive dynamics of large fire ant rafts," Communicative & Integrative Biology. Paper is currently being rewritten per first round of reviewer's comments.

Manuscript under review

Mlot NJ, Foster P, Lin A, Hu DL. "Fire ants actively control spacing and orientation within self-assemblages," *under review with The Journal of Experimental Biology.*

Planned publication

Mlot NJ, Tovey CA and Hu DL. "Fire ants self-assemble into towers of constant strength."

Conference presentations

Mlot NJ, Tovey CA and Hu DL. "Fire ant towers." SICB. Dec 2013. San Francisco, CA
Mlot NJ and Hu DL. "Fire ants as a fabric." New Frontiers in Fiber Materials Science. Oct 2011. Charleston, SC

Mlot NJ, Shinotsuka S and Hu DL. "Ant Towers." APS: Division of Fluid Dynamics. Nov 2010. Long Beach, CA

Mlot NJ and Hu DL. "Fire ant self-assemblages - Poster" Social Biomimicry: Insect Societies and Human Design. Feb 2010. Tempe, AZ

Mlot NJ, Tovey CA and Hu DL. "Fire ant rafts." APS: Division of Fluid Dynamics. Nov 2009. Minneapolis, MN

APPENDIX B

DERIVATION OF DIFFERENTIAL EQUATION MODELS FOR ANT RAFT FORMATION

B.1 Straight movement in random direction model

Let N = the total number of ants. Let t denote time in seconds. Let $n(t)$ denote the number of ants in the bottom layer at time t = area of the raft at time t. The number of ants in the bottom layer can be converted to cm^2 with conversion factor 34 ants = 1 cm^2. Let h denote the eventual thickness of the raft, experimentally determined to be approximately 2.5 (ant heights). In the straight movement model we assume that only ants in the top layer move, and they move by picking a random direction and going straight until they hit a boundary. When they hit a boundary they "bounce" with probability $p = 0.65$ (this value determined by observation), picking a random direction away from the boundary, and "stick" with probability $1 - p$. If they bounce, they go again until they hit a boundary, where again they "bounce" with probability p and stick with probability $1-p$. They repeat this process until they stick, at which time they join the bottom h layers there. The expected number of "bounces" before sticking is therefore $\frac{1}{1-p} - 1 = 1.86$.

Lemma: Let x be a random point in a circle of radius r, and let θ be a direction randomly chosen from the interval $[0, 2\pi]$. Then the expected distance from x to the circle boundary, in the direction θ, equals $\frac{8r}{3\pi} \approx 0.8488r$. Now let x be a point on the circle boundary and let θ be a direction randomly chosen from the interval $[0, \pi]$ where $\theta = \pi/2$ means the direction towards the circle center. Then the expected distance from x to the circle boundary in the direction θ equals $4r/\pi \approx 1.27r$.

Proof: given later so as not to disrupt the exposition of the model.

Let u denote the speed of an ant in cm/sec. When $N \geq (h+1)n(t)$ there is a full top layer of ants who can move. A single ant in that layer takes on average $(0.849+(1.86)(1.27))r/u = 3.21r/u$ seconds to reach a boundary and stick, where $\pi r^2 = n(t)/34$ so $r = \sqrt{n(t)/34\pi}$ is the radius of the raft in cm. There are $n(t)$ ants in the moving layer so on average $n(t)u/3.21r$ ants reach and stick to the boundary per second. This equals $\sqrt{34\pi n(t)}u/3.21$ ants per second. These ants form a new exterior boundary h ants thick. So

$$\frac{dn(t)}{dt} = u\sqrt{34\pi n(t)}/3.21h.$$

When $hn(t) \leq N \leq (h+1)n(t)$ there is a partial layer of $N - hn(t)$ ants who can move. So

$$\frac{dn(t)}{dt} = u(N - hn(t))/3.21hr = u\sqrt{34\pi}(N - hn(t))/3.21h\sqrt{n(t)}.$$

B.2 Brownian Motion Model

Let $N, t, n(t), h$ be as in the Straight Motion model. We assume that only ants in the top layer move, and they move in brownian motion until they hit a boundary. It is more or less obvious that the expected time to reach a boundary from the center of a circle of radius r

is r^2 (up to scaling by ant speed). It is not as obvious what the expected time to reach a boundary is from a random point in the circle.

Lemma: Let x be a random point in a circle of radius r. Execute standard brownian motion from x. The expected time until the circle boundary is reached is $r^2/4$.

Proof: From page 125 of Stochastic differential equations: an introduction with applications By Bernt Karsten Øksendal 6th edition 2003 Springer, the expected first hitting time is $(r^2 - |x|^2)/2$ where $|x|^2$ is the squared distance to the circle center from x. The rest is calculus, given later.

When $N \geq (h+1)n(t)$ there is a full top layer of ants who can move. A single ant in that layer takes $r^2/4 = n(t)/136\pi$ seconds to reach a boundary, since $\pi r^2 = n(t)/34$. There are $n(t)$ ants in the moving layer so on average $136\pi n(t)/n(t) = 136\pi$ ants reach the boundary per second. Notice this is independent of the size of the raft and of N.

$$\frac{dn(t)}{dt} = 136\pi/h.$$

When $hn(t) \leq N \leq (h+1)n(t)$ we have $N - hn(t)$ ants in the moving layer. On average $136\pi(N - hn(t))/n(t)$ reach the boundary per second. For this time period,

$$\frac{dn(t)}{dt} = 136\pi(N - hn(t))/hn(t).$$

Notes: This model has to be scaled by some unknown factor which is the ant speed, but the ant speed here is not the usual cm/sec but rather the brownian motion scaling compared with standard brownian motion. This model's predictions don't match the data. In the data, rafts grow faster when N is bigger. We changed the model to let every ant except those in the lowest h layers move. The formula is simply the 2nd formula used for all t, that is,

$$\frac{dn(t)}{dt} = 136\pi(N - hn(t))/hn(t).$$

However, this model did not fit the data, either.

B.3 Calculus Derivations

For the Brownian Motion Model, we want the average value of $(r^2 - x^2)/2$ in a circle of radius r, where x^2 is the squared distance to the circle center. This is

$$\frac{1}{\pi r^2} \int_{x=0}^{r} \frac{r^2 - x^2}{2} 2\pi x \; dx = r^2/4.$$

For the Straight Motion Model, we first need a geometric lemma. Suppose the ant is at distance x from the circle center. Consider the chord that is perpendicular to the line segment from the circle center to the ant, and passes through the ant. Let z denote the length of the chord. Then $(z/2)^2 = (r-x)(r+x)$ whence $z/2 = \sqrt{r^2 - x^2}$. Now suppose the ant moves at angle θ to the chord. If $\theta = 0$ or $\theta = \pi$ the distance to the circle boundary is $z/2$. If $\theta = \pi/2$ the distance is $r + x$ and if $\theta = 3\pi/2$ the distance is $r - x$. We need a formula for the general case of θ. By symmetry it suffices to consider the cases $0 \leq \theta \leq \pi/2; \pi \leq \theta \leq 3\pi/2$. The two cases $\theta, \theta + \pi$ define a chord passing through the ant. Let y denote the length of the shorter segment of the chord (where the chord intersects the ant). Then the longer segment has length $2x \sin\theta + y$. From this we obtain

$$y(2x \sin\theta + y) = (r-x)(r+x) \Rightarrow y^2 + 2x \sin\theta y - (r^2 - x^2) = 0.$$

One of the roots to this quadratic is negative. Hence

$$y = -x\sin\theta + \sqrt{x^2\sin^2\theta + (r^2 - x^2)}.$$

If the ant randomly chooses between θ and $\theta+\pi$ the expected distance traveled is $\frac{1}{2}(2x\sin\theta + 2y) = \sqrt{x^2\sin^2\theta + r^2 - x^2} = \sqrt{r^2 - x^2\cos^2\theta}$.

(Check this against the two extremes: when $\theta = \pi/2$ we have $\cos\theta = 0$ and the expected distance is r, which is correct. When $\theta = 0$ we have $\cos\theta = 1$ and the expected distance is $\sqrt{r^2 - x^2} = z/2$ which is correct.)

We assume that the ant chooses a random direction. The expected distance traveled by the ant to a boundary is therefore

$$\frac{2}{\pi}\int_0^{\pi/2} \sqrt{r^2 - x^2\cos^2\theta}\ d\theta.$$

Taking the mean value of this as x ranges from 0 to r gives an overall expected distance of

$$\frac{1}{\pi r^2}\int_0^r 2\pi x\ dx \int_0^{\pi/2} \frac{2}{\pi}\sqrt{r^2 - x^2\cos^2\theta}\ d\theta.$$

Putting the factor of r on the left (this is obvious by scaling, we could have done it earlier) gives

$$r\int_0^1 4x/\pi\ dx \int_0^{\pi/2} \sqrt{1 - x^2\cos^2\theta}\ d\theta = 8r/3\pi \approx 0.8488r.$$

The integral was calculated both numerically and with Mathematica 7. (Check this against the two extremes. At the two extremes of integration, the values are $2r/\pi$ at $x = r$, and r at $x = 0$. The average value ought to be somewhere between $0.64 \approx 2/\pi$ and 1.)

After the ant reaches the boundary, the situation is slightly different. We assume that the ant moves in a random direction *away* from the boundary. In terms of our model, we assume that the ant chooses a random value of θ from the interval $0 \le \theta \le \pi$. The expected distance to the (next) boundary is

$$\frac{2}{\pi}r\int_0^{\pi/2} 2\sqrt{1 - cos^2\theta}\ d\theta = \frac{4r}{\pi}\int_0^{\pi/2} \sin\theta\ d\theta = \frac{4r}{\pi} = 1.27r$$

APPENDIX C

DATA PROCESSING TO PRODUCE 3-D ANT STRUCTURE RENDERINGS

The processing proceeded in three phases:

Overview

Image processing: Segmenting the ants from the scan. Filling in voids left due to body cavities and scan noise.

Object segmentation, identification, and association: Breaking up the scan into body segments and appendages. Associating the body segments together and tracing appendage segments. (This part required nearly all of the hand corrections, mostly in body part association and solving Y intersections of appendages.)

Measurements: Gathering various statistics.

Details

Image Processing:

1. The ant balls were scanned as 3D 1600x1600x1600 voxel images with 7 micron voxel size.
2. The images were thresholded to segment the ants from background noise. Due to brightness variations between scans, the threshold was manually adjusted for each scan.
3. Small bits of noise were removed using the "bwareaopen" command.
4. The internal body cavities were filled in. This was the trickiest image processing operation because the ants often contained large cavities close to the exoskeleton, leading to aliasing at the surface. To do this we used a trick similar to a visual hull computation:
a. The 3D image was sliced into 2D planes in the (1 0 0) axis (i.e. planes perpendicular to the x direction)
b. The 2D images were filled with "imfill"
c. steps a. and b. were repeated for slices in the 1 0 0 , 1 1 0 , and 1 1 1 plane families (i.e. perpendicular to the axes, perpendicular to the short diagonals of a cube, and perpendicular to the long diagonals of a cube.)
d. Any voxels that were filled in at least two slices are filled in the original image
e. Repeat entire procedure until convergence
This was found to fill in essentially all of the body cavities without creating spurious connections.

Object Segmentation and Association:

Body:

Because it was hard to algorithmically segment whole bodies from appendages, we used an approach where we over-segmented the ants into individual body segments and appendage segments and then associating the body and appendage segments together to form complete bodies and appendages.

1. Segmentation:
A watershed transform of the distance transform of the image was used to cut up the image into segments. An extended maxima transform was applied to the distance transformed image to prevent noise from causing spurious segments.
We found that the bodies would segment into head, thorax, petioles and gaster, and that petioles, thorax, and head would sometimes remain connected to each other after segmentation.

2. Body Association:
Under the assumption that each ant body should contain a head, thorax, and gaster, we labelled the body segments head-or-gaster, head-and-thorax, or thorax.
a. The appendage segments and unconnected petioles were removed by a morphological opening using "imopen".
b. The ellipticity of the moment of inertia ellipsoid was used to classify the remaining segments, with low ellipticity marking head-or-gaster, medium ellipticity marking thorax, and high ellipticity marking head-and-thorax.
c.The two points on the thorax farthest from each other along the direction of the thorax's principle moment of inertia were designated as connection points. The head-or-gaster segments that came closest to each connection point were associated with the thorax to form a full ant body. The procedure for the head-and-thorax segments was similar except that only the connection point farthest from the centroid was used.
This part of the algorithm was prone to errors, so mistakes were corrected by reviewing each ant and manually fixing incorrect associations.

3. Appendage Association:
Segments that were not used in the bodies and had high aspect ratio (as measured by ellipticity of the moment of inertia ellipsoid) were classified as appendage segments. Starting from these segments, our algorithm defines connection points in the same way as for the thorax. Each appendage segment was then associated with the nearest other appendage segment to form an appendage.
Appendages were considered complete when they all connection points were either connected to a body segment, too far from another segment, or terminated at an intersection. Appendage segments were connected through intersections when their principal axis closely aligned with the principal axis of another segment approaching the intersection (meaning they were probably the same leg and just crossing over another leg).
This part of the algorithm was also prone to errors at Y intersections where legs terminated on one another, so mistakes were corrected by hand reviewing all of the connections.

Measurements:

Number of Connected Neighbors:
Any two ants where an appendage started at one and stopped at another were considered neighbors.

Connections per Ant:
The connections for a given ant were the number of appendages that connect that ant to another ant, which was measured as the number of appendages terminating on the ant's body or on appendages terminating on the ants body. In cases where both ends of an appendage terminated on body segments and another appendage terminated on it, the result was hand reviewed.
Packing Fraction:
Packing fraction was defined as the ratio of volume occupied by ant bodies and limbs to occupied volumedetermined by dilating the ant ball, using "imdilate", until 95% of the interior was filled.
Ant spacing:
Center of mass for each ant was estimated as the centroid of all of its body segments, excluding appendages. From this we determined spacing as the distance from each centroid to its nearest neighbor.
Orientation:
Described in structure paper

APPENDIX D

DETAILS FOR APPROXIMATING TOWER GROWTH RATE

We can use values for other parameters to estimate g. The volume of layer i is $Rn(i)/\chi cm^3$ since each segment follows the shape law. The thickness is ψcm. The cross section surface area of the segments, taken together, is $Rn(i)/\chi\psi$. The cross section surface area of the segments plus the cross section area of the pole is $Rn(i)/\chi\psi + \pi D^2/4$. The diameter is $2\sqrt{(\pi D^2/4 + Rn(i)/\chi\psi)/\pi}$. The circumference is $2\sqrt{(\pi^3 D^2/4 + \pi Rn(i)/\chi\psi)}$. The area of the surface of layer i of the tower is approximately the circumference times the thickness which equals

$$2\sqrt{(\pi(\pi\psi D/2)^2 + \pi\psi Rn(i)/\chi)}.$$

The surface area of the first $k+1$ layers is approximated by the integral

$$\int_0^k 2\sqrt{\pi(\pi\psi D/2)^2 + \pi\psi Rn(i)/\chi}di \approx 2\sqrt{\pi}\int_0^k \sqrt{2.1D^2 + 0.48Re^{.29i}}di.$$

This integral has no simple closed form solution (unless we use inverse hyperbolic tangents) so we approximate the integrand with a Taylor series as

$$\sqrt{0.48R}e^{.15i} + 2.1D^2/2\sqrt{0.48R}e^{.15i} - 0.25(2.1)^2D^4/(0.48R)^{3/2}e^{.45i}.$$

This gives an approximation of surface area as

$$2\sqrt{\pi}\int_0^k \sqrt{0.48R}e^{.15i} + 2.1D^2/2\sqrt{0.48R}e^{.15i} - 0.25(2.1)^2D^4/(0.48R)^{3/2}e^{.45i}di =$$
$$3.5\int_0^k 0.69\sqrt{R}e^{.15i} + 1.5D^2e^{-.15i}/\sqrt{R} - 3.3D^4e^{-0.45i}R^{-3/2} =$$
$$16\sqrt{R}(e^{.15k} - 1) - 35D^2(e^{-.15k} - 1)/\sqrt{R} + 26D^4(e^{-0.45k} - 1)R^{-3/2}. \quad (12)$$

At $d/\psi = 4/.93 \approx 4.3$ layers we estimate the surface area. Set $k = 3.3$ (since the first layer is layer 0). Set $R = 22D$. Then at $D = 0.5$ we have the values $R = 11, \sqrt{R} = 3.3, 1/\sqrt{R} = 0.30, D = 0.5, e^{.15k} = 1.6, e^{-.15k} = 0.61, e^{-0.45k} = 0.23$. The surface area estimate is

$$16 \times 3.3 \times 0.6 + 35/4 \times 0.39 \times 0.3 - 26/16 \times 0.77 \times 0.027$$

which equals $31.7 + 1.02 - 0.034 = 32.6 \approx 33$. At $R = 22$ sections, the top d cm of each section has surface area $33/22 = 1.5cm^2$. The density ρ is 0.3 ants per cm^2. The expected number of ants is .45 and the number of ants is Poisson distributed with mean 0.45.

Probability $X = 0 : 0.64$. Probability $X = 1 : 0.29$. Probability $X = 2 : 0.06$. Probability $X > 2 : 0.01$. The key probability is for $X \geq 1 : 0.36$.

Idealize the movement of ants into time steps of time length $d/v = 4cm/0.4cm/sec = 10sec$. In one time step, with probability 0.64 there are no ants so nothing happens. With probability .29 there is one ant. It moves up with probability .5. With probability 0.06 there are two ants but only the top ant has a chance of filling the empty spot and that

has probability 0.5. So the chance the spot gets reached is 0.36×0.5=0.18. The chance an ant that reaches the empty spot stays, rather than bouncing, is p. Hence the expected time until the spot is filled is $10sec \times 1/0.18 \times 1/p = 56/p$ seconds. Using $p = 0.3$ from ant raft data gives 185 seconds or about 3 minutes. The growth rate is $(60/185(layer/min)) \times (.93(cm/layer)) = 0.30cm/minute$. Once the tunnels start operating the speed should decrease to $.30 - s = .3 - .05 = 0.25cm/minute$.

Suppose we double D from $0.5cm$ to $1cm$. R doubles. In equation 12, the first term increases by a factor of $\sqrt{2}$. The second term increases by a factor of $2^2/\sqrt{2} = 2^{1.5} \approx 2.828$. The third term increases by a factor of $2^4/2^{1.5} = 2^{2.5} \approx 5.656$. The number of sections R has doubled so the total surface area is divided by twice as much. The net effect is that the 1st term decreases by a factor of $\sqrt{2}$ to give $31.7/1.414 = 22.4$. The 2nd term increases by factor $2.828/2 = 1.414$ to give $1.02 \times 1.414 = 1.44$ and the 3rd term increases by factor 2.828 to give $-.034 \times 2.828 = -0.96$. The surface area of a segment is $22.9 \times 1/22 = 1.04cm^2$. Multiply by .3 ants per square centimeter to get .31 for the expected number of ants. From the Poisson distribution the chance of zero ants is $e^{-.31} = 0.73$. The probability $X \geq 1$ is 0.27 rather than 0.36. The predicted speed of growth is slower, namely $0.30 \times 0.27/0.36 = .225cm/minute$. After the tunnels start operating the speed should decrease to $.225 - s = .225 - 0.05 = 0.175cm/minute$.

REFERENCES

[1] N. Gravish, S. Franklin, D. Hu, and D. Goldman, "Entangled granular media," *Physical Review Letters*, vol. in review, 2012.

[2] A. Wouterse, S. R. Williams, and A. P. Philipse, "Effect of particle shape on the density and microstructure of random packings," *Journal of Physics: Condensed Matter*, vol. 19, no. 40, p. 406215, 2007.

[3] W. Tschinkel, *The fire ants*. Belknap Press, 2006.

[4] K. Stokely, A. Diacou, and S. V. Franklin, "Two-dimensional packing in prolate granular materials," *Physical Review E*, vol. 67, no. 5, p. 051302, 2003.

[5] Y. Liu and K. Passino, "Swarm intelligence: Literature overview," *Department of Electrical Engineering, the Ohio State University*, 2000.

[6] P. Miller, *The smart swarm: how understanding flocks, schools, and colonies can make us better at communicating, decision making, and getting things done*. Avery Pub Group, 2010.

[7] S. Garnier, J. Gautrais, and G. Theraulaz, "The biological principles of swarm intelligence," *Swarm Intelligence*, vol. 1, no. 1, pp. 3–31, 2007.

[8] C. Nicolson, A. Starfield, G. Kofinas, and J. Kruse, "Ten heuristics for interdisciplinary modeling projects," *Ecosystems*, vol. 5, no. 4, pp. 376–384, 2002.

[9] W. Gotwald, "Army ants," *Social insects*, vol. 4, pp. 157–254, 1982.

[10] C. Anderson, G. Theraulaz, and J. Deneubourg, "Self-assemblages in insect societies," *Insectes Sociaux*, vol. 49, no. 2, pp. 99–110, 2002.

[11] C. Anderson and D. W. McShea, "Intermediate-level parts in insect societies: adaptive structures that ants build away from the nest," *Insectes Sociaux*, vol. 48, no. 4, pp. 291–301, 2001.

[12] W. Allee, "Animal aggregations," *Quarterly Review of Biology*, vol. 2, no. 3, pp. 367–398, 1927.

[13] J. Halley and D. Winkler, "Consistent concepts of self-organization and self-assembly," *Complexity*, vol. 14, no. 2, pp. 10–17, 2008.

[14] C. Anderson and N. Franks, "Teamwork in animals, robots, and humans," *Advances in the Study of Behavior*, vol. 33, pp. 1–48, 2003.

[15] S. Cully and T. Seeley, "Self-assemblage formation in a social insect: the protective curtain of a honey bee swarm," *Insectes sociaux*, vol. 51, no. 4, pp. 317–324, 2004.

[16] A. Lioni, C. Sauwens, G. Theraulaz, and J. Deneubourg, "Chain formation in Oecophylla longinoda," *Journal of Insect Behavior*, vol. 14, no. 5, pp. 679–696, 2001.

[17] N. Mlot, C. Tovey, and D. Hu, "Fire ants self-assemble into waterproof rafts to survive floods," *Proceedings of the National Academy of Sciences*, vol. 108, no. 19, p. 7669, 2011.

[18] A. Lioni and J. Deneubourg, "Collective decision through self-assembling," *Naturwissenschaften*, vol. 91, no. 5, pp. 237–241, 2004.

[19] H. Azzag and M. Lebbah, "A new approach for auto-organizing a groups of artificial ants," *Advances in Artificial Life. Darwin Meets von Neumann*, pp. 440–447, 2011.

[20] E. Bonabeau, G. Theraulaz, J. Deneubourg, A. Lioni, F. Libert, C. Sauwens, and L. Passera, "Dripping faucet with ants," *Physical Review E*, vol. 57, no. 5, pp. 5904–5907, 1998.

[21] G. Theraulaz, E. Bonabeau, C. Sauwens, J. Deneubourg, A. Lioni, F. Libert, L. Passera, and R. Solé, "Model of droplet dynamics in the Argentine ant Linepithema humile (Mayr)," *Bulletin of Mathematical Biology*, vol. 63, no. 6, pp. 1079–1093, 2001.

[22] R. Harkness and N. Maroudas, "Central place foraging by an ant (cataglyphis bicolor fab.): a model of searching," *Animal behaviour*, vol. 33, no. 3, pp. 916–928, 1985.

[23] I. Helland, "Diffusion models for the dispersal of insects near an attractive center," *Journal of Mathematical Biology*, vol. 18, no. 2, pp. 103–122, 1983.

[24] E. Bonabeau, G. Theraulaz, J. Deneubourg, S. Aron, and S. Camazine, "Self-organization in social insects," *Trends in Ecology & Evolution*, vol. 12, no. 5, pp. 188–193, 1997.

[25] S. Camazine, *Self-organization in biological systems*. Princeton Univ Pr, 2003.

[26] I. D. Couzin and J. Krause, "Self-organization and collective behavior in vertebrates," *Advances in the Study of Behavior*, vol. 23, pp. 1–75, 1999.

[27] R. Goldstone and T. Gureckis, "Collective behavior," *Topics in Cognitive Science*, vol. 1, no. 3, pp. 412–438, 2009.

[28] D. Sumpter, "The principles of collective animal behaviour," *Philosophical Transactions of the Royal Society B: Biological Sciences*, vol. 361, no. 1465, p. 5, 2006.

[29] S. Nouyan, R. Groß, M. Bonani, F. Mondada, and M. Dorigo, "Teamwork in self-organized robot colonies," *Evolutionary Computation, IEEE Transactions on*, vol. 13, no. 4, pp. 695–711, 2009.

[30] H. Hess, "Self-assembly driven by molecular motors," *Soft Matter*, vol. 2, no. 8, pp. 669–677, 2006.

[31] I. Couzin and N. Franks, "Self-organized lane formation and optimized traffic flow in army ants," *Proceedings of the Royal Society of London. Series B: Biological Sciences*, vol. 270, no. 1511, p. 139, 2003.

[32] C. Anderson, "Self-organization in relation to several similar concepts: Are the boundaries to self-organization indistinct?," *The Biological Bulletin*, vol. 202, no. 3, pp. 247–255, 2002.

[33] M. Moussaid, S. Garnier, G. Theraulaz, and D. Helbing, "Collective information processing and pattern formation in swarms, flocks, and crowds," *Topics in Cognitive Science*, vol. 1, no. 3, pp. 469–497, 2009.

[34] G. Beni and J. Wang, "Swarm intelligence in cellular robotic systems," *Robots and Biological Systems: Towards a New Bionics?*, pp. 703–712, 1993.

[35] E. Bonabeau, M. Dorigo, and G. Theraulaz, *Swarm intelligence: from natural to artificial systems*. Oxford University Press, USA, 1999.

[36] Y. Cao, A. Fukunaga, and A. Kahng, "Cooperative mobile robotics: Antecedents and directions," *Autonomous robots*, vol. 4, no. 1, pp. 7–27, 1997.

[37] M. Dorigo, V. Trianni, E. Şahin, R. Groß, T. Labella, G. Baldassarre, S. Nolfi, J. Deneubourg, F. Mondada, D. Floreano, *et al.*, "Evolving self-organizing behaviors for a swarm-bot," *Autonomous Robots*, vol. 17, no. 2, pp. 223–245, 2004.

[38] F. Ducatelle, G. Di Caro, C. Pinciroli, and L. Gambardella, "Self-organized cooperation between robotic swarms," *Swarm Intelligence*, pp. 1–24, 2011.

[39] R. Groß, M. Bonani, F. Mondada, and M. Dorigo, "Autonomous self-assembly in swarm-bots," *Robotics, IEEE Transactions on*, vol. 22, no. 6, pp. 1115–1130, 2006.

[40] C. Kube and H. Zhang, "Collective robotics: From social insects to robots," *Adaptive Behavior*, vol. 2, no. 2, p. 189, 1993.

[41] R. Pfeifer, M. Lungarella, and F. Iida, "Self-organization, embodiment, and biologically inspired robotics," *science*, vol. 318, no. 5853, p. 1088, 2007.

[42] E. Şahin, "Swarm robotics: From sources of inspiration to domains of application," *Swarm Robotics*, pp. 10–20, 2004.

[43] D. Floreano and C. Mattiussi, *Bio-inspired artificial intelligence: theories, methods, and technologies*. The MIT Press, 2008.

[44] S. Kernbach, E. Meister, F. Schlachter, K. Jebens, M. Szymanski, J. Liedke, D. Laneri, L. Winkler, T. Schmickl, R. Thenius, *et al.*, "Symbiotic robot organisms: Replicator and symbrion projects," in *Proceedings of the 8th Workshop on Performance Metrics for Intelligent Systems*, pp. 62–69, ACM, 2008.

[45] J. Deneubourg, S. Goss, N. Franks, A. Sendova-Franks, C. Detrain, and L. Chrétien, "The dynamics of collective sorting robot-like ants and ant-like robots," in *Proceedings of the first international conference on simulation of adaptive behavior on From animals to animats*, pp. 356–363, 1991.

[46] R. Groß, *Self-assembling robots*. PhD thesis, Citeseer, 2007.

[47] S. Ramaswamy, "The mechanics and statistics of active matter," *Annual Review of Condensed Matter Physics*, vol. 1, pp. 323–345, 2010.

[48] T. Vicsek and A. Zafeiris, "Collective motion," *Physics Reports*, 2012.

[49] T. Endlein and W. Federle, "Walking on smooth or rough ground: passive control of pretarsal attachment in ants," *Journal of Comparative Physiology A*, vol. 194, no. 1, pp. 49–60, 2008.

[50] A. Lipp, H. Wolf, and F.-O. Lehmann, "Walking on inclines: energetics of locomotion in the ant camponotus," *Journal of experimental biology*, vol. 208, no. 4, pp. 707–719, 2005.

[51] B. Hölldobler and E. Wilson, *The ants*. Belknap Press, 1990.

[52] R. Albert, I. Albert, D. Hornbaker, P. Schiffer, and A.-L. Barabási, "Maximum angle of stability in wet and dry spherical granular media," *Physical Review E*, vol. 56, no. 6, pp. R6271–R6274, 1997.

[53] P. B. Umbanhowar and D. I. Goldman, "Low density fragile states in cohesive powders," *American journal of physics*, vol. 74, p. 720, 2006.

[54] D. Hornbaker, R. Albert, I. Albert, A.-L. Barabási, and P. Schiffer, "What keeps sandcastles standing?," *Nature*, vol. 387, no. 6635, p. 765, 1997.

[55] E. Brown, A. Nasto, A. G. Athanassiadis, and H. M. Jaeger, "Strain stiffening in random packings of entangled granular chains," *Physical Review Letters*, vol. 108, no. 10, p. 108302, 2012.

[56] W. Thorpe and D. Crisp, "Studies on plastron respiration," *Journal of Experimental Biology*, vol. 24, no. 3-4, pp. 227–269, 1947.

[57] M. Flynn and J. Bush, "Underwater breathing: the mechanics of plastron respiration," *Journal of Fluid Mechanics*, vol. 608, pp. 275–296, 2008.

[58] A. Cassie and S. Baxter, "Wettability of porous surfaces," *Transactions of the Faraday Society*, vol. 40, pp. 546–551, 1944.

[59] R. Wenzel, "Resistance of solid surfaces to wetting by water," *Industrial & Engineering Chemistry*, vol. 28, no. 8, pp. 988–994, 1936.

[60] J. Bush, D. Hu, and M. Prakash, "The integument of water-walking arthropods: form and function," *Advances in Insect Physiology*, vol. 34, pp. 117–192, 2007.

[61] J. Bush and D. Hu, "Walking on water: biolocomotion at the interface," *Annu. Rev. Fluid Mech.*, vol. 38, pp. 339–369, 2006.

[62] D. Hu, B. Chan, J. Bush, *et al.*, "The hydrodynamics of water strider locomotion," *Nature*, vol. 424, no. 6949, pp. 663–666, 2003.

[63] D. Hu and J. Bush, "The hydrodynamics of water-walking arthropods," *Journal of Fluid Mechanics*, vol. 644, no. 1, pp. 5–33, 2010.

[64] K. Haight, "Defensiveness of the fire ant, solenopsis invicta, is increased during colony rafting," *Insectes sociaux*, vol. 53, no. 1, pp. 32–36, 2006.

[65] S. Vinson *et al.*, "Invasion of the red imported fire ant (hymenoptera: Formicidae): spread, biology, and impact.," *American Entomologist*, vol. 43, no. 1, pp. 23–39, 1997.

[66] W. Morrill, "Dispersal of red imported fire ants by water," *Florida Entomologist*, pp. 39–42, 1974.

[67] M. Goodisman and K. Ross, "Relationship of queen number and worker size in polygyne colonies of the fire ant Solenopsis invicta," *Insectes Sociaux*, vol. 43, no. 3, pp. 303–307, 1996.

[68] W. Wheeler, *Ants: their structure, development, and behavior*. Columbia Univ Pr, 1960.

[69] S. McGrail, *Ancient boats and ships*, vol. 31. Shire, 2008.

[70] R. C. Highsmith, "Floating and algal rafting as potential dispersal mechanisms in brooding invertebrates.," *Marine ecology progress series. Oldendorf*, vol. 25, no. 2, pp. 169–179, 1985.

[71] S. H. Suhr, Y. S. Song, S. J. Lee, and M. Sitti, "Biologically inspired miniature water strider robot," in *Proceedings of the Robotics: Science and Systems I*, pp. 319–325, Boston, USA, 2005.

[72] W. Federle, M. Riehle, and A. Curtis, "An integrative study of insect adhesion: Mechanics and wet adhesion of pretarsal pads in ants," *Integrative and Comparative Biology*, vol. 42, no. 6, p. 1100, 2002.

[73] T. Merton, "On a barrier against insect pests," *Proceedings of the Royal Society of London. Series A, Mathematical and Physical Sciences*, pp. 218–220, 1956.

[74] W. Banks, "Techniques for collecting, rearing, and handling imported fire ants.," *Advances in Agricultural Technology, Science and Education Administration, United States Department of Agriculture*, no. AAT-S-21, 1981.

[75] J. Chen, "Advancement on techniques for the separation and maintenance of the red imported fire ant colonies," *Insect Science*, vol. 14, no. 1, pp. 1–4, 2007.

[76] A. Dejean, C. Leroy, B. Corbara, O. Roux, R. Céréghino, J. Orivel, and R. Boulay, "Arboreal ants use the velcro® principle to capture very large prey," *PloS one*, vol. 5, no. 6, p. e11331, 2010.

[77] W. Federle, K. Rohrseitz, and B. Holldobler, "Attachment forces of ants measured with a centrifuge: better wax-runners have a poorer attachment to a smooth surface," *Journal of Experimental Biology*, vol. 203, no. 3, pp. 505–512, 2000.

[78] W. Federle and T. Endlein, "Locomotion and adhesion: dynamic control of adhesive surface contact in ants," *Arthropod structure & development*, vol. 33, no. 1, pp. 67–75, 2004.

[79] S. Gorb, "Smooth attachment devices in insects: functional morphology and biomechanics," *Advances in insect physiology*, vol. 34, pp. 81–115, 2007.

[80] D. Cassill, A. Greco, R. Silwal, and X. Wang, "Opposable spines facilitate fine and gross object manipulation in fire ants," *Naturwissenschaften*, vol. 94, no. 4, pp. 326–332, 2007.

[81] H. Stewart, "Ontogenetic changes in buoyancy, breaking strength, extensibility, and reproductive investment in a drifting macroalga turbinaria ornata (phaeophyta) 1," *Journal of phycology*, vol. 42, no. 1, pp. 43–50, 2006.

[82] D. Hu and J. Bush, "Meniscus-climbing insects," *Nature*, vol. 437, no. 7059, pp. 733–736, 2005.

[83] C. Neinhuis and W. Barthlott, "Characterization and distribution of water-repellent, self-cleaning plant surfaces," *Annals of Botany*, vol. 79, no. 6, pp. 667–677, 1997.

[84] X. Gao and L. Jiang, "Biophysics: water-repellent legs of water striders," *Nature*, vol. 432, no. 7013, pp. 36–36, 2004.

[85] P. De Gennes, F. Brochard-Wyart, and D. Quéré, *Capillarity and wetting phenomena: drops, bubbles, pearls, waves*. Springer Verlag, 2004.

[86] D. Quéré, "Wetting and roughness," *Annu. Rev. Mater. Res.*, vol. 38, pp. 71–99, 2008.

[87] A. Yarin, "Drop impact dynamics: splashing, spreading, receding, bouncing," *Annu. Rev. Fluid Mech.*, vol. 38, pp. 159–192, 2006.

[88] S. Rafaï, D. Bonn, and A. Boudaoud, "Spreading of non-newtonian fluids on hydrophilic surfaces," *Journal of Fluid Mechanics*, vol. 513, no. 1, pp. 77–85, 2004.

[89] F. Brochard-Wyart, G. Debregeas, and P. Gennes, "Spreading of viscous droplets on a non viscous liquid," *Colloid & Polymer Science*, vol. 274, no. 1, pp. 70–72, 1996.

[90] B. Øksendal, *Stochastic differential equations: an introduction with applications*. Springer Verlag, 2003.

[91] G. Whitesides and B. Grzybowski, "Self-assembly at all scales," *Science*, vol. 295, no. 5564, p. 2418, 2002.

[92] R. Wool, "Self-healing materials: a review," *Soft Matter*, vol. 4, no. 3, pp. 400–418, 2008.

[93] L. Henderson, "On the fluid mechanics of human crowd motion," *Transportation research*, vol. 8, no. 6, pp. 509–515, 1974.

[94] V. Fourcassié, C. Bredard, K. Volpatti, and G. Theraulaz, "Dispersion movements in ants: spatial structuring and density-dependent effects," *Behavioural processes*, vol. 63, no. 1, pp. 33–43, 2003.

[95] D. Gordon, "Group-level exploration tactics in fire ants," *Behaviour*, pp. 162–175, 1988.

[96] B. Fristedt and L. Gray, *A Modern Approach to Probability Theory*. Birkhauser, Boston, 1996.

[97] T. Friedrich and L. Levine, "Fast simulation of large-scale growth models," *Approximation, Randomization, and Combinatorial Optimization. Algorithms and Techniques*, pp. 555–566, 2011.

[98] F. Schweitzer, W. Ebeling, and B. Tilch, "Statistical mechanics of canonical-dissipative systems and applications to swarm dynamics," *Physical Review E*, vol. 64, no. 2, p. 021110, 2001.

[99] G. Theraulaz, E. Bonabeau, S. Nicolis, R. Solé, V. Fourcassié, S. Blanco, R. Fournier, J. Joly, P. Fernández, A. Grimal, *et al.*, "Spatial patterns in ant colonies," *Proceedings of the National Academy of Sciences*, vol. 99, no. 15, p. 9645, 2002.

[100] F. Bartumeus, M. G. E. da Luz, G. Viswanathan, and J. Catalan, "Animal search strategies: a quantitative random-walk analysis," *Ecology*, vol. 86, no. 11, pp. 3078–3087, 2005.

[101] C. Detrain and J. Deneubourg, "Self-organized structures in a superorganism: do ants "behave" like molecules?," *Physics of Life Reviews*, vol. 3, no. 3, pp. 162–187, 2006.

[102] J.-L. Deneubourg and S. Goss, "Collective patterns and decision-making," *Ethology Ecology & Evolution*, vol. 1, no. 4, pp. 295–311, 1989.

[103] R. Beckers, J.-L. Deneubourg, S. Goss, and J. Pasteels, "Collective decision making through food recruitment," *Insectes sociaux*, vol. 37, no. 3, pp. 258–267, 1990.

[104] D. Gordon, R. Paul, and K. Thorpe, "What is the function of encounter patterns in ant colonies?," *Animal Behaviour-London*, vol. 45, pp. 1083–1083, 1993.

[105] T. C. Schneirla, "Army ants: A study in social organization.," 1971.

[106] A. Lioni, C. Sauwens, G. Theraulaz, and J.-L. Deneubourg, "Chain formation in oecophylla longinoda," *Journal of Insect Behavior*, vol. 14, no. 5, pp. 679–696, 2001.

[107] E. Bonabeau, G. Theraulaz, J.-L. Deneubourg, A. Lioni, F. Libert, C. Sauwens, and L. Passera, "Dripping faucet with ants," *Physical Review E*, vol. 57, no. 5, p. 5904, 1998.

[108] A. Donev, I. Cisse, D. Sachs, E. A. Variano, F. H. Stillinger, R. Connelly, S. Torquato, and P. Chaikin, "Improving the density of jammed disordered packings using ellipsoids," *Science*, vol. 303, no. 5660, pp. 990–993, 2004.

[109] K. Desmond and S. Franklin, "Jamming of three-dimensional prolate granular materials," *Physical Review E*, vol. 73, no. 3, p. 031306, 2006.

[110] J. Blouwolff and S. Fraden, "The coordination number of granular cylinders," *EPL (Europhysics Letters)*, vol. 76, no. 6, p. 1095, 2007.

[111] J. Zhao, S. Li, R. Zou, and A. Yu, "Dense random packings of spherocylinders," *Soft Matter*, vol. 8, no. 4, pp. 1003–1009, 2012.

[112] R. Haralick and L. Shapiro, *Computer and robot vision*. Addison-Wesley, 1992.

[113] A. Wouterse, S. Luding, and A. Philipse, "On contact numbers in random rod packings," *Granular Matter*, vol. 11, no. 3, pp. 169–177, 2009.

[114] L. A. Wood and W. R. Tschinkel, "Quantification and modification of worker size variation in the fire antsolenopsis invicta," *Insectes Sociaux*, vol. 28, no. 2, pp. 117–128, 1981.

[115] K. S. Toohey, N. R. Sottos, J. A. Lewis, J. S. Moore, and S. R. White, "Self-healing materials with microvascular networks," *Nature materials*, vol. 6, no. 8, pp. 581–585, 2007.

[116] T. Lo and H. Cui, "Effect of porous lightweight aggregate on strength of concrete," *Materials Letters*, vol. 58, no. 6, pp. 916–919, 2004.

[117] C. Hernandez, G. Beaupré, T. Keller, and D. Carter, "The influence of bone volume fraction and ash fraction on bone strength and modulus," *Bone*, vol. 29, no. 1, pp. 74–78, 2001.

[118] R. Al-Raoush and M. Alsaleh, "Simulation of random packing of polydisperse particles," *Powder technology*, vol. 176, no. 1, pp. 47–55, 2007.

[119] N. Mlot, C. Tovey, and D. Hu, "Dynamics and circularity of large fire ant rafts," *Communicative & Integrative Biology*, vol. 5, no. 6, pp. 0–1, 2012.

[120] N. Gravish, D. Monaenkova, M. A. Goodisman, and D. I. Goldman, "Climbing, falling and jamming during ant locomotion in confined environments," *arXiv preprint arXiv:1305.5860*, 2013.

[121] L. Zirbes, Y. Brostaux, M. Mescher, M. Jason, E. Haubruge, and J.-L. Deneubourg, "Self-assemblage and quorum in the earthworm eisenia fetida (oligochaete, lumbricidae)," *PLoS One*, vol. 7, no. 3, p. e32564, 2012.

[122] J. Jones and B. Oldroyd, "Nest thermoregulation in social insects," *Advances in Insect Physiology*, vol. 33, pp. 153–191, 2006.

[123] N. FRANKS, "Thermoregulation in army ant bivouacs," *Physiological Entomology*, vol. 14, no. 4, pp. 397–404, 1989.

[124] J.-H. Dirks, C. J. Clemente, and W. Federle, "Insect tricks: two-phasic foot pad secretion prevents slipping," *Journal of The Royal Society Interface*, vol. 7, no. 45, pp. 587–593, 2010.

[125] W. Federle and T. Endlein, "Locomotion and adhesion: dynamic control of adhesive surface contact in ants," *Arthropod Structure & Development*, vol. 33, no. 1, pp. 67–75, 2004.

[126] P. Drechsler and W. Federle, "Biomechanics of smooth adhesive pads in insects: influence of tarsal secretion on attachment performance," *Journal of Comparative Physiology A*, vol. 192, no. 11, pp. 1213–1222, 2006.

[127] M. Nilsson, R. Daniello, and J. Rothstein, "A novel and inexpensive technique for creating superhydrophobic surfaces using teflon and sandpaper," *Journal of Physics D: Applied Physics*, vol. 43, p. 045301, 2010.

[128] P. Català i Roca, "The castells, a popular creation," *Catalònia*, no. 7, pp. 46–47, 1988.

[129] H. A. Barnes, J. F. Hutton, and K. Walters, *An introduction to rheology*, vol. 3. Elsevier, 1989.

[130] R. G. Larson, *The structure and rheology of complex fluids*, vol. 2. Oxford university press New York, 1999.

[131] T. G. Mezger, *The rheology handbook: for users of rotational and oscillatory rheometers.* Vincentz Network GmbH & Co KG, 2006.

[132] R. B. Bird, R. C. Armstrong, and O. Hassager, "Dynamics of polymeric liquids. vol. 1: Fluid mechanics," 1987.

[133] A. Deshpande, *Rheology of complex fluids.* Springer, 2010.

[134] J. Gachelin, G. Miño, H. Berthet, A. Lindner, A. Rousselet, and É. Clément, "Non-newtonian viscosity of e-coli suspensions," *arXiv preprint arXiv:1210.2102*, 2012.

[135] T. B. Liverpool and M. C. Marchetti, "Rheology of active filament solutions," *arXiv preprint cond-mat/0607285*, 2006.

[136] Y. Hatwalne, S. Ramaswamy, M. Rao, and R. A. Simha, "Rheology of active-particle suspensions," *Physical review letters*, vol. 92, no. 11, p. 118101, 2004.

[137] P. Coussot, Q. D. Nguyen, H. Huynh, and D. Bonn, "Avalanche behavior in yield stress fluids," *Physical review letters*, vol. 88, no. 17, p. 175501, 2002.

[138] S. Wolfram, *Cellular automata and complexity: collected papers*, vol. 1. Addison-Wesley Reading, 1994.

[139] E. Bonabeau, "Agent-based modeling: Methods and techniques for simulating human systems," *Proceedings of the National Academy of Sciences of the United States of America*, vol. 99, no. Suppl 3, pp. 7280–7287, 2002.

[140] A. M. Bruckstein, "Why the ant trails look so straight and nice," *The Mathematical Intelligencer*, vol. 15, no. 2, pp. 59–62, 1993.

[141] M. Resnick, *Turtles, termites, and traffic jams: Explorations in massively parallel microworlds.* Mit Press, 1994.

[142] U. Wilensky, "{NetLogo}," 1999.

[143] M. Ostoja-Starzewski, P. Sheng, and K. Alzebdeh, "Spring network models in elasticity and fracture of composites and polycrystals," *Computational Materials Science*, vol. 7, no. 1, pp. 82–93, 1996.

[144] R. Picu, "Mechanics of random fiber networksa review," *Soft Matter*, vol. 7, no. 15, pp. 6768–6785, 2011.

[145] K. Nichol, A. Zanin, R. Bastien, E. Wandersman, and M. van Hecke, "Flow-induced agitations create a granular fluid," *Physical review letters*, vol. 104, no. 7, p. 078302, 2010.

[146] I. Goldhirsch, "Introduction to granular temperature," *Powder Technology*, vol. 182, no. 2, pp. 130–136, 2008.

[147] M. Yim, D. G. Duff, and K. D. Roufas, "Polybot: a modular reconfigurable robot," in *Robotics and Automation, 2000. Proceedings. ICRA'00. IEEE International Conference on*, vol. 1, pp. 514–520, IEEE, 2000.

[148] S. Powell and N. R. Franks, "How a few help all: living pothole plugs speed prey delivery in the army ant¡ i¿ eciton burchelliii¡/i¿," *Animal behaviour*, vol. 73, no. 6, pp. 1067–1076, 2007.

[149] B. Hölldobler and E. O. Wilson, "The multiple recruitment systems of the african weaver ant oecophylla longinoda (latreille)(hymenoptera: Formicidae)," *Behavioral Ecology and Sociobiology*, vol. 3, no. 1, pp. 19–60, 1978.

References